

REMOVAL OF CIPROFLOXACIN AND CARBAMAZEPINE BY ADSORPTION
ON INORGANIC POROUS MATERIALS

Ms. Thitikamon Sitthisorn

A Thesis Submitted in Partial Fulfillment of the Requirements
for the Degree of Master of Science Program in Environmental Management
(Interdisciplinary Program)
Graduate School
Chulalongkorn University
Academic Year 2009
Copyright of Chulalongkorn University

การกำจัดสารตกค้างจากซีโปรฟล๊อกซาซินและคาร์บามาซีเฟน
โดยการดูดซับด้วยวัสดุมีรูพรุนอินทรีย์

นางสาวจิตติภมล สิทธิสอน

วิทยานิพนธ์นี้เป็นส่วนหนึ่งของการศึกษาตามหลักสูตรปริญญาวิทยาศาสตรมหาบัณฑิต
สาขาวิชาการจัดการสิ่งแวดล้อม (สหสาขาวิชา)
บัณฑิตวิทยาลัย จุฬาลงกรณ์มหาวิทยาลัย
ปีการศึกษา 2552
ลิขสิทธิ์ของจุฬาลงกรณ์มหาวิทยาลัย

Thesis Title REMOVAL OF CIPROFLOXACIN AND CARBAMAZEPINE
BY ADSORPTION ON INORGANIC POROUS MATERIALS

By Ms. Thitikamon Sitthisorn

Field of Study Environmental Management

Thesis Advisor Patiparn Punyapalakul, Ph.D.

Accepted by the Graduate School, Chulalongkorn University in Partial
Fulfillment of the Requirement for the Master's Degree

.....Dean of the Graduate School
(Associate Professor Pornpote Piumsomboon, Ph.D.)

THESIS COMMITTEE

.....Chairman
(Chantra Tongcumpou, Ph.D.)

.....Thesis Advisor
(Patiparn Punyapalakul, Ph.D.)

.....Examiner
(Associate Professor Jin Anotai)

.....External Examiner
(Punjaborn Weschayanwivat, Ph.D.)

ฐิติกมล สิทธิสอน : การกำจัดสารตกค้างจากซิโปรฟล็อกซาซินและคาร์บามาซีพินโดยการดูดติดผิวบนวัสดุที่มีรูพรุนอนินทรีย์ (REMOVAL OF CIPROFLOXACIN AND CARBAMAZEPINE BY ADSORPTION ON INORGANIC POROUS MATERIALS) อ. ที่ปริกษาวิทยานิพนธ์หลัก: อาจารย์.ดร.ปฎิภาณ ปัญญาพลกุล, 123หน้า

ซิโปรฟล็อกซาซินและคาร์บามาซีพินเป็นยาที่มีการใช้อย่างแพร่หลายในการรักษาโรคต่าง ๆ สารจำพวกยาทั้งสองชนิดนี้มีความคงตัวสูง ย่อยสลายได้ยาก จึงตกค้างอยู่ในแหล่งน้ำ ซิโปรฟล็อกซาซินและคาร์บามาซีพินสามารถส่งผลกระทบต่อจุลินทรีย์และระบบนิเวศทางน้ำแม้ในระดับความเข้มข้นต่ำ วัตถุประสงค์ของงานวิจัยนี้มุ่งศึกษาการดูดซับซิโปรฟล็อกซาซินและคาร์บามาซีพินโดยอาศัยเฮกซะ โกนอลมีโซพอร์สซิลิเกต (HMS) และเฮกซะ โกนอลมีโซพอร์สซิลิเกตที่ผ่านการปรับปรุงพื้นผิวด้วยการต่อติดหมู่ฟังก์ชันทั้งแบบหมู่เดี่ยว (SF-HMS) และสองหมู่ (BF-HMS) ได้แก่ หมู่อะมิโน หมู่เมอร์แคปโต และหมู่อัลคิล นอกจากนี้ยังใช้มีโซพอร์สซิลิเกตชนิด SBA-15 รวมไปถึงตัวกลางดูดซับที่มีสมบัติซูเปอร์พาราแมกเนติกประเภทแมกนีไทต์ (Fe_3O_4) โดยเปรียบเทียบประสิทธิภาพการดูดซับกับการใช้ถ่านกัมมันต์ชนิดผง จากผลการทดลองพบว่า เฮกซะ โกนอลมีโซพอร์สซิลิเกตที่ต่อติดหมู่เมอร์แคปโตมีประสิทธิภาพการดูดซับทั้งซิโปรฟล็อกซาซินและคาร์บามาซีพินได้สูงสุด แต่อย่างไรก็ตามประสิทธิภาพการดูดซับซิโปรฟล็อกซาซินและคาร์บามาซีพินยังน้อยกว่าการใช้ถ่านกัมมันต์ชนิดผง ในด้านระยะเวลาสัมผัสที่สมดุลระหว่างตัวกลางดูดซับและมลสารนั้น กลุ่มของเฮกซะ โกนอลมีโซพอร์สซิลิเกตใช้เวลาสัมผัส 9 ชั่วโมง ส่วนกรณีของมีโซพอร์สซิลิเกตชนิด SBA-15 และตัวกลางดูดซับที่มีสมบัติซูเปอร์พาราแมกเนติกประเภทแมกนีไทต์ (Fe_3O_4) ใช้เวลาเพียง 3 ชั่วโมง จากผลการศึกษาด้านศาสตร์การดูดซับเป็นไปตามแบบจำลองอันดับสองเสมือน โดยสมมติความไม่ชอบน้ำและพันธะไฮโดรเจนมีบทบาทสำคัญต่อกระบวนการดูดซับ นอกจากนี้การแปรผันค่า pH ของสารละลายยังส่งผลต่อประสิทธิภาพการดูดซับด้วยความแรงของพันธะไฮโดรเจนระหว่างมลสารและตัวกลางดูดซับ การดูดซับซิโปรฟล็อกซาซินและคาร์บามาซีพินด้วยตัวกลางที่ศึกษานั้น อธิบายได้ดีโดยอาศัยแบบจำลองของแลงเมียร์ ซึ่งอธิบายได้ว่า กลไกการดูดซับที่เกิดขึ้นเป็นการดูดติดผิวแบบชั้นเดี่ยว

สาขาวิชา การจัดการสิ่งแวดล้อม
ปีการศึกษา 2552

ลายมือชื่อนิสิต
ลายมือชื่ออาจารย์ที่ปรึกษาวิทยานิพนธ์หลัก

5187528020 : MAJOR ENVIRONMENTAL MANAGEMANT

KEYWORDS: CIPROFLOXACIN, CARBAMAZEPINE, HEXAGONAL MESOPOROUS SILICATES (HMS), FUNCTIONALIZED HMS, SUPERPARAMAGNETIC MAGNETITE, ADSORPTION

THITIKAMON SITTHISORN: REMOVAL OF CIPROFLOXACIN AND CARBAMAZEPINE BY ADSORPTION ON INORGANIC POROUS MATERIALS. THESIS ADVISOR: PATIPARN PUNYAPALAKUL, Ph.D., 123 pp.

Ciprofloxacin (CIP) and Carbamazepine (CBZ) are widely used pharmaceutical products for treatment of many symptoms. It was reported that they are persistent and can be detected from several water sources. The discharged CIP and CBZ in environment can affect to microorganism or aquatic ecology even for very low concentration; therefore, the elimination of CIP and CBZ from water has to be investigated. The objectives of this research were to study the adsorption of CIP and CBZ by using synthesized hexagonal mesoporous silicate (HMS), functionalized HMSs, SBA-15, and superparamagnetic magnetite, comparing with powdered activated carbon (PAC). The results showed that mercapto functional groups grafted on HMS provided highest CIP and CBZ adsorption capacities; however, it was still lower than that of PAC. The saturation time of HMSs and PAC were achieved at 9 hr, while 3 hr for SBA-15 and superparamagnetic magnetite. The kinetic results were compatible with pseudo-second order. The hydrophobicity and hydrogen bonding might play a key role on the adsorption. Furthermore, the capacities were impacted by varying pH values due to the strength of hydrogen bonding between targeted compounds and adsorbents. The adsorption capacities of both CIP and CBZ on the studied adsorbents were fitted with Langmuir isotherm model implying that the adsorption phenomena of the targeted compounds were monolayer adsorption.

Field of Study: Environmental Management Student's Signature.....

Academic Year : 2009 Thesis Advisor's Signature.....

ACKNOWLEDGEMENTS

To complete my thesis work, many people should be mentioned to express my deep grateful as following:

First of all, I would like to express my thankfulness to my thesis advisor, Dr. Patiparn Punyapalakul, for his valuable knowledge and time –sharing even on recreational time. Moreover, inspiration support throughout this thesis works. I am also grateful to Dr. Chantra Tongcumpao, chairman of the committee and my committee, Dr. Punjaporn Weschayanwiwat, and Associate Professor Jin Anotai for their creative and useful comments.

I express my gratitude to the National Center of Excellence of Environmental and Hazardous waste management (NCE-EHWM) for financial support and research grants.

My cordial thanks should be given to all the NCE-EHWM staffs for their kind cooperation and help including NCE-EHWM laboratory for assistance DI water supply and glassware as well as Department of Environmental Engineering, Faculty of Engineering, Chulalongkorn University for support UV- visible spectrophotometer.

Furthermore, I am very appreciative to Dr. Chavalit Ngamcharussrivichai, lecturer of Department of Chemical Technology, Faculty of Science, Chulalongkorn University, for his beneficial suggestion in SBA-15 synthesis and providing Pluronic. In addition, I impressed my laboratory co - workers for their contribution and good friendship.

Finally, I would like to express my sincere gratitude to my parents and council for their encouragement, understanding and spirit support.

CONTENTS

	Page
ABSTRACT (IN THAI)	iv
ABSTRACT (IN ENGLISH)	v
ACKNOWLEDGEMENTS	vi
CONTENTS	vii
LIST OF TABLES	x
LIST OF FIGURES	xi
ABBREVIATIONS	xiii
CHAPTER I Introduction.....	1
1.1 State of problems.....	1
1.2 Objectives.....	2
1.3 Hypotheses.....	2
1.4 Scopes of the study.....	3
CHAPTER II Theoretical Background and Literature Review.....	5
2.1 Pharmaceutical residues.....	5
2.1.1 Sources and pathway of pharmaceutical residues.....	5
2.2 Ciprofloxacin (CIP).....	8
2.2.1 Mechanisms.....	8
2.2.2 Physical and chemical properties.....	8
2.2.3 World consumption.....	9
2.2.4 Environmental concentration.....	9
2.2.5 Environmental toxicity.....	11
2.3 Carbamazepine (CBZ).....	12
2.3.1 Physical and chemical properties.....	12
2.3.2 World consumption.....	13
2.3.3 Environmental concentration.....	13
2.3.4 Environmental toxicity.....	15
2.4 Nanoporous materials.....	15

2.4.1	Synthesis of ordered mesoporous silicate.....	17
2.4.2	Synthesis route.....	18
2.5	Hexagonal mesoporous silicates (HMS).....	20
2.5.1	Surface functionalization of ordered nanoporous silicates.....	21
2.6	Magnetism.....	24
2.6.1	Types of magnetic materials.....	24
2.7	Synthesis of the magnetic iron oxide nanoparticles in solution.....	25
2.7.1	Application of magnetic nanoparticles.....	26
2.7.2	Superparamagnetic magnetite (Fe_3O_4).....	27
2.8	Adsorption theory.....	28
2.8.1	Mechanism of adsorption onto porous adsorbent.....	28
2.8.2	Adsorption kinetic.....	29
2.8.3	Adsorption isotherm.....	30
2.9	Literature review.....	32
2.9.1	Removal of pharmaceutical residue.....	32
2.9.2	Mesoporous silicate synthesis method.....	33
2.9.3	Application of mesoporous silicates in micro-pollutants removal...	34
2.9.4	Superparamagnetic materials.....	36
2.9.5	Application of superparamagnetic material in micro-pollutant Adsorption.....	37
CHAPTER III Materials and Methods.....		39
3.1	Materials.....	39
3.1.1	Chemical reagents.....	39
3.1.2	Instruments.....	40
3.2	Experiment procedure.....	40
3.2.1	Preparation of adsorbents.....	40
3.2.2	Physico-chemical characterization of adsorbents.....	43
3.2.3	Adsorption study.....	44
CHAPTER IV Results and discussion.....		48
4.1	Physico-chemical characterization.....	48

4.1.1	Pore structure.....	48
4.1.2	Surface area and pore size.....	50
4.1.3	Surface functional groups.....	52
4.1.4	Elemental analysis.....	53
4.1.5	Surface charge.....	54
4.2	Adsorption kinetic.....	57
4.3	Adsorption isotherm.....	62
4.3.1	Effect of surface functional groups at pH 6.8 – 7.2.....	62
4.3.2	Effect of surface functional groups density.....	67
4.4	Adsorption mechanisms.....	71
4.4.1	Effect of pH.....	71
CHAPTER V Conclusion and Recommendations.....		81
5.1	Conclusions.....	81
5.2	Recommendations.....	82
REFERENCES.....		83
APPENDICES.....		91
APPENDIX A.....		92
APPENDIX B.....		98
BIOGRAPHY.....		123

LIST OF TABLES

	Page
Table 2.1 Physico-chemical properties of CIP.....	9
Table 2.2 Concentration of detected CIP in environment.....	10
Table 2.3 Physico-chemical properties of CBZ.....	12
Table 2.4 Annual consumption of CBZ in various countries.....	13
Table 2.5 CBZ concentration detected from many sources.....	14
Table 2.6 Definition of nanoporous powder.....	15
Table 2.7 Definition of porous solids.....	16
Table 2.8 The interaction between surface/inorganic (S/I) in cooperative assembly reaction pathways.....	19
Table 2.9 Comparison of two surface modified method.....	23
Table 3.1 Molar ratio of APTES and MPTES for varied BF-HMS types.....	42
Table 3.2 The studied parameters in adsorption kinetic studies.....	45
Table 3.3 The studied parameters in adsorption isotherm.....	46
Table 3.4 The determination parameters in study of pH effect.....	47
Table 4.1 BET surface area, porous volume, and pore diameter of the studied adsorbents.....	51
Table 4.2 pH_{zpc} of adsorbents used in this study.....	55
Table 4.3 Kinetics values calculated for CIP adsorption onto HMS, functionalized HMSs, PAC, SBA-15, and superparamagnetic magnetite.....	61
Table 4.4 Kinetics values calculated for CBZ adsorption onto HMS, functionalized HMSs, PAC, SBA-15, and superparamagnetic magnetite.....	61
Table 4.5 Densities of amino- and mercapto- functional group per area.....	69
Table 4.6 Charge types of studied adsorbents at different pH.....	74
Table 4.7 Parameters of Langmuir and linear isotherm model for CIP adsorption on applied adsorbents.....	78
Table 4.8 Parameters of Langmuir and linear isotherm model for CBZ adsorption on applied adsorbents.....	79

LIST OF FIGURES

	Page
Figure 2.1 Source and fate of pharmaceutical residual enter to the environment...	6
Figure 2.2 The route of exposed pharmaceutical residues to drinking water treatment plant.....	7
Figure 2.3 Structure and speciation in various pH of CIP.....	8
Figure 2.4 Molecular structure of carbamazepine.....	12
Figure 2.5 Cross-section of a hypothetical porous grain showing various type of pore.....	17
Figure 2.6 Synthesis pathway with different interaction of surfactant and inorganic molecule.....	20
Figure 2.7 The synthesis route of HMS mesoporous molecular sieve.....	21
Figure 2.8 Grafting or post-synthesis and co-condensation or direct synthesis.....	22
Figure 2.9 The overview of magnetite synthesis.....	27
Figure 4.1 XRD pattern of HMS.....	48
Figure 4.2 XRD pattern of functionalized HMSs.....	49
Figure 4.3 XRD pattern of SBA-15.....	49
Figure 4.4 FT-IR spectra of HMS and functionalized HMSs.....	52
Figure 4.5 Total nitrogen and sulfur content in functionalized HMSs.....	53
Figure 4.6 Surface charge of HMS and functionalized HMSs.....	55
Figure 4.7 Adsorption kinetic results of CIP.....	55
Figure 4.8 Adsorption kinetic results of CBZ.....	59
Figure 4.9 Adsorption capacities of CIP on HMS, SF-HMSs, SBA-15, and superparamagnetic magnetite.....	63
Figure 4.10 Adsorption capacities of CIP on M-HMS, A-HMS, and A-HMS.....	65
Figure 4.11 Adsorption capacities per specific surface area of CIP on HMS, SF- HMSs, SBA-15, and superparamagnetic magnetite.....	66
Figure 4.12 Adsorption capacities per specific surface area of CIP on M-HMS, A-HMS, and A-HMS.....	67
Figure 4.13 Adsorption capacities of CBZ on HMS, SF-HMSs, SBA-15, and superparamagnetic magnetite.....	68
Figure 4.14 Adsorption capacities of CBZ on M-HMS, A-HMS, and A-HMS.....	69

	Page
Figure 4.15 Adsorption capacities per specific surface area of CBZ on HMS, SF-HMSs, SBA-15, and superparamagnetic magnetite.....	70
Figure 4.16 Adsorption capacities per specific surface area of CBZ on M-HMS, A-HMS, and A-HMS.....	70
Figure 4.17 Adsorption capacities of CIP on HMS, SF-HMSs, BF-HMSs, SBA-15, and superparamagnetic magnetite.....	73
Figure 4.18 Adsorption capacities per specific surface area of CBZ on HMS, SF-HMSs, BF-HMSs, SBA-15, and superparamagnetic magnetite.....	77

ABBREVIATIONS

CIP	=	Ciprofloxacin
CBZ	=	Carbamazepine
PAC	=	Powdered Activated Carbon
HMS	=	Hexagonal Mesoporous Silicates
SF-HMS	=	Single –functional Hexagonal Mesoporous Silicates
BF-HMS	=	Bi - functional Hexagonal Mesoporous Silicates
A-HMS	=	Amino functionalized Hexagonal Mesoporous Silicates
M-HMS	=	Mercapto functionalized Hexagonal Mesoporous Silicates
OD-HMS	=	Alkyl functionalized Hexagonal Mesoporous Silicates
A3M7	=	Combination of Amino and Mercapto functional Hexagonal Mesoporous Silicates at ratio 3:7
A5M5	=	Combination of Amino and Mercapto functional Hexagonal Mesoporous Silicates at ratio 5:5
A7M3	=	Combination of Amino and Mercapto functional Hexagonal Mesoporous Silicates at ratio 7:3
TEOS	=	Tetraethoxysilane or Tetraethylorthosilane
MPTMS	=	Mercaptopropyltrimethoxysilane
APTES	=	Aminopropyltriethoxysilane
ODS	=	N-Octyldimethylchlorosilane
XRD	=	X-ray diffraction
BET	=	Brunauer-Emmett-Teller
BJH	=	Barrett-Joyner-Halenda
FT-IR	=	Fourier Transform Infrared Spectroscopy
ICP-AES	=	Inductively Coupled Plasma Optical Emission Spectroscopy

CHAPTER I

INTRODUCTION

1.1 State of problems

Pharmaceutical residue is the emerging micro-pollutant that widely detected in various source of water in the recent years. Although the detected concentration level is quite low, the adverse effects of the residue cannot be negligible because of their toxicity and persistence. Hence, the methods for eliminating pharmaceutical residue from water have to be investigated. The pharmaceuticals detected in environment are in many groups, for instance, antibiotics, epileptic, etc.

Ciprofloxacin (CIP) is one of antibiotics in fluoroquinolone group that is widely used for treatment of infectious symptoms. The annually consumption rate of CIP was report at a high level. The rejected CIP was generated from several sources including, household usage, hospital wastewater, and pharmaceutical industry. Moreover, it can be detected in water from many sources such as, surface and ground water, municipal sewage, and even in the effluent of wastewater treatment plant. Likewise, carbamazepine (CBZ) is also reported as the occasional detected pharmaceuticals in environment. CBZ is pharmaceutical belonged to epileptic group that used for remediation of nervous system disorders. Both CIP and CBZ were reported as the persistent substance found in water that should be eliminated. Hence, these pharmaceuticals might be used as pharmaceutical residues model to study for removal method.

In order to remove the pharmaceutical residue from water, many methods such physical and chemical processes have been applied; for example, coagulation and flotation, since the residue tend to have no biodegradation. However, many studies reported that the treatment efficiencies were still low. Adsorption process is one of the widely physico-chemical processes used for water and wastewater treatment, since it can efficiently remove various targeted pollutants from water even for very low

concentration. However, the major disadvantage of adsorption process is its low selectivity, especially for the universal adsorbent like Powdered Activated Carbon (PAC). Moreover, used PAC is frequently regenerated by thermal treatment; it is not applied in case of micro-pollutant containing halogen atom. Therefore, the adsorbent that have higher selectivity and conveniently separate from water should be developed. Therefore, the objective of this study is to evaluate the possibility to remove CIP and CBZ from wastewater by adsorption on synthesized hexagonal mesoporous silicates (HMS), single - functionalized HMSs (i.e. amino-, mercapto-, and octyl- functional groups), bi – functionalized HMSs (i.e. amino- and mercapto-functional groups), and superparamagnetic magnetite, comparing with adsorption by PAC. Moreover, effects of physico-chemical characteristic of adsorbents and pH of solution on the adsorption capacities were also determined and discussed.

1.2 Objectives

The main objective of this study is to evaluate the possibility of using mesoporous silicates and superparamagnetic magnetite for removal of pharmaceutical residues by adsorption process. The specific objectives can be expressed as following:

1. To determine adsorption capacities of ciprofloxacin (CIP) and carbamazepine (CBZ) on mesoporous silicates and superparamagnetic magnetite comparing with powdered activated carbon (PAC) in aqueous phase.
2. To determine the effect of surface functional groups on ciprofloxacin (CIP) and carbamazepine (CBZ) adsorption capacity.
3. To determine the effect of pH on the adsorption capacities of mesoporous silicates and superparamagnetic magnetite.

1.3 Hypotheses

1. CIP and CBZ might be adsorbed by hydrogen bonding and/or Van der Waals interaction between organic surface functional group of adsorbents.

2. Adsorption capacities of CIP and CBZ in aqueous phase can be affected by changing pH due to electrostatic interaction.
3. Surface characteristics, for example, type of surfaces, pore structure, surface charge, surface area and pore size, etc., might affect CIP and CBZ adsorption capacities.

1.4 Scopes of the study

This study was operated at Department of Environmental Engineering, Faculty of Engineering and NCE-EHWM laboratory, Chulalongkorn University. The studies were conducted in batch experiment. The overall of this research can be divided into 4 steps including:

1. ***Synthesis of adsorbent materials***

The aim of this step is to synthesize the various adsorbent materials; for example, hexagonal mesoporous silicate (HMS) and modified surface HMS with several organic functional groups (i.e. amino-, mercapto-, and octyl-functional groups) as single functional group HMS (SF-HMS) and bi functional group HMS (BF-HMS). Moreover, super paramagnetic magnetite was also synthesized.

2. ***Characterization of synthetic adsorbents***

The purpose of this part is to determine the physico-chemical properties of synthesized adsorbents in order to discuss the effect of adsorbent characteristics on adsorption capacity of CIP and CBZ on adsorbent materials.

3. ***Adsorption study of ciprofloxacin (CIP) and carbamazepine (CBZ) on adsorbents***

The adsorption efficiencies of those synthesized adsorbents will be investigated by using synthesized wastewater containing Ciprofloxacin (CIP) and Carbamazepine (CBZ) at concentration range of 0.4-8 mg/L and 0.5-16 mg/L, respectively. The adsorption studies are divided into 2 parts: adsorption kinetic

and adsorption capacity. The capacity results were compared to PAC, which is the widely used adsorbent.

4. *Effect of pH on adsorption capacity study*

The adsorption experiments of CIP and CBZ will be operated under various pH values; including 5, 7, and 9 for determine the effect of pH value on the adsorption capacity. The results were compared to PAC as well.

CHAPTER II

THEORETICAL BACKGROUND AND LITERATURE REVIEW

2.1 Pharmaceutical residues

Pharmaceutical residues in the environment have been widely studied in recent years. The number of detected pharmaceutical in aquatic system is steadily increasing; hence, their effects to aquatic life and human health should be considered. Due to the numerous quantity of used pharmaceuticals and regular discharge to the environment, the pharmaceuticals residues were become an emerging pollutant in several aquatic environments, for instance, the final hospital effluent from wastewater treatment plants in Canada (Miao, *et al.*, 2004) and also natural water resources (Zuccato, *et al.*, 2005, CBS News, 2008, and Hektoen, *et al.*, 1995). These data indicated that pharmaceuticals do not only pollute in effluent of sewage treatment plants, but also contaminate in both surface and ground water, and even in drinking water system. Although their detected concentrations were very little amount, generally in ng/L to µg/L range, which are lower than level prescribed pharmaceutical doses, they have been reported the adverse effects to the marine bacterium *Vibrio fischeri* and the crustacean *Daphnia magna* (Zurita, *et al.*, 2007). Furthermore, there was phytotoxic injury to aquatic plants such as, *Myriophyllum sibiricum* and *Lemna gibba* (Brain, *et al.*, 2004). Therefore, the control of pharmaceutical residues in the environment is still necessary in order to achieve safe water quality.

2.1.1 Sources and pathway of pharmaceutical residues

The common sources of pharmaceutical are the usage for human and animal therapy, which expose to environment via excretion. The other sources are as resulting from the improper disposal of expired pharmaceuticals to environment with unknown quantity from pharmaceuticals manufacturing. The sources of pharmaceutical residues were highly variable in many countries as described in Figure 2.1. Nevertheless, the previous studies pointed out that hospital effluents (Ort, *et al.*, In Press) and sewage treatment plants (STPs) (Andreozzi, *et al.*, 2003) were the major sources of the

residues. The misunderstanding of expired pharmaceuticals disposal by dropping in toilet or throw away with garbage causes the difficult to management and control. As reported in 2009, several groups of pharmaceutical waste composed in municipal solid waste (MSW) in Florida (Musson *et al.*, 2009). The reason to explain their behavior is their understanding that the expired pharmaceuticals can degrade in environment like the organic substance, which is the huge mistake.

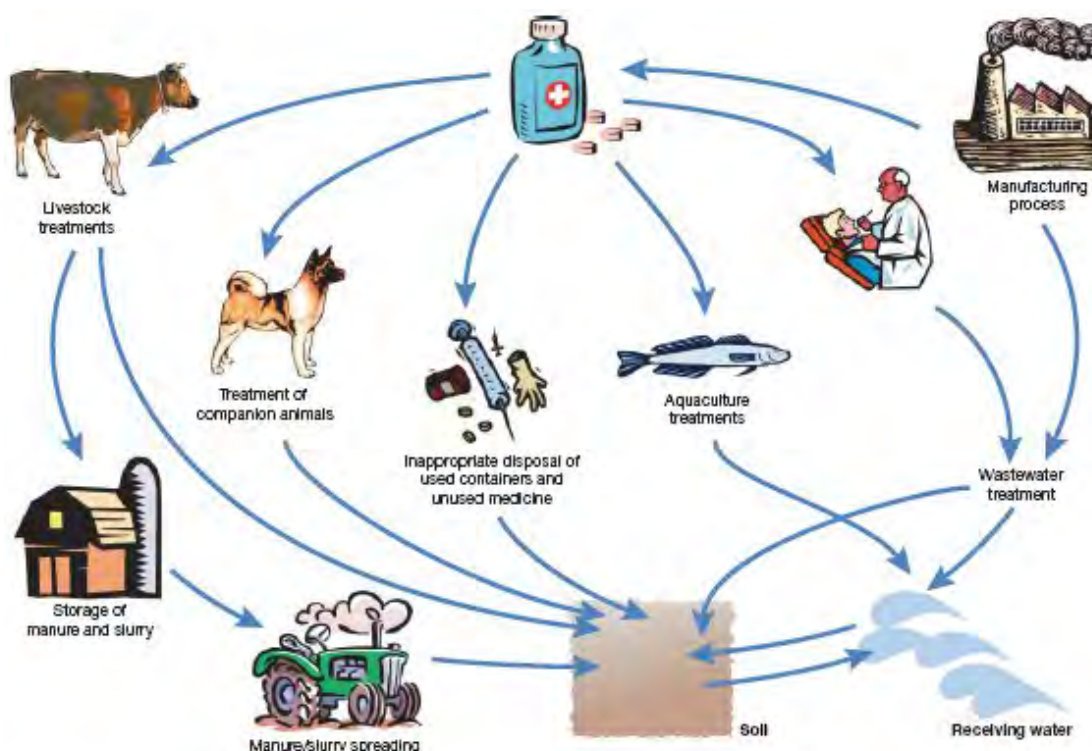


Figure 2.1 Source and fate of pharmaceutical residue enter to the environment
(Boxall *et al.*, 2004).

The reuse of wastewater, sewage water irrigation, and application of sewage sludge on agricultural land causes the pharmaceuticals pass through the unsaturated ground zone before reaching an aquifer. There were several studies on the contaminant of pharmaceutical in groundwater, for example, Ekel *et al.*, (1984) reported the contamination of pharmaceuticals (pentobarbital) nearby shallow groundwater in sampling well 300 m-depth from landfill, which used containing waste in 1968 and 1969 in Florida. Holm *et al.*, (1995) reported the occurrence of pharmaceuticals, i.e. sulfonamide and propyphenazone, from landfill, which served for household and the manufacturers in Denmark.

Fate of metabolism and transformation of used pharmaceuticals is studied by Mompelat and co-worker (2009) as displayed in Figure 2.2. First of all, both human and animal were treated with pharmaceuticals as parent compounds to relieve illness, and then most of them were metabolized in human/animal body to transform as metabolite. After that, the used products were discharged to aquatic environment via effluent of wastewater treatment plant. The effluent and sewage were generally either discharged into surface water, used for irrigation, or groundwater recharge, and finally, they can soak into the drinking water treatment and cause many adverse effects to human health by bacterial resistance. The therapy become more difficult and the illness need new kind of pharmaceutical to heal the same symptom or disease.

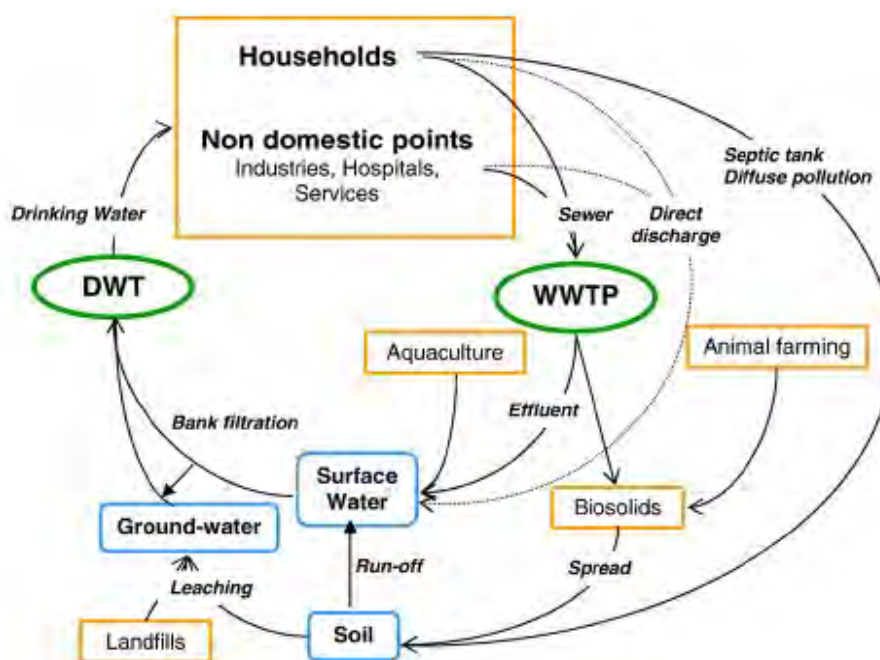


Figure 2.2 The route of exposed pharmaceutical residues to the drinking water treatment (Mompelat *et al* , 2009).

Pharmaceutical was transferred from wastewater or surface water and end up in groundwater with several ways such as;

- river bank filtration
- artificial groundwater recharge

- naturally occurring
- influent groundwater flow conditions
- leaky sewage systems

2.2 Ciprofloxacin (CIP)

Ciprofloxacin is a second-generation antibiotic in fluoroquinolone group that was synthesized to substitute the first one to expand the antibacterial activity, which can cover treatment of diseases occurring from Gram negative bacteria and also Gram positive bacteria, including urinary tract infection, respiratory tract infection, alimentary infection, etc.

2.2.1 Mechanisms

The mechanism of ciprofloxacin was proposed for inhibit enzyme activity for DNA replication, transcription, and repair in bacteria; moreover, it can inhibit the bacteria's enzyme for cell cleavage.

2.2.2 Physical and Chemical properties (Halling-Sørensen et al., 2000 and Wako Pure, 2005)

The molecular structure and speciation of ciprofloxacin in various pHs are respectively shown in Figure 2.3 (a) and (b).

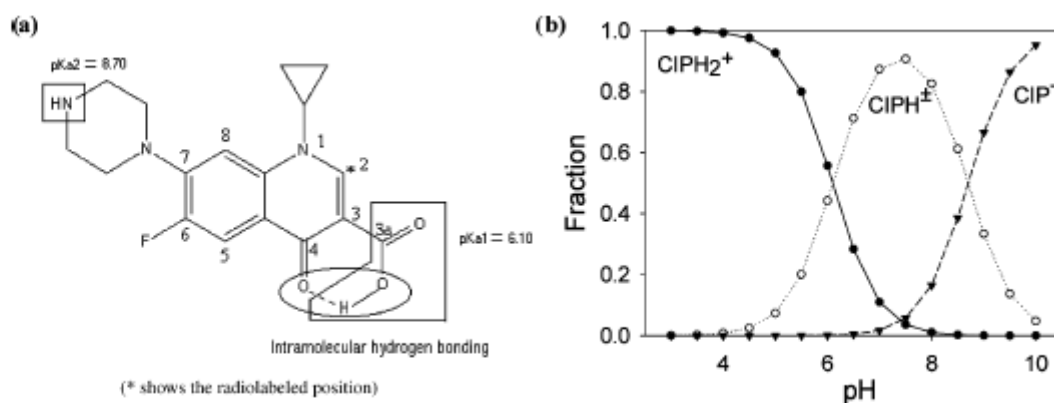


Figure 2.3 (a) Structure and (b) speciation in various pH of CIP

(Gu and Karthikeyan, 2005)

The physical and chemical properties of ciprofloxacin can be summarized in Table 2.1 (Halling-Sørensen *et al.*, 2000; Gu and Karthikeyan, 2005).

Table 2.1 Physicochemical properties of CIP

Parameters	Descriptions
Appearance	White - pale yellow, crystals - powder
Molecular weight	331 g/mol
Aqueous solubility	0.21-9.89
pKa	6.10 and 8.70
Log K _{ow}	-1.51 to -1.13
Solubility in water	> 2 g/L (but soluble in Hydrochloride monohydrate form)
pH	3.0-4.5 (25g/L at 25 °C)
Melting point	318-320 °C

2.2.3 World Consumption

The antibacterial agent in fluoroquinolones group are reliable in healing infection disease and suitable for seriously illness treatment. Thus, consumption of CIP is in high level and still increasing as reports by many literatures (Per *et al.*, 2004). The annually consumption of antibiotic drugs reported in 2002 were estimated to reach the range of 100,000 – 200,000 tons (Sukul and Spitteller, 2007) It was reported that fluoroquinolone antibiotic was applied in Switzerland since 1992 in amount of 4.8 t per year, and the major human-use of fluoroquinolones is “ciprofloxacin” (Giger *et al.*, 2003), which the global sales of CIP in 1999 were mentioned as more than 1.3 billion dollars (Nakata *et al.*, 2005).

2.2.4 Environmental concentration

Ciprofloxacin was detected in many aquatic environments as reported by several researchers. Environment risk studies had estimated the environmental loadings of CIP from European sewage treatment plants to be as high as 186.2 tones per year in

1999 (Halling- Sørensen, 2000). The other detection of CIP in environment can be summarized as in Table 2.2.

Table 2.2 Concentration of detected CIP in environment

Researchers	Year	Matrix	Country	Environment Concentration
Hartmann <i>et al.</i>	1999	- Effluent from hospital wastewaters	Germany	0.7-124.5 µg/L
Golet <i>et al.</i>	2001	- Effluent from urban wastewater treatment plant ○ Primary wastewater ○ Tertiary wastewater	Switzerland	0.249 µg/L 0.405 µg/L
Miao <i>et al.</i>	2004	- Final effluent of wastewater treatment plant	Canada	120 µg/L maximum
Per <i>et al.</i>	2004	- Effluent from hospital sewage line - Sediment	Sweden	0.5 µg/L 151.4 µg/L
Renew and Huang	2004	- Secondary effluent from municipal wastewater	US	0.1-0.16 µg/L
Larsson <i>et al.</i>	2007	- Effluent from treatment plant serving 90 drug manufacturers	India	28,000-31,000 µg/L
Duong <i>et al.</i>	2008	- Hospital wastewater	Vietnam	1.1 µg/L
Diwan <i>et al.</i>	2009	- Hospital effluent	India	236.6 µg/L

2.2.5 Environmental toxicity

Halling - Sørensen et al., 2000 studied the effect of 3 antibiotics, including mecillinam, ciprofloxacin, and trimethopim, which fed in sludge sampling from Denmark. The biodegradation test indicated that no biodegradation occur during 28 day of operation. The compound that consisted of CIP was persistent and tended to not mineralized in every test condition. The results of toxicity confirmed that ciprofloxacin was quite harm to bacteria in activated sludge, green algal (*Selenastrum carpicornutum*), and cyanobacterium (*Microcystis. aerogenosa*), with EC₅₀ values of 0.61 mg/L, 2.97 mg/L, and 5 µg/L, respectively. Moreover, an environment risk assessment in Europe indicated that CIP tended to be hazard to the environment due to its high annually consumption as mentioned above. Hence, CIP was needed to beware its fate and effect on environment.

Brain et al., 2004 assessed for the effect of phytotoxicity of the 25 pharmaceuticals compounds covering 22 antibiotics to the aquatic higher plant *Lemna gibba*. The growth media contained pharmaceutical with concentration range of 0 – 1,000 µg/l were feed to the aquatic plant. The results shown that 3 major antibiotic groups, which comprised of fluoroquinolone, sulfonamide, and tetracycline, expressed the significant phytotoxicity to the plant. Effective Concentration (EC₁₀) value of ciprofloxacin in long –term exposure was 0.106 mg/l.

Cordova-Kreylos et al., 2007 determined the effects of ciprofloxacin on the microbial community from three salt marshes in California. It was found that the exposure of 0.02-200 µg/L of ciprofloxacin to microcosms in sediment can affect sulfate-reducer bacteria, especially *Desulfovibrio*. Moreover, they reported that ciprofloxacin loss its antibacterial activity against CIP exposed anaerobic bacteria in anaerobic condition or sediment.

2.3 Carbamazepine (CBZ)

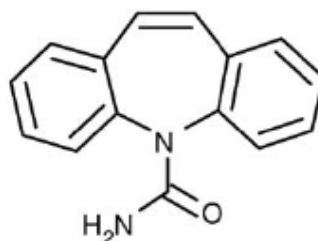


Figure 2.4 Molecular structure of carbamazepine (Scheytt *et al.*, 2006).

Carbamazepine is a worldwide drug belongs to epileptic group. It is widely used for remediation several diseases or symptoms such as alcoholism (Sternebring *et al.*, 1992), opiate withdrawal (Montgomery *et al.*, 2000), relieve depressant (Bertschy *et al.*, 1997), and epileptic (Tixier *et al.*, 2003). The molecular structure and properties of CBZ are shown in Figure 2.4 and Table 2.3, respectively.

Table 2.3 Physico-chemical properties of the CBZ considered in this work (Wako Pure, 2004 ; Comerton, *et al.*, 2008 and Yu *et al.*, 2008)

Properties	Value
Molecular weight (g/mol)	236
Water solubility (mg/L)	17.7 (Practically insoluble)
pK _a	2.3 and 13.9
logK _{ow}	2.45
logK _d	0.1
Dipole moment (μ) (D)	1.67
Molecular width (Å)	5.7
Molecular length (Å)	9.5
Molecular volume (Å ³)	693.3
Appearance	White - slightly yellow, powder
Melting point	189 - 193 °C/372.2 - 379.4 °F

2.3.1 *World consumption: (Oetken et al., 2005; Scheytt et al., 2006; Fent et al., 2006; Kim et al., 2007; Yamamoto et al., 2009 and Zhang et al., 2008)*

High production rate of carbamazepine is consequent to it is prescribed to the patient for long period with high dosages in range 100-2,000 mg per day. The report of annual consumption of CBZ in many countries is summarized in Table 2.4.

Table 2.4 Annual consumption of CBZ in various countries

Country	Year	Annual consumption (ton)
Austria	1997	6.330
	1998	9.970
Germany	1999	120.000
	2000	87.710
	2001	87.600
	2003	78.000
England	2000	40.350
USA	2000	43.000
	2003	35.000
Canada	2001	28.000
France	2001	40.000
Korea	2003	9.155
Japan	2003	45.000
Switzerland	2004	4.400
Finland	2005	4.600

2.3.2 *Environmental concentration*

Carbamazepine was frequently detected in the environment including water and soil phase, particular in the sandy soil. Scheytt and colleagues (2006) reported that no microbial degradation in sandy sediment. Moreover, several reports indicated that CBZ cannot be eliminate or partly removed approximately less than 10% in

wastewater treatment (Ternes, 1998 and Heberer, 2002 and Oetken *et al.*, 2005). It was concluded that carbamazepine behaved as a very persistent substance. The detections of CBZ were reported from many sources as summarized in Table 2.5.

Table 2.5 CBZ concentration detected from many sources

Researchers	Year	Matrix	Country	Environmental concentration
Herberer <i>et al.</i>	1999	3STPs influent	Berlin, Germany	Average 1.78 ng/l
		3STPs effluent	Berlin, Germany	Average 1.63 ng/l
	2000	Surface water	Berlin, Germany	25 – 1075 ng/l
	2001	Lake Wannsee	Berlin, Germany	235 ng/l
		Shallow well from bank filtration site	Berlin, Germany	160 – 360 ng/l
		Water supply well	Berlin, Germany	20 ng/l
Ternes	2000	STP effluent	USA	6300 ng/l maximum
		40 rivers and streams	Germany	250 ng/l maximum
		Drinking water with different facilities	Germany	30 ng/l maximum
Sacher <i>et al.</i>	2000	13 groundwater samples	Baden- Württemberg, Germany	900 ng/l maximum
Drewes <i>et al.</i>	2002	Ground water	California, Arizona USA	610 ng/l
Mompelat <i>et al.</i>	2009	Tap water	Canada	24 ng/l maximum
			USA	140 –258 ng/L maximum
			France	43.20 ng/l maximum
			Germany	60.00 ng/l maximum

In 2009, **Yamamoto and co-worker** reported the persistent of carbamazepine by (1) photolysis experiments with direct sunlight energy source, It was the reported that carbamazepine was high resistance against sunlight due to its half-life ($t_{1/2}$) obtained in 2007 (2100 h) higher than those in 2006 (84 h) approximately 25 times with the similar initial concentration of carbamazepine 100 µg/L. (2) Biodegradation test at 25 °C in the dark was determined the decreasing of carbamazepine concentration 100 mg/L which applied to filtrate water samples from Tamiya River and Tsumeta River in Tokushima City, Japan in 2006 and 2007, respectively. The results showed that

carbamazepine was hardly eliminated by activated sludge with removal rate lesser than 1% and half-life ($t_{1/2}$) value which calculated in 2007 was 5,600 h which was greater than value in 2006 with 2600 h.

2.3.3 Environmental toxicity

Kim and co-worker (2007) determined acute aquatic toxicity of carbamazepine with a marine bacterium (*Vibrio fischeri*), a freshwater invertebrate (*Daphnia magna*), and the Japanese medaka fish (*Oryzias latipes*). The results showed that the median effective concentrations for *V. fischeri* and *D. magna* were 52.5 mg/L (5 min exposure) and 76.3 mg/L (96 h exposure), respectively. For carbamazepine, LC50 test results for the Japanese medaka fish (*O. latipes*) was 35.4 mg/L (48 h exposure). The PEC (potential environmental concentration) of carbamazepine was estimated at 0.14 µg/L calculated based on the population Korean in 2005 (48 million people), which consumed carbamazepine 9,155 kg annually. Moreover, it was reported by Wako Pure Chemical Industries (2004) that the LC50 value of CBZ on the aquatic plankton *zebra danio* was 43 mg/L (96hr exposure).

2.4 Nanoporous-materials (Rouquerol *et al.*, 1999)

The definitions of technical term for powder are summarized as in Table 2.6.

Table 2.6 Definition of powders

Term	Definition
Powder	Dry material composed of discrete particles with maximum dimension less than about 1 mm
Fine powder	Powder with particle size below about 1 µm
Aggregate	Loose, unconsolidated assemblage of particles
Agglomerate	Rigid, consolidated assemblage of particles
Compact	Agglomerate formed by compression of powder
Acicular	Needle-shaped

Term	Definition
Specific surface area	Surface area of unit mass of powder, as determined under stated conditions
External surface	Area of external surface of particles, as taking account of roughness, but not porosity
Roughness	Ratio of external surface area to area of smoothed envelope around particles
Divided solid	Solid made up of more or less independent particles, which may be in the form of a powder, aggregate or agglomerate

The classification of pores according to size has been under discussion for many years. IUPAC attempt to clarify the limits of size of the different categories of pores included in Table 2.7.

Table 2.7 Definition of porous solids

Term	Definition
Porous solid	Solid with cavities or channels which are deeper than they are wide
Open pore	Cavity or channel with access to the surface
Interconnect pore	Pore which communicates with other pores
Blind pore	Pore with single connection to the surface (Dead- End Pore)
Closed pore	Cavity not connected to the surface
Void	Space between particles
Micropore	Pore of internal width less than 2 nm
Mesopore	Pore of internal width between 2 and 50 nm
Macropore	Pore of internal width greater than 50 nm
Pore size	Pore width (diameter of cylindrical pore or distance between opposite walls of slit)
Pore volume	Volume of pores determined by stated method

Term	Definition
Porosity	Ratio of total pore volume to apparent volume of particle or powder
Total porosity	Ratio of volume of void and pores (open and closed) to volume occupied by solid
Open porosity	Ratio of volume of voids and open pores to volume occupied by solid
Surface area	Extent of total surface area as determined by given method under stated conditions
External surface area	Area of surface outside pores
Internal surface area	Area of pore walls
True density	Density of solid, excluding pores and voids
Apparent density	Density of material including closed and accessible pores as determined by stated method

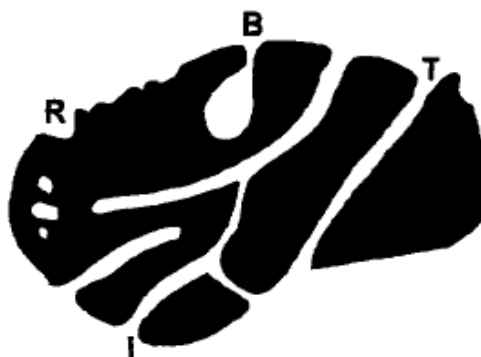


Figure 2.5 Cross-section of a hypothetical porous grain showing various types of pores: Blind (B), Through (T), Interconnected (I) and Roughness (R) (Rouquerol *et al.*, 1999).

2.4.1 Synthesis of ordered mesoporous silicates (Wong, 2004)

The preparation of mesoporous silicates is capable controlled and justified as easy to prepare. Due to the main reasons such as

- Surfactant resists synthesis parameters for example: aging temperature, aging time, pH of synthesis medium and initial precursor ratios in surfactant or silicate mesostructure synthesis.
- Silicate framework can stability in removing of surfactant process which lead structure collapse

2.4.2 *Synthesis route*

2.4.2.1 Surfactant as template routes

Surfactant molecules is become a template for preparation of ordered mesoporous silicates MCM-41 since early 1990s. It was recognized as useful material that give the desirable material properties such as high surface areas (more than 1000 m²/g), uniform pore size (2-10nm), long-range ordering of the pores, structural stability, and ease in surface functionalizations as well as compositional tailoring of the inorganic framework. Application of silicate-based surfactant-template mesoporous materials is popular especially in the separation process. Generally, the synthesis of surfactant-templated mesoporous materials is divided in two parts:

- Forming the surfactant or inorganic mesostructure
- Removing the surfactant from the mesostructure to achieve mesoporous materials

2.4.2.2 Cooperative assembly

The surfactant/inorganic mesostructure occur from the interaction between the surfactant and inorganic precursor molecules. The general types of binding behavior between surfactant head group (S) and inorganic precursor (I) are expressed in Table 2.8 based on the precursors and synthesis conditions.

Table 2.8 The interaction between surfactant/inorganic (S/I) in cooperative assembly reaction pathways

S/I interactions	Chemical Interaction	Example of surfactant/inorganic mesostructure	Reaction conditions
S^+T^-	Electrostatic	MCM-41 mesoporous SiO_2	Prepared with sodium silicate and CTAB* at basic pH
ST^+	Electrostatic	Al- dodecylphosphate mesostructure	Prepared at acidic pH
S^+XT^-	Electrostatic	SBA-3 mesoporous SiO_2	Prepared with CTAB at low pH Counterion X^- is Cl^-/Br^-
$S^+M^+T^-$	Electrostatic	Al- dodecylphosphate mesostructure	Prepared at basic pH Counterion M^+ is Na^+
S/I interactions	Chemical Interaction	Example of surfactant/inorganic mesostructure	Reaction conditions
S^0T^0	Hydrogen bonding	HMS mesoporous SiO_2	Prepared with TEOS** and dodecylamine at neutral pH
N^0T^0	Hydrogen bonding	MSU-1 mesoporous SiO_2	Prepared with nonionic Tergitol T15-S-9 surfactant at neutral pH
$(S^0H^+)(XT^-)$	Hydrogen bonding / Electrostatic	SBA-15 mesoporous SiO_2	Prepared with nonionic Triblock copolymer Pluronic P123 at acidic pH
S-I	Covalent	Nb-TMS1 mesoporous Nb_2O_5	Prepared with niobium ethoxide and dodecylamine

*CTAB = Cetyltrimethyl ammonium

**TEOS = Tetraethoxylorthosilicate

The long- range arrangement or mesophase of the mesostructure is a unique characteristic of surfactant-templated materials. Mesostructure can be disordered or ordered mesostructures can be lamellar, cubic, or hexagonal phase. As shown in Figure 2.6.

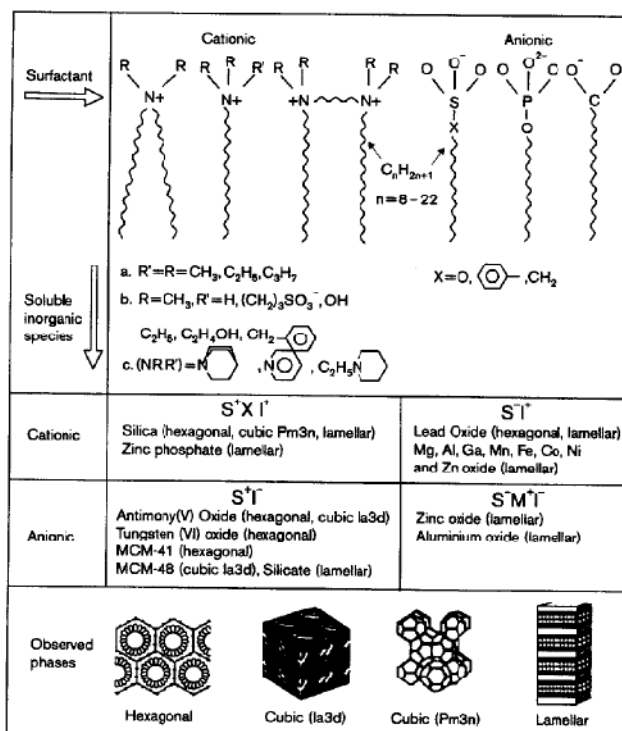


Figure 2.6 Synthesis pathways with different interaction of surfactant and inorganic molecule (Beck, 1996).

The lamellar mesophase comprises an alternating stack of inorganic sheets and surfactant bilayers which quite common for surfactant/non-silicate mesostructures. Moreover, the lamellar phase recognized as containing and the hexagonal and cubic phase can be regarded as rod-like and spherical micelles that close-packed within an inorganic matrix.

2.5 Hexagonal Mesoporous Silicates (HMS) (Tanev and Pinnavaia, 1996)

Mesoporous silicates were applied in most of adsorption work for several years, major of them were HMS and MCM-41. Due to their mesostructure, they can let the molecule trap internal surface so that their adsorption capacity is high. HMS was first synthesized by Tanev and Pinnavaia (1996). Neutral primary amine surfactants and alkyl chain lengths equivalent to the cationic quaternary ammonium analogues were mixed under various range of temperature of reaction. Tetraethoxyorthosilicate

(TEOS) was used as silica source and neutral primary amine surfactant was dodecylamine, which are widely used.

From their work, a neutral synthesis pathway (S^0I^0) was proposed as shown in Figure 2.7. This route was used to synthesis the mesoporous molecular sieves that is based on hydrogen bonding and self-assembly between neutral primary amine surfactants (S^0) and inorganic precursors (I^0). This route provided a noticeable subset of hexagonal mesoporous sieves, which denoted as HMS.

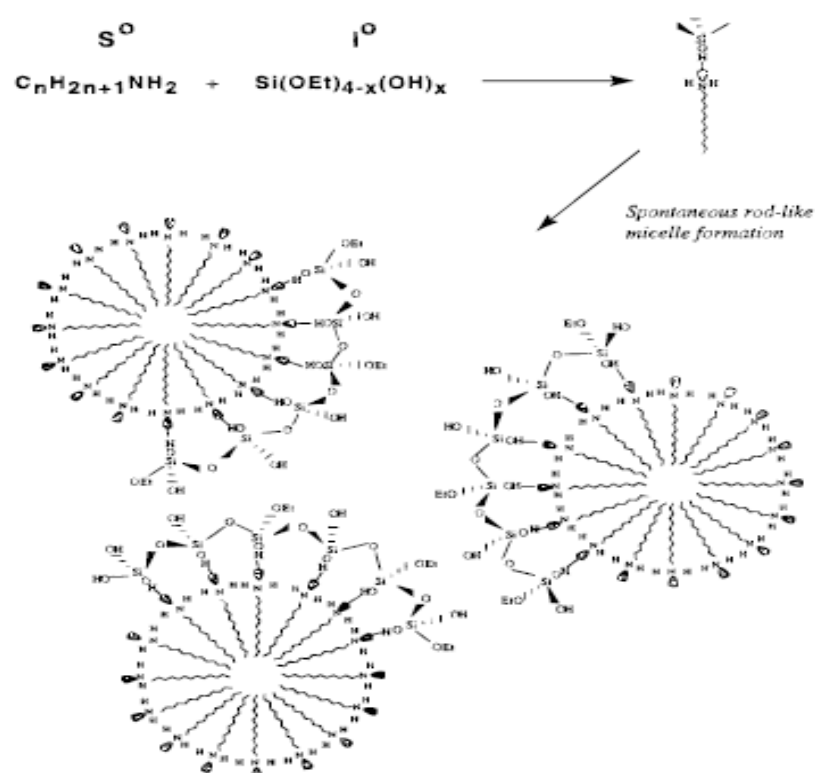


Figure 2.7 The synthesis route of HMS mesoporous molecular sieves
(Tanev and Pinnavaia, 1996)

2.5.1 Surface functionalization of ordered nanoporous silicates (Chong, 2004)

The surface functionalized ordered nanoporous silicate was remarkable and capable in several field such as catalysis, adsorption, optic electronics, sensors, nanotechnology and biology, etc. The main reason is both pore and functional group position can be controlled in order to improve the thermal/hydrothermal stability in this preparation

method. The improvement of surface on ordered nanoporous silicates can be conducted in 2 steps as shown in Figure 2.8.

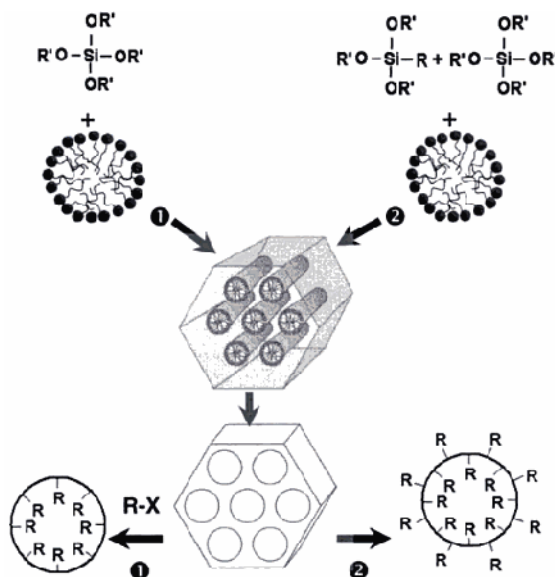


Figure 2.8 (a) Grafting or post-synthesis and (b) Co-condensation or direct synthesis
(Chong, 2004).

1. Grafting or post-synthesis/ post-modification

The preparation method refers to attachment part of functional group to terminal hydroxyl groups or silanol groups (Si-OH). In this process, the functional groups are substituted for silanol groups and placed on the pore surface, resulting in the decrease of pore volume diameter. This method is suitable for organic and inorganic, which do not include every kind of functional group due to limitation of access to silanol group, and also the heterogeneity of surface functional group

The products obtained from this manner are limit in density, and non uniform distribution of the grafted functional group, but the original one still uniform.

2. Co-condensation or direct synthesis

The products obtained from this method are organic- inorganic composite with uniformly distribution of organic on the surface and pore, but loss in long-range structure ordering due to functional group disrupts the original structure.

The comparison between grafting method and co-condensation method are summarized in Table 2.9.

Table 2.9 Comparison of two surface modified methods

Grafting method	Co-condensation method
<p>Advantage:</p> <ul style="list-style-type: none"> - Good preservation of mesostructure after functionalization 	<p>Advantage:</p> <ul style="list-style-type: none"> - Higher and more uniform surface coverage of functionality - Capable control in surface properties.
<p>Disadvantage:</p> <ul style="list-style-type: none"> - Time consuming - Obtain low density and non uniformity of functionality 	<p>Disadvantage:</p> <ul style="list-style-type: none"> - Loss in original structure ordering such as aminopropyltriethoxsilane (APTES)

The surface functionalization of ordered nanoporous silicates is advantage, since the surface functional group can be controlled in type, location, and density in the modified process. Surface modification can extend the limit in application of pure silicate component; for example, increase in the hydrophobicity of surface causes the increasing in hydrothermal of material. These properties can apply in novel catalysis, adsorbents and advanced materials. In term of environmental treatment, surface functional group modified on ordered mesoporous silicates were practically used, such as, adsorption of heavy metal in water by grafted thiol- functional group on ordered nanoporous silicates (*Chong, 2004*).

2.6 Magnetism

Magnetic nanostructures are remarkable among the researches since the first application in biomolecular separation by Robinson and co-worker (1973), in this works the silica-coated magnetic iron oxide and cellulose-coated magnetic iron oxide were prepared (Bruce *et al.*, 2004). The exclusive property of magnet in form of nano-magnetic materials was well known ever since, as can see in many literature reviews involved preparing silica coated magnetic nanoparticles (Jolivet *et al.*, 2002 and Xu *et al.*, 2009)

2.6.1 *Types of magnetic materials (Willis, 2002)*

Magnetic materials can be classified into five basic types based on their behaviors in magnetic fields with varied temperature including:

1. Ferromagnetic materials

These material types are strongly attracted to magnets. They include iron, nickel, cobalt, and steel. The atoms of these substances contain electrons which are all spinning in the same direction. They are strongly influenced by a magnetic field, and the atoms can be turned to point their poles in the same direction. These metals can become strong magnets themselves even without magnetic field.

2. Paramagnetic materials

This type is weakly attracted to magnets. They include metals like aluminum, gold, and copper. The atoms of these substances contain almost all electrons spin in the same direction. This gives the atoms some polarity. Paramagnetic materials can exhibit the magnetism properties only in the presence of magnetic fields.

3. Ferrimagnetic materials

The main ferrimagnetic material is magnetite, a crystal which occurs naturally in rocks. The crystal structure of the mineral allows only some of the atoms to line up

when a magnetic field is present, so it is only weakly attracted to a magnet. The crystal itself is only a weak magnet.

4. Diamagnetic materials

Diamagnetic substances show no visible reaction to the presence of a magnetic field, because the electrons in their atoms are equally spinning in opposite directions. These materials are magnetically neutral. However, the molecules of these substances have a very small polarity, because they are usually not symmetric. When they are exposed to a strong magnetic field, they can express the magnetism properties, which usually are the repulsive force.

2.7 Synthesis of magnetic iron oxide nanoparticles in solution (Gupta and Gupta, 2005 and Ma *et al.*, 2007)

Magnetic nanoparticles preparation methods can be normally divided in 3 routes.

1. Physical methods: These methods are complex and incapable to control the particles' size in range of nanometer, for example, gas phase deposition and electron beam lithography.
2. The wet chemical routes: These methods are simple, flexible, and more efficient in the control of size composition, and sometimes even the shape of the nanoparticles.
3. Biological methods

Among them, the wet chemical methods are widely used due to their straightforward nature and ease of control the characteristics of nanoparticles. Co-precipitation is commonly used for the preparation of magnetic iron oxide nanoparticles for biotechnology. There are two main methods for the synthesis of both Fe_3O_4 and $\gamma\text{-Fe}_2\text{O}_3$ nanoparticles in solution.

In the first, ferrous hydroxide suspensions are partially oxidized with different oxidizing agents, such as nitrate ions, aqueous hydrogen peroxide solution in an open

atmosphere or inert atmosphere spontaneously. The other consists in the co-precipitation of Fe^{2+} to Fe^{3+} aqueous salt solutions by addition of a base. Several factors involve in the characteristics of nanomaterials (i.e. size, shape, and composition) are type of salts used (e.g. chlorides, sulfates, nitrates, per chlorates, etc.), ratio of Fe^{2+} and Fe^{3+} , and pH values as well as ionic strength of the media.

The disadvantages of this bulk solution synthesis are the sensitivity of pH of the reaction mixture, which have to be adjusted during the synthesis, and also the ability in control of particles' size for large quantity production.

2.7.1 Applications of magnetic nanoparticles

The magnetic nanoparticles having suitable surface characteristics have a high potential for using in a wide range application. In all cases, superparamagnetic particles are of interest because they do not retain any magnetism after removal of magnetic field. The application of these particles such as:

- Cellular labeling/cell separation
- Detoxification of biological fluids
- Tissue repair
- Drug delivery
- Magnetic Resonance Imaging (MRI)
- Hyperthermia
- Magnetofection

In the last decade, investigations with several types of iron oxides have been increasingly carried out in the field of nano-sized magnetic particles (mostly maghemite, $\gamma\text{-Fe}_2\text{O}_3$, or magnetite, Fe_3O_4 , single domains of about 5–20 nm in diameter).

2.7.2 Super paramagnetic magnetite (Fe_3O_4)

Magnetite and maghemite nanoparticles have found extensive applications because of their unique magnetic and electronic properties. Especially, Magnetite is the most famous among the magnetic nanomaterials in adsorption process due to weakly force between pollutants and its own that a consequence to easy to separation or regeneration with external magnetic field. (Yuan *et al.*, 2010). There are various ways to prepare magnetite nanoparticles, such as co-precipitation, microemulsions, high temperature decomposition of organic precursors, and oxidization of magnetite nanoparticles. The size and shape of magnetic particles can be controlled in the synthesis route.

The synthesis of magnetite via co-precipitation method and the reaction as showed in Figure 2.9 and Equation 2.1, respectively.

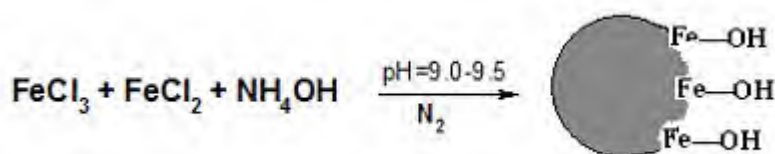
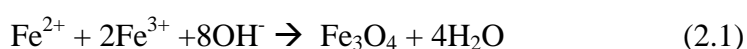


Figure 2.9 The overview of magnetite synthesis
(Durdureanu-Angheluta *et al.*, 2008)



Nanoparticles have attracted great attention in relation with their distinguishable magnetic properties and device miniaturization. These specific properties of magnetic materials can be usefully applied in the wastewater treatment field in adsorption process, for example, removal of heavy metals and arsenic. These applications are known as the Magnetically Assisted Chemical Separation (MACS) process. Moreover, it was reported that the adsorption efficiency of the magnetic materials can be improved by modifying its surface. In the other hand, the functionalization of the particles' surface provided opportunities for selective removal of target chemicals

from polluted water. The application of the magnetic particles for water treatment processes could benefit from its characteristics that can be controlled; for example, specificity, adsorption/ desorption rates, and separation of adsorbed by magnetic force (Auffan, *et al.*, 2007).

2.8 Adsorption Theory

2.8.1 *Mechanism of adsorption onto porous adsorbent*

Adsorption is the inter-phase accumulation of substances at a surface or interface. This process can occur at an interface of any two phases, such as liquid-liquid, gas-solid, or liquid-solid interfaces. The driving force of the process is the imbalance between two phases: the sorbate molecules in the solution and the empty sorbent particles. The sorbate will generate layer on the sorbent's surface and then gradually penetrate deeper into the sorbents. Surface phenomena in term of adsorption can be distinguished into 2 parts, including physical adsorption, which the solute molecules are attracted to the solid by relatively weak force (i.e. covalent, electrostatic, and Van der Waals force), and chemisorption that involves with much stronger force that those of physical sorption such as metals chelation.

Many factors influence the adsorptive capacity for solutes on the adsorbents, which can be classified into 3 groups as following:

1. Properties of sorbent materials: surface area, surface charge, charge density, pore size, etc.
2. Properties of sorbates: chemical structure, pK_a values, functional groups contained, molecular weight, etc.
3. Solution conditions: temperature, pH, ionic strength, presence of other ions.

2.8.2 Adsorption Kinetic (Punyapalukul and Takizawa, 2006; Ho, 2006)

- **The pseudo-first order model**

A simple kinetic of sorption is the pseudo-first order model as expressed in Equation 2.2.

$$\frac{dq_t}{dt} = k_1(q_e - q_t) \quad (2.2)$$

Where k_1 is the pseudo-first order rate constant (h^{-1}). q_e and q_t are the adsorbate uptake at equilibrium (mg g^{-1}) and at time t (mg g^{-1}), respectively. Equation 1 can be derived as shown in Equation 2.3.

$$\ln(q_e - q_t) = \ln(q_e) - k_1 t \quad (2.3)$$

The pseudo-first order (k_1) can be obtained from slope from linear plot between $\ln(q_e - q_t)$ and t .

- **The pseudo-second order model**

The pseudo-second order rate model is used for explaining chemisorptions that involve with valency forces through the sharing or exchange of electrons between adsorbent and adsorbate as covalent forces. The rate of pseudo-second order reaction might be dependent on the amount of adsorbed solute on the surface of adsorbent and the amount sorbed at equilibrium. The kinetic rate equation can be written as Equation 2.4.

$$\frac{dq_t}{dt} = k_2(q_e - q_t)^2 \quad (2.4)$$

Where k_2 is the pseudo-second order rate constant ($\text{g mg}^{-1} \text{h}^{-1}$). By integrating Equation 2.4 with boundary conditions from $t=0$ to t and $q_t = 0$ to q_t , Equation 2.5 are obtained.

$$\frac{t}{q_t} = \frac{1}{2k_2 q_e^2} + \frac{t}{q_e} \quad (2.5)$$

Moreover, the initial adsorption rate can also be acquired from this model as Equation 2.6.

$$h = k_2 q_e^2 \quad (2.6)$$

Where h is the initial sorption rate ($\text{mg}\cdot(\text{g}\cdot\text{min})^{-1}$)

2.8.3 Adsorption Isotherm (Punyapalakul and Takizawa, 2006)

Sorption isotherms are plot between the equilibrium adsorption capacity (q) and the final equilibrium concentration of the residual solute remaining in the solution (C_e). The capacity q ($\text{mg}\cdot\text{g}^{-1}$) can be calculated by Equation 2.7.

$$q = \frac{(C_0 - C_e)V}{m} \quad (2.7)$$

Where C_0 is the initial concentration ($\text{mg}\cdot\text{l}^{-1}$), C_e is the residual concentration at equilibrium ($\text{mg}\cdot\text{l}^{-1}$), V is the solution volume (l), and m is the adsorbent mass (g). The adsorption isotherm relationship can also be mathematically expressed by many models. Langmuir and Freundlich isotherm are the most commonly used for describing the relationship.

- **Langmuir Isotherm**

The Langmuir relationship is a hyperbolic form as show in Equation 2.8.

$$q = \frac{q_m b C_e}{1 + b C_e} \quad (2.8)$$

Where b is Langmuir isotherm coefficient related to the affinity between sorbent and sorbate, and q_m is the monolayer adsorption capacity. This isotherm considers sorption as a chemical phenomenon. It is assumed that the forces between sorbent and sorbate are exerted by chemically unsaturated atoms and do not extend further than the diameter of one sorbed molecule. Therefore, the sorption is restricted to a monolayer.

- **Freundlich Isotherm**

The Freundlich isotherm relationship is in exponential form as expressed in Equation 2.9.

$$q = kC_e^{(1/n)} \quad (2.9)$$

Where k and n are Freundlich constants. The constant k measures the relative adsorption capacity of the adsorbent while $(1/n)$, ranging between 0 and 1, indicates the adsorption affinity or surface heterogeneity. These constants can be obtained from linearized plotting between q and C_e .

The Freundlich relationship is an empirical equation, which does not indicate a limited sorption capacity of the sorbent. This model can only be reasonably applied in case of low to intermediate concentration ranges.

Performances of sorbent are usually implied by its uptake (q). The sorbent can be compared by the specific q_m values, which are calculated from the Langmuir isotherm fitting to the actual experimental data (if it fits). A good sorbent would provide a high uptake capacity (q_m). However, affinity between the sorbent and sorbate is also desired to be high that reflect in considerably uptake value at low concentrations. This performance value is indicated from Langmuir coefficient (b).

2.9 Literature reviews

2.9.1 Removal of pharmaceutical residues

Gu and Karthikeyan (2005) investigated the sorption capacity of ciprofloxacin on hydrous oxides of Al (HAO) and Fe (HFO) which represented as sink of micro-pollutant in the environment. The study indicated that sorption capacity of HFO is higher than that of HAO with $0.066 \text{ mmol}\cdot\text{kg}^{-1}$ and $0.041 \text{ mmol}\cdot\text{kg}^{-1}$, respectively. The sorption isotherm of both HFO and HAO were fitted with Langmuir model ($R^2 = 0.98$). Moreover, pH and zwitterionic form of ciprofloxacin plays a key role in its solubility and sorption, while increasing ionic strength as 0.5 M obtained higher sorption capacity.

Carballa *et al.* (2005) studied the removal of Carbamazepine in primary sewage treatment by using coagulation and dissolved air flotation (DAF) processes. The coagulants employed in this study were FeCl_3 , $\text{Al}_2(\text{SO}_4)_3$, and PAX (aluminum polychloride). It is found that CBZ concentration in water was not affected by adding coagulants in every tested condition; for example, different types of coagulants, coagulants concentration varied, and operating temperature. Its low removal efficiency was discussed to be responsible by its low K_d values. For DAF study, CBZ was particularly removed with highest efficiency of 35% in case of high fat wastewater, which contained 150 mg/L grease, was used.

Mestre *et al.*, (2007) synthesized two types of activated carbon from cork powder waste namely chemical activation of cork with K_2CO_3 (CAC) and physical activation of CAC with steam (CPAC), and then studied the adsorption kinetic of ibuprofen solution on the activated carbons in initial concentration of 20, 40, and 60 mg dm^{-3} . The equilibrium contact time of 4 h was obtained and fitted with pseudo-second order model. From the adsorption capacity of ibuprofen with concentration range 20–120 mg dm^{-3} in different pH conditions and temperatures, they concluded that the higher adsorption capacities were obtained at pH values of 2 – 4. At higher pH value until 11, the lesser capacity was taken and operating temperature did not affect to any

adsorption efficiency. The ibuprofen adsorption isotherms for both activated carbons in every condition were fitted with Langmuir model. It was concluded that CPAC was the best adsorbent for removing ibuprofen due to the preparation of super microporous structure, resulting in higher initial adsorption rate and efficiency.

Comertan *et al.* (2008) applied the nano-filtration and reverse osmosis (R.O.) process for treating CBZ in water. It is reported that the CBZ can be considerably removed by these processes. However, the equilibrium time of 24 h was considered as a too long operating time to achieve the feasibility of treatment by these methods.

Putra *et al.*, (2009) studied the adsorption capacity of amoxicillin, which is an antibiotic drug in penicillin group onto bentonite and activated carbon. The results showed that the equilibrium contact time of amoxicillin solution with initial concentration of 300 mg/L on bentonite and activated carbon were 8 h and 35 min, respectively, and can be explained by pseudo-second order with $R^2 = 0.99$.

In the study of adsorption capacity at various pH, the reported claimed that the highest adsorption capacity of amoxicillin on bentonite (53.9315 mg/g) was obtained at pH = 2.31, whereas the adsorption capacity of amoxicillin on activated carbon was achieved at 189.551 mg/g at pH = 7.04. The phenomena of amoxicillin adsorption on bentonite and activated carbon were fitted with both Langmuir and Freundlich model. Moreover, the study also tested these two adsorbents with real pharmaceutical wastewater, which contained amoxicillin with initial concentration of 317 mg/L. It was found that activated carbon and bentonite could remove amoxicillin as 94.67 % (16.9 mg/L).

2.9.2 *Mesoporous silicates synthesis methods*

Punyapalaku and Takizawa (2006) studied the synthesis method for hexagonal mesoporous silicates (HMS), which have uniform mesopores, large surface area, and uniform functional group. Moreover, the surface of HMS was modified by grafting 3 organic function group including aminopropyltriethoxy-, mercaptopropyl-, and n-

octyldimethyl functional group as well as substitution with Titanium. HMS was synthesized by using surfactant-templating methods, which can be thoroughly described as the silica source – tetraethoxysilane (TEOS) 1.0 mol was dissolved into a mixture of water 29.6 mol, a surfactant – dodecylamine 0.27 mol, and 9.09 mol of ethanol under vigorous stirring. The reaction mixture was aged at ambient temperature for 18 h, and then filtered and air-dried on a glass plate. The product was calcined in air under static conditions at 923 K for 4 h to remove organic template.

2.9.3 *Application of mesoporous silicates in micropollutants removal*

Punyapalaku and Takizawa (2004) prepared the functionalized-HMS by grafting with organic functional groups such as n-octyldimethyl, 3-aminopropyltriethoxy, and 3-mercaptopropyl groups (denoted as OD-, AM-, and MP-HMS). Moreover, titanium was used to improve on HMS's surface and varied ratio of 3-aminopropyltriethoxy and 3-mercaptopropyl to synthesized bi-functional HMS (BF-HMS) were also determined. These adsorbents were used for study the adsorption of DCAA under 298 K temperature. The concentrations of DCAA in solutions were monitored by using UV spectrophotometer or HPLC-MS depended on the concentration of DCAA. For HMS and single functionalized HMSs, the results indicated that scarcely hydrophilic (HMS and Ti-HMS) and hydrophobic surface (M- and OD-HMS) barely adsorbed DCAA, while AM-HMS and PAC that contain strong positive charge can adsorb DCAA. It was discussed that hydrophobicity and surface charge have strong impact on the adsorption, as well as Coulomb force in case of AM-HMS. The results also showed that the adsorption capacities of DCAA were strongly influenced by the initial DCAA concentration. The surface charge of DCAA played a key role for low concentration range where the charge became neutralized at high concentration. In case of BF-HMS, it was found that the grafting of mercapto functional group with amino functional group can significantly enhanced the adsorption capacities. The ratio between amino- and mercapto- functional group of 5:5 and 7:3 provided the highest capacity in this study.

Pérez-Quintanilla *et al.*, (2006) conducted the adsorption study of Hg (II) on the functionalized mesoporous silicates (i.e. SBA-15 and MCM-41) by 3-chloropropyltriethoxysilane and 2-mercaptopyridine with different synthesis route; for example, heterogeneous and homogeneous route. The adsorption study was conducted at pH 6 for 4 hr with 0.2 g of silica. The concentration of Hg solution was 0.1 M and the operating temperature was controlled at 25 °C. The determination method of remaining Hg concentration was analyzed by using an UV-vis spectrophotometer. It was founded that the modified silicates obtained from homogeneous route provided higher adsorption capacity of Hg (II) than those obtained from heterogeneous route. The adsorption results were discussed by comparing the physico-chemical characteristics of adsorbent materials. It was stated that employment of mesoporous silicates that contain higher surface area with controlled pore size and narrow pore size distribution can improve the adsorption of Hg (II) from aqueous media. These abilities of mesoporous silicates can be explored for application to use in clean technologies.

Punyapalakul *et al.*, (2009) reported the effects of the crystalline structure and surface functional group of porous inorganic materials on the adsorption of haloacetic acids. The adsorbent materials used in this study were hexagonal mesoporous silicates (HMS) and modified HMS with amino- and mercapto- functional group, denoted as A-HMS and M-HMS, respectively. The adsorption study was divided into 2 parts including adsorption kinetics and isotherms. The kinetic study was conducted under batch process with dichloroacetic acid (DCAA) and adsorbent concentration of 100 µg/L and 2 g/L, respectively. The contact time was varied for 0 – 72 hr. The pH value at 7 and 0.1 M ionic strength were controlled by phosphate buffer. Samples were agitated by shaker at 150 rpm with 25°C temperature controlled by water bath. The sample was filtered and analyzed for concentration by gas chromatography using an electron capture detector (GC/ECD). The kinetic results were analyzed by pseudo-first and pseudo-second order model. For isotherm study, the concentrations of DCAA were varied for 10 – 400 µg/l with the 2 g/L adsorbent. The 0.1 M ionic strength was controlled and pH value were varied for 5, 7, and 9. The results were analyzed by applying Langmuir and Freundlich isotherm models.

The results showed that the kinetic results of all adsorbent were compatible with pseudo-second order model. The adsorption capacities of DCAA were strongly affected by the physical properties of adsorbent, especially at low concentration. It is stated that the hydrogen bonding and electrostatic force were play an important role in the adsorption. Moreover, pH values can affect the adsorption capacity. Decreasing of pH to less than the pH_{zpc} of the adsorbents resulted in the increase of adsorption capacities.

2.9.4 *Super paramagnetic materials*

Woo and Lee (2004) synthesized hematite and maghemite nanoparticles through sol-gel mediated reaction. The results showed that both of them were rod-shaped and achieved 5-nm in diameters. Their lengths were 16 and 17 nm-lengths, respectively. To investigate magnetic behavior, they performed with a superconducting quantum interference device (SQUID) and hematite was ferromagnetic type at temperature higher than 5 and below 300K. In the other hand, maghemite showed the superparamagnetic property at temperature at around 130 K.

Wang *et al.*, (in press) reported the synthesis method of super paramagnetic mesoporous silica. The overall preparation was divided in two main steps including Fe^{3+} was filled into the silica pore, and then the sample was dried. After that, the dried sample was soaked by ethylene glycol in order to reduce Fe^{3+} to Fe^{2+} , which essential for the formation of iron oxides ferrite. The second step was to determine the best condition of superparamagnetic mesoporous silica preparation, the temperature in the heat treatment range were varied from 350-450°C. It was concluded that in the condition of 350°C heating, the materials contained large surface area, 377.4m²/g and obtained 0.65 cm³/g pore volume with large pore size (7.05 nm).

2.9.5 *Application of Super paramagnetic materials in micropollutants adsorption*

Hu et al., (2006) synthesized the maghemite nanoparticles ($\gamma\text{-Fe}_2\text{O}_3$) via sol-gel method to obtain the nanoparticles with average diameter of around 10 nm and surface area was $198 \text{ m}^2/\text{g}$. After that, they determined the adsorption capacity of heavy metals including Cr (VI), Cu (II), and Ni (II) by those nanoparticles. The adsorption kinetic study indicated that heavy metals with concentration 100 mg/L were adsorbed with high adsorption rate in the first period approximately within 10 min and then steady until 120 min. The adsorption capacity of Cr (VI), Cu (II), and Ni (II) at equilibrium contact time was calculated as 17.0, 26.8, and 23.6 mg/g, respectively. Moreover, it was also reported that the optimum pH for Cr (VI), Cu (II) and Ni (II) removal was reported as 2.5, 6.5, and 9.5, respectively. Additionally, they performed adsorption study of Cr (VI) on conventional hematite ($\alpha\text{-Fe}_2\text{O}_3$) in order to compare the adsorption study with the maghemite one. It was explored that the equilibrium contact time of Cr (VI) on hematite was achieved at 24 hr, which was longer than obtained from maghemite nanoparticles study, and the adsorption capacity was found to be 5 mg/g. From the adsorption capacity study by maghemite, they found that adsorption behavior of Cr (VI), Cu (II) and Ni (II) by maghemite nanoparticles can be described by the Langmuir model with $R^2 = 0.99$.

Afkhami and Moosavi (2010) synthesized maghemite nanoparticles ($\gamma\text{-Fe}_2\text{O}_3$) with diameter 45 nm through co-precipitation method and then, they performed adsorption capacity of Congo-red, anionic dye solution with those synthesized particles at different concentrations (20 -600 mg/L) including determine the effect of contact time and pH of solution in the range 4.0-7.6. The results showed that the decreasing of Congo red concentration was almost completely adsorbed within 30 minutes and the appropriate pH to achieve high removal rate was pH= 5.9. The mechanism of adsorption was reported that it was proceeded by electrostatic force between Congo-red molecule and synthesized adsorbent in different pH condition. From Langmuir model, they calculated the maximum adsorption capacity (q_m) of maghemite nanoparticles

to achieve 208.33 mg/g which the highest adsorption rate than the other adsorbents could in the previous studies.

According to many studies, pharmaceutical residues are emerging as the micro-pollutant that still lack of effective removal method. The residues were inefficiently eliminated in biological treatment and partially removed by physical treatment (i.e. DAF). Adsorption process was report as the treatment method that can be applied in order to remove this micro-pollutant from water. The Powdered activated carbon (PAC) was stated as the effective adsorbent to be employed; however, this widely used adsorbent might contain the disadvantage in low selectivity and regeneration since the thermal regeneration of PAC after used could cause the toxic compound from halogen atom presented on the molecule of pollutants. Therefore, the adsorbent that is capable to adsorb the micro-pollutant without limitation in regeneration should be developed or explored to handle with pharmaceutical residues. In this work, ciprofloxacin and carbamazepine were selected as the representative of pharmaceutical residues in wastewater due to their high consumption rate and frequency detection in water source, especially, carbamazepine which recognized as persistent substance and difficult removal by conventional wastewater treatment plant, and Hexagonal Mesoporous Silicate (HMS) was synthesized and employed as the adsorbent, since it was expected to have high selectivity and containing uniform functional group on its surface. The adsorbed compounds can be desorbed from the materials without causing any toxic substances by solvent extraction. The crystalline structure of used adsorbent was lost only 10 %; therefore HMS can be used in adsorption for several times. Moreover, the adsorption capacity of HMS will be enhanced by surface modifying via organic functional group (amino-, mercapto-, and octyl- group) grafting. Furthermore, the superparamagnetic magnetite are synthesized and used as adsorbent as well in order to solve the problem in hardly separation between of used adsorbents and micro-pollutant. The adsorption capacities of these materials will be compared with the result obtained from PAC.

CHAPTER III

MATERIALS AND METHODS

3.1 Materials

3.1.1 Chemical reagents

1. Dodecylamine	98%	ACROS ORGANICS
2. Tetraethoxysilane	98%	ACROS ORGANICS
3. 3-aminopropyltriethoxysilane	>98%	Fluka
4. 3-mercaptopropyltrimethoxysilane	>98%	Fluka
5. N-Octyldimethylchlorosilane	97%	Fluka
6. Powdered activated carbon	ShirasakiS-10	Japan enviroChemicals, Ltd.
7. Ethyl alcohol absolute	RPE-ACS	CARLO ERBA
8. Sodium hydroxide	AR grade	LAB SCAN
9. Hydrochloric acid	37%	CARLO ERBA
10. Sulfuric acid	98%	LAB SCAN
11. Potassium dihydrogenphosphate	AR grade	Riedel-de-Haen
12. Dipotassium hydrogenphosphate	AR grade	Riedel-de-Haen
13. Ciprofloxacin Hydrochloride monohydrate	97%	Wako pure Co.Ltd.
14. Carbamazepine	98%	Wako pure Co.Ltd.
15. Potassium persulfate (K ₂ S ₂ O ₈)	AR grade	Riedel-de-Haen
16. Nitric acid	65%	Ajax Finechem
17. Hydrofluoric acid	40%	Fluka
18. Iron (II) chloride tetrahydrate	99%	Sigma Aldrich
19. Iron (III) chloride hexahydrate	96%	Ajax Finechem
20. Ammonium hydroxide	28-30%	J.T. Baker
21. Sodium chloride	99%	LAB SCAN

3.1.2 Instruments

1. X-ray diffraction (XRD): Bruker AXS Model D8
2. Fourier transform Infrared Spectroscopy: Nicolet Impact 410
3. Inductively coupled plasma atomic emission spectroscopy (ICP-AES): Varian
4. UV- vis spectrophotometer: Shimadzu UV 1601S with 1 and 5- cm quartz cells
5. Shaker: Green SSriker II
6. Magnetic stirrer : AS ONE Rexim RS 6D model
7. Porosity Analyzer Micromeritic Model: ASAP 2020 version 1.04H
8. Scanning Electron Microscope (SEM): JSM -6400
9. pH meter: Sartorius PB-10 model

3.2 Experimental procedure

3.2.1 Preparation of Adsorbents

- *Synthesis of Hexagonal Mesoporous Silicates (HMS) (Tanev and Pinnavaia, 1996)*

This material was prepared by mixing 29.6 mol of water with 0.27 mol of dodecylamine and 9.09 mol of ethanol to form as organic template of HMS. Add 1.0 mol of tetraethoxysilane (TEOS) in the mixture and were then mixed under vigorous stirring. The reaction mixture was aged at an ambient temperature for 18 h. The resulting mixture was filtered and air-dried on a glass plate. The product was calcined in air under static condition at 650 °C for 4 h to remove organic template.

- *Synthesis of Single-functional HMS (SF- HMS: A-HMS and M-HMS (Lee et al., 2001)*

These materials were synthesized by mixing 50 mol of water with 0.25 mol of dodecylamine and 10.25 mol of ethanol to form an organic template to HMS. Add 1.0 mol of tetraethoxysilane (TEOS) in the mixture and were then mixed under vigorous stirring for 30 min. Then 0.25 mol of 3-aminopropyltriethoxysilane (APTES) or 3-mercaptopropyltrimethoxysilane (MPTMS) was added in the mixture. The reaction mixture was vigorously stirred for 20 h at ambient temperature and the resulting were filtered and air-dried on a glass plate for 24 h. Residual organosilane and organic template were removed by solvent extraction for 72 h with ethanol.

- *Single-functional HMS synthesis (SF-HMS): OD-HMS (Punyapalukul and Takizawa, 2004)*

Octyldimethyl-functional HMS (OD-HMS) was prepared by these following method: drying 5 g of HMS was put in a 250 ml three-neck round flash which containing 140 ml of dichloromethane and stirrer bead. The mixture is stirred, and then 1.8 g of 1-methyl-2-pyrrolidine and 3.6 g of n-octyldimethylchlorosilane (ODS) were added under N₂ flow. The mixture was maintained stirred under reflux at 60°C for 4 hr, after that, filtrated and wash with 50 ml of chloroform twice and 50 ml of ethanol. The sample was drying under vacuum at 40 °C for 4 hr; the OD-HMS was obtained.

- *Synthesis of Bi-functional HMS (BF-HMS) (Punyapalukul and Takizawa, 2004)*

Preparation of BF-HMS was performed by mixing 50 mol of water with 0.25 mol of dodecylamine and 10.25 mol of ethanol to form an organic template to HMS. Tetraethoxysilane (TEOS) of 1.0 mol was added in the mixture, and were then mixed under vigorous stirring for 30 min. Then 0.25 mol of 3-aminopropyltriethoxysilane (APTES) or 3-mercaptopropyltrimethoxysilane (MPTMS) was added in the mixture. The molar ratios of APTES and MPTES for BF-HMS synthesis are exhibited in Table 3.1.

The reaction mixture was vigorously stirred for 20 h at ambient temperature and the resulting were filtered and air-dried on a glass plate for 24 h. Residual organosilane and organic template were removed by solvent extraction for 72 h with ethanol.

Table 3.1 Molar ratios of APTES and MPTMS for varied BF-HMS type

Chemicals Adsorbents	3-aminopropyltriethoxysilane (APTES) (mol)	3-mercaptopropyltrimethoxysilane (MPTMS) (mol)
A7M3	0.175	0.075
A5M5	0.125	0.125
A3M7	0.075	0.175

- *Synthesis of SBA-15 (Imperor Clerc et al., 2000)*

Pluronic 4 g is acidified with 0.24 mol of HCl and then, mixed in 6.46 mol of DI water. The solution is mixed under constant stirring at temperature of reaction 40 °C. After mixture become homogeneous, TEOS (0.0409 mol) is dropped into the mixture and the solution is maintain stirring under 40 °C for 24 hr. The sample is transfered into Teflon container and submit to hydrothermal treatment at 100°C for 24 hr. After filtration and calcination in air at 450°C for 6 hr, the SBA-15 will be obtained.

- *Synthesis of superparanagmetic magnetite (Fe₃O₄) (Lui et al., 2004; Kim et al., 2006)*

The synthesis method of superparanagmetic magnetite (Fe₃O₄) was conducted with co-precipitation method between Fe²⁺ and Fe³⁺ with 1:2 molar ratios under basic condition as following. FeCl₂.4H₂O 0.86 g and 2.36 g of FeCl₃.6H₂O were dissolved in beaker containing 40 ml of DI water under N₂ gas flow. Then, the orange solution was shaken at 250 rpm under temperature 85°C and became instantly black solution after adding 5 ml of NH₄OH. After precipitation Fe₃O₄ with a permanent magnet, the resultant was wash with DI water twice and 0.02 Molar of NaCl.

3.2.2 Physico-Chemical characterization of adsorbents

- *Pore structure*

The synthesized adsorbents were characterized crystalline structure by using X-ray diffraction (XRD), Bruker AXS Model D8 Discover equipped with Cu K α radiation source in the 2θ range 0.35-6 $^{\circ}$.

- *Surface area and pore size*

The schematic for determine surface area were applied with Nitrogen adsorption-desorption isotherms (BET) at 77 K on a surface area and Porosity Analyzer Micromeritic Model: ASAP 2020 version 1.04H. The BET specific surface areas were calculated by using adsorption data in the relative pressure from 0.06-0.14. Pore size distributions were calculated from adsorption branches of isotherms using the Barrett-Joyner-Helenda (BJH) formula.

- *Surface functional group*

Surface functional groups of the synthesized adsorbents were determined by Fourier Transform Infrared (FT-IR) Spectroscopy Nicolet Impact 410. KBr was used as background and sample mixer (KBr: Sample ratio=10:1). In preparation sample, the sample was heated at 110 $^{\circ}$ C for reducing the effect of H $_2$ O at 3750 and 3457 cm $^{-1}$.

- *Elemental analysis*

1. Nitrogen content analysis

The synthesized adsorbents were digested by potassium persulfate (K $_2$ S $_2$ O $_8$) under base condition in autoclave. After that, the sample was determined by UV spectrophotometer at 220 nm.

2. Sulfur content analysis

The synthesized adsorbents were digested with 7 ml- 65% of HNO₃ and 2ml-40% HF in Microwave equipment. The temperature of the reaction was hold at 240°C in 10 min and hold for 20 min. adding 10ml- 5% of H₃BO₃ to remove HF and then the sample was analyzed by Inductively Coupled Plasma Atomic Emission Spectroscopy (ICP-AES).

3. Surface Charge

Acid-Base titrations of all synthesized adsorbents were used to determined surface charge of each adsorbent. Each adsorbent of 2 g was added to 0.01 M of HCl or 0.01 M of NaOH solution in order to vary pH of each sample. There was one sample do not containing acid or base to prepare Blank sample. After adjusting pH with NaCl solution, the samples were shaken in water bath at 25°C for 12 h. The suspension pH of each sample after equilibrating was referred as surface charges.

3.2.3 Adsorption study

The adsorption study can be divided into 3 parts, including:

- *Adsorption kinetic*

1. HMS of 0.04 g was transferred into 50 ml Erlenmeyer flask with 6 mg/l CIP solution for 20 ml. The pH value and ionic strength of solution were controlled at 7 and 0.01 M by using phosphate buffer.
2. Shaking the flasks in controlled temperature at 25 ± 2 °C.
3. The samples were taken at time interval until reach 48 h, and then filtered through the GF/C filter paper. The filtered solution was analyzed for CIP concentration by applying an UV-visible spectrophotometer at 271 nm.
4. This procedure was repeated with concentration of 9 mg/l Carbamazepine solution (CBZ) with UV-visible spectrophotometer at 286 nm.

5. The procedure was repeated with changing adsorbents, including SF-HMS, BF-HMS, SBA-15, superparamagnetic materials and PAC.

The considered variables in adsorption kinetic can be concluded in Table 3.2.

Table 3.2 The studied parameters in adsorption kinetic study

Studied parameters	Values
- Time	- 0, 30, 60, 120, 240 min and then every 2 h until reach 48 h
- Adsorbent types	- HMS, SF-HMSs, BF-HMSs, SBA-15, superparamagnetic material and PAC
- Pollutant types	- Ciprofloxacin (CIP) and Carbamazepine (CBZ)
Analytical parameters	Analytical method
- Concentration of CIP and CBZ	- UV-visible spectrophotometer (1 and 5 - cm quart cell)
Controlled parameters	Values
- pH	- pH value 7 controlled by phosphate buffer
- Ionic strength	- 0.01 M
- Temperature	- 25 ± 2 °C
- Adsorbent weight	- 0.04 g
- Solution volume	- 20 ml

- *Adsorption isotherm*

1. HMS of 0.04 g was transferred into 50 ml Erlenmeyer flask with various range of CIP concentration from 0.4 to 8 mg/L for 20 ml in volume each. The pH value of solution was controlled at 7 and 0.01 M ionic strength by using phosphate buffer.
2. Shaking the flasks in controlled temperature at 25 ± 2 °C.

3. The sample was taken at the contact time obtained from adsorption kinetic. The sample was filtered through the GF/C filter paper, and then analyzed for CIP concentration by applying an UV-visible spectrophotometer at 271 nm.
4. This procedure was repeated with carbamazepine solution (CBZ) with 0.5 to 16 mg/L in concentration. The sample was analyzed for remaining CBZ concentration by UV-visible spectrophotometer at 286 nm.
5. The procedure was repeated with changing adsorbents, including SF-HMS, BF-HMS, SBA-15, superparamagnetic materials and PAC.

The considered variables in adsorption kinetic can be concluded in Table 3.3.

Table 3.3 The studied parameters in adsorption isotherm study

Studied parameters	Values
- Adsorbent types	- HMS, SF-HMSs, BF-HMSs, SBA-15, superparamagnetic material and PAC
- Pollutant types	- Ciprofloxacin (CIP) and Carbamazepine (CBZ)
Analytical parameters	Analytical method
- Concentration of CIP and CBZ	- UV-visible spectrophotometer (1 and 5- cm quart cell)
Controlled parameters	Values
- pH	- pH value 7 controlled by phosphate buffer
- Ionic strength	- 0.01 M
- Temperature	- 25 ± 2 °C
- Adsorbent weight	- 0.04 g
- Solution volume	- 20 ml
- Time	- As obtain from result 3.1

- *Effects of pH*

1. HMS 0.04 g was transferred into 50 ml Erlenmeyer flask with various range of CIP solution including 0.4 – 8 mg/L for 20 ml each. The pH value of solution was

adjusted and controlled to 5, 7, and 9 with 0.01 M ionic strength by using phosphate buffer.

2. Shaking the flasks in controlled temperature at 25 ± 2 °C.
3. The sample was taken at the contact time obtained from adsorption kinetic. The sample will be filtered through the GF/C filter paper and analyzed for CIP concentration by applying an UV-visible spectrophotometer.
4. This procedure was repeated with carbamazepine solution (CBZ) with concentration range of 0.5 to 16 mg/L.
5. The procedure was repeated with varying adsorbents, including SF-HMS, BF-HMS, SBA-15, superparamagnetic materials and PAC.

The considered variables in determining of pH effect can be concluded in Table 3.4.

Table 3.4 The determined parameters in study of pH effects

Studied parameters	Values
- Adsorbent types	- HMS, SF-HMSs, BF-HMSs, SBA-15, superparamagnetic material and PAC
- Pollutant types	- Ciprofloxacin (CIP) and Carbamazepine (CBZ)
Analytical parameters	Analytical method
- Concentration of CIP and CBZ	- UV-visible spectrophotometer (1 and 5 - cm quart cell)
Controlled parameters	Values
- pH	- pH value 7 controlled by phosphate buffer
- Ionic strength	- 0.01 M
- Temperature	- 25 ± 2 °C
- Adsorbent weight	- 0.04 g
- Solution volume	- 20 ml
- Time	- As obtain from result in 3.1

CHAPTER 4

RESULTS AND DISCUSSION

4.1 Physico-Chemical Characterization

Physico-chemical characteristics of synthesized adsorbents (HMS, functionalized HMSs, SBA-15, and superparamagnetic magnetite) were investigated and compared with PAC. The obtained data were applied with the adsorption experiment results for study the relationships between physico-chemical characteristics (i.e. crystalline structure, surface characteristics, water affinity, etc.) and the adsorption phenomena of CIP and CBZ.

4.1.1 Pore Structure

Figure 4.1 and Figure 4.2 displays the X-Ray Powder Diffraction (XRD) pattern of synthesized HMSs. From Figure 4.1, the XRD pattern of pristine HMS exhibited a strong single diffraction peak at $2\theta = 2.2^\circ$ and weak peak at approximately 4.3° as an evidence of the hexagonal crystalline structure. However, XRD pattern of functionalized HMSs indicated that crystalline structure was lost by co-condensation method compared with pristine HMS.

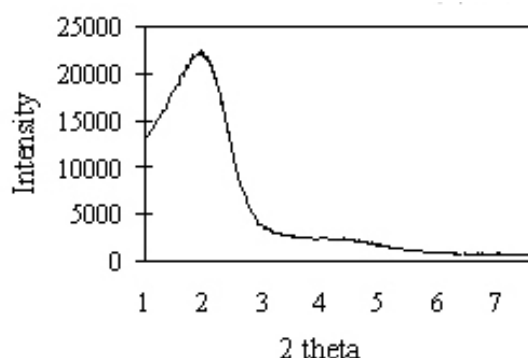


Figure 4.1 XRD patterns of HMS

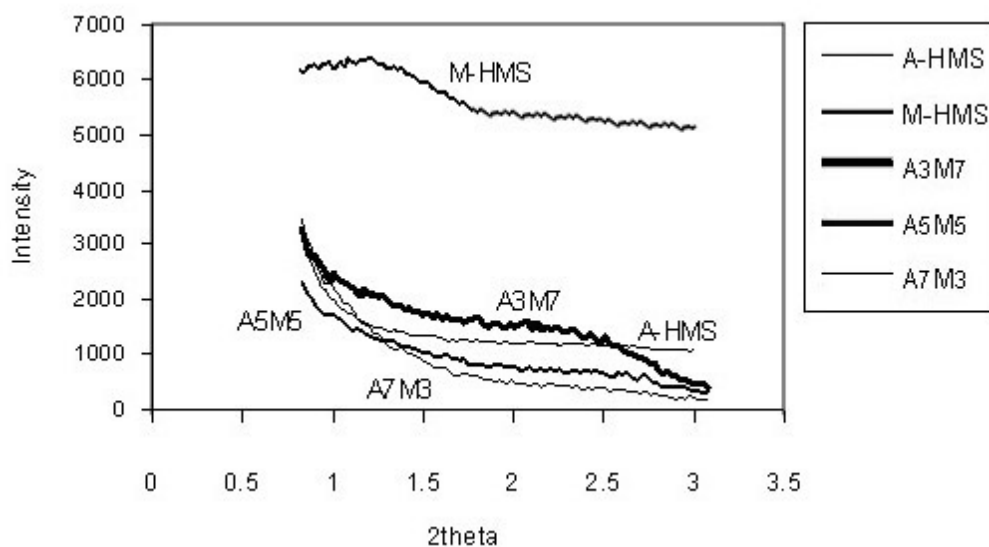


Figure 4.2 XRD patterns of functionalized HMSs

For BF-HMSs, the XRD patterns exhibited very broad peak indicating that the meso-structure of functionalized HMSs became disorder. It might be caused by protonation of APTES under acid or neutral condition. Protonated APTES can cross-link with surface silanol groups of silicate species. On the other hand, protonated APTES might play a strong influence on the self assembly of surfactant, leading to weaker interactions of the silicate species with surfactant template (Chong *et al.*, 2004)

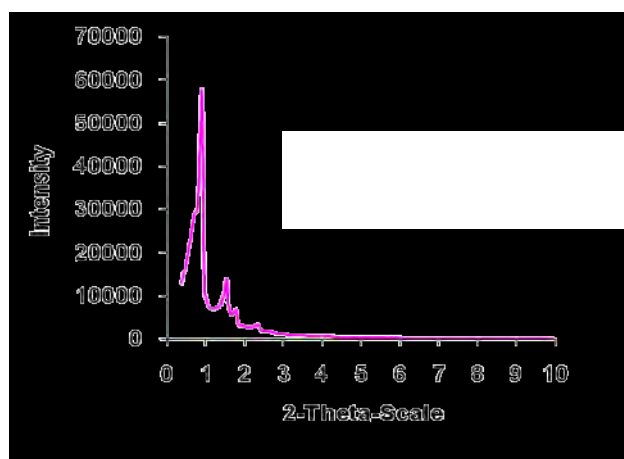


Figure 4.3 XRD patterns of functionalized SBA-15.

The synthesized SBA-15 was confirmed a crystallized structure as a hexagonal symmetry with a well resolved peaks from the XRD pattern which showed a well-resolved peaks at 2θ at $0.5^\circ - 3^\circ$ (Bui T.X. and Choi, H., 2009).

4.1.2 Surface Area and Pore Size

The Brunauer-Emmett-Teller (BET) method was the most widely used method for determination of surface area, pore volumes, and pore size distributions of porous materials from nitrogen adsorption-desorption isotherm data. The nitrogen isotherms (BET) were measured at 77 K on a surface area and porosity analyzer. The BET equation was expressed in Equation 4.1.

$$\frac{p}{v(p_0 - p)} = \frac{1}{v_m c} + \frac{c-1}{v_m c} \cdot \frac{p}{p_0} \quad (4.1)$$

Where, v is volume of N_2 adsorbed by the analyzed sample under pressure p ;
 p_0 is the saturated vapor pressure at the same temperature;
 v_m is the volume of N_2 adsorbed when the surface is covered with a uni-molecular layer;
 and c is constant for a given adsorbate

The specific surface areas of samples were calculated from the adsorption data by Equation 4.2.

$$S = \frac{N_0 v_m A}{22414m} \quad (4.2)$$

Where S is specific surface area;
 N_0 is Avogadro number;
 m is amount of solid adsorbent;
 and A is cross-section of the gas molecules (16.2 \AA^2 for N_2)

The BET model was use for calculating pore size distributions of materials. The obtained BET surface areas, pores volumes, and pores size distributions of HMS, functionalized HMSs, PAC, SBA-15, and superparamagnetic magnetite were shown in Table 4.1.

Table 4.1 BET surface area, pores volumes, and pore diameter of the studied adsorbents

Adsorbents	Pore diameter (nm)	BET surface area (m ² /g)	Pore volume (mm ³ /g)	Surface functional groups	Nitrogen content (μmol/m ²)	Sulfur Content (μmol/m ²)
HMS	2.60	712.24	773.42	Silanol	-	-
A-HMS	3.95	262.28	147.26	Amino	3.84	-
M-HMS	2.48	912.68	433.47	Mercapto	-	3.39
OD-HMS	2.36	477	500	Alkyl	-	-
PAC	1.90	980.46	276.00	Carboxyl, Phenyl, and others	-	-
A3M7	2.50	482.76	151.98	Amino and Mercapto	0.90	4.58
A5M5	2.60	426.40	220.46	Amino and Mercapto	1.29	4.39
A7M3	3.58	200.23	186.82	Amino and Mercapto	4.65	5.38
SBA-15 (Imperor-Clerc, 2000)	3 – 6	841	1,110	Silanol	-	-
Superparamagnetic magnetite (Fe ₃ O ₄)	-	95.3 (Tombácz <i>et al.</i> , 2006)	-	Fe-OH (Bruce <i>et al.</i> , 2004)	-	-

According to Table 4.1, the specific surface area of PAC was higher than the other adsorbents that might result in highest adsorption capacity. Moreover, it was found that the surface area of HMS was decreased due to increasing of grafted amino functional group. It was clearly seen that the amino functional group considerably impacted the structure of mesoporous silicate, which was indicated by the decrease of BET surface area. On the contrary, M-HMS contained higher specific surface area than HMS, which indicated that the mercapto functional group did not disorder the mesostructure of materials.

For pore size distribution, PAC contained the smallest pore size among the used adsorbents. In case of HMS and functionalized HMSs, their average pore sizes were in the range of 2 – 50 nm that conformed to the mesoporous structures category. However, existence of organo-functional groups on HMS influenced to the contained

pore size, for instance, mercapto functional groups on M-HMS provided smaller pore size than the pristine HMS. From this part, it can be concluded that presence of amino functional group might deform hexagonal mesostructure, which causing the increment of average pore size.

4.1.3 Surface Functional Groups

Surface functional groups of used adsorbents were investigated by Fourier Transform Infrared (FT-IR) in order to confirm the presence of functional groups on the adsorbents surface after synthesis. The FT-IR spectra of the HMS and functionalized HMSs were illustrated in Figure 4.4.

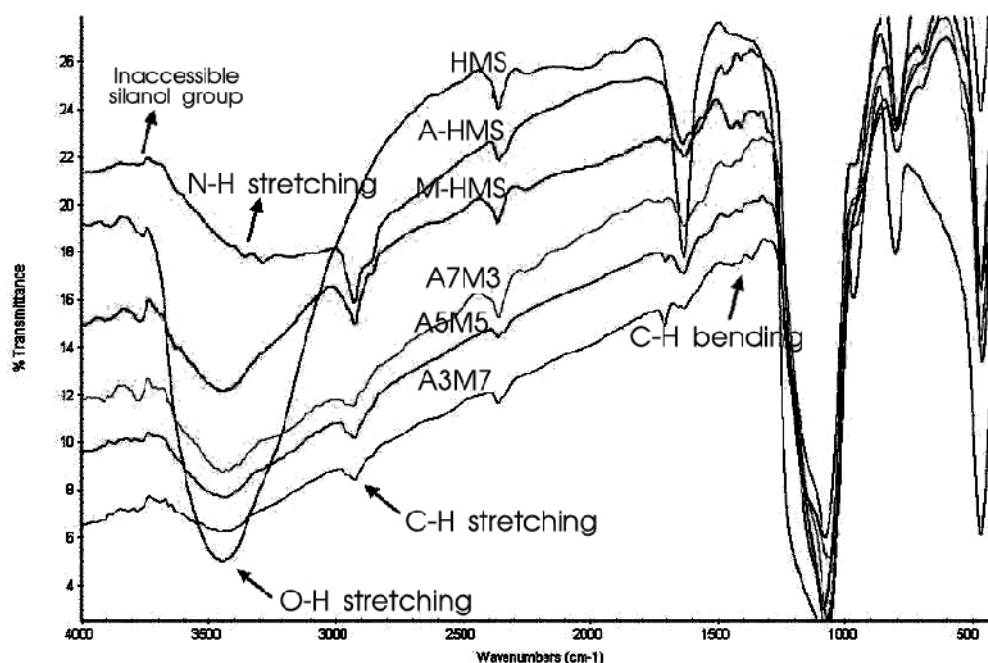


Figure 4.4 FT-IR spectra of HMS and functionalized HMSs

From Figure 4.4, it can be seen that all adsorbents exhibited O-H stretching peak at wave number of $3400 - 3500 \text{ cm}^{-1}$. It indicated that silanol functional group still presented on the surface of materials. Nevertheless, HMS provided the highest transmittance percentage of FT-IR spectra exhibited that it comprised of silanol groups more than the other materials. For functionalized HMSs, they expressed C-H stretching peak and C-H bending of CH_2 -methylene group at less than 3000 cm^{-1} and

1450 cm^{-1} wave number, respectively, in spite of disappearance in pristine HMS. Moreover, A-HMS showed two N-H stretching peak at wave number of 3300 – 3400 cm^{-1} indicating the presence of NH_2 on surface of HMS. However, the mercapto functional group cannot be identified in case of BF-HMSs, which might be caused by low sensitivity of FT-IR to analyze S-H stretching of mercapto groups.

4.1.4 Elemental Analysis

The quantities of N and S in A-HMS, M-HMS, and BF-HMSs were investigated for confirming the presence of N and S, which were used as the evidence of the obtained FT-IR spectra. The total nitrogen and sulfur contents in amino- and mercapto-functionalized HMS were displayed in Figure 4.5.

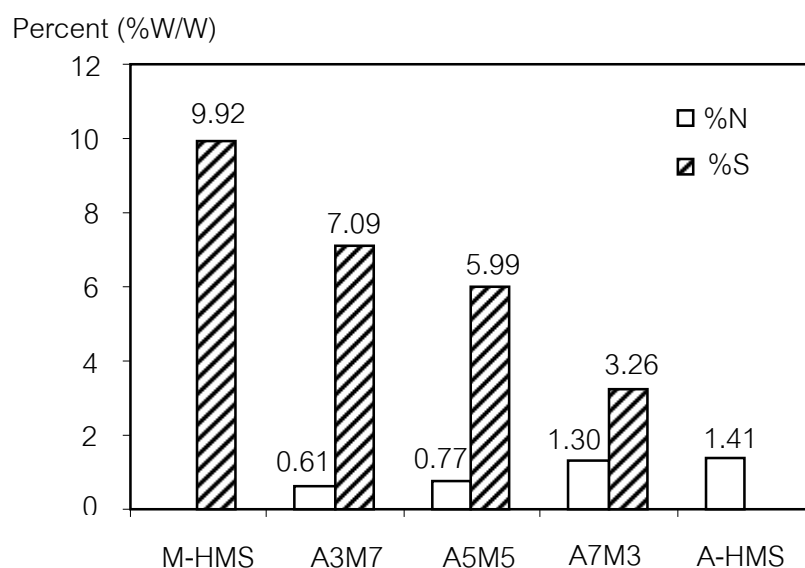


Figure 4.5 Total nitrogen and sulfur content in functionalized HMSs

From Figure 4.5, nitrogen contents of A-HMS, A7M3, A5M5, and A3M7 were detected as 1.41, 1.30, 0.77, and 0.61%, respectively, which were decreasing along to the reduction of amino-functional groups in materials. Whereas, the sulfur content in M-HMS, A3M7, A5M5, and A7M3 were found to be 9.92, 7.09, 5.99, and 3.26%, respectively. The results exhibited that the detected sulfur contents were close to the amount of MPTMS applied in synthesis process. It implied that the mercapto

functional groups were not impacted by reaction between surfactant templates and silica precursor, unlike in case of amino functional groups. Moreover, ratios of amino- and mercapto-functional groups of BF-HMSs as in Figure 4.5 corresponded to the ratios of each functional group used in synthesis of BF-HMSs as in chapter 3, and also the amounts of each functional group presented on the surface.

4.1.5 Surface Charge

Acid/base titration technique was applied for determining the surface charge of used materials. The surface charges can be calculated from the principle of electroneutrality as shown in Equation 4.3.

$$\text{Surface charge (C/g)} = \{[\text{HCl}]_{\text{add}} - [\text{NaOH}]_{\text{add}} - [\text{H}^+] + [\text{OH}^-]\} \times 96500 / W \quad (4.3)$$

Where $[\text{HCl}]_{\text{add}}$ is concentration of added HCl (mol/l)
 $[\text{NaOH}]_{\text{add}}$ is concentration of add NaCl (mol/l)
 $[\text{H}^+]$ is concentration of proton (mol/l) calculated from $\text{pH} = -\log[\text{H}^+]$
 $[\text{OH}^-]$ is concentration of hydroxide ion (mol/l) calculated from
 $\text{pOH} = -\log[\text{OH}^-]$ and $\text{pOH} = 14 - \text{pH}$
 96500 is Faraday's constant (C/mol)
 W is weight of adsorbent (g/l)

The surface charge density of PAC, HMS, SF-HMSs, and BF-HMSs were displayed in Figure 4.6.

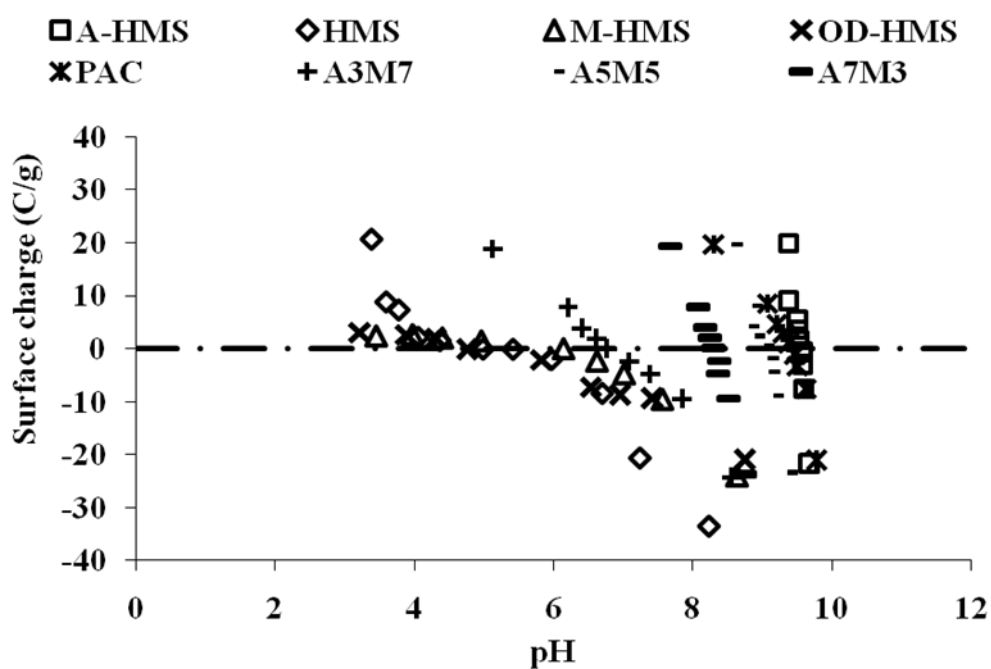


Figure 4.6 Surface charges of HMS and functionalized HMSs

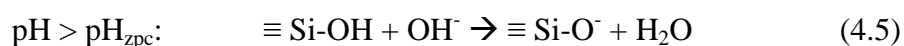
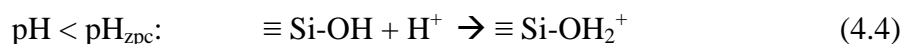
Figure 4.6 illustrated the surface charge density of applied adsorbents as function of pH. The pH value that gives zero surface charge was defined as the zero point of charge (pH_{zpc}), which is summarized in Table 4.2 for all used adsorbents.

Table 4.2 pH_{zpc} of adsorbents used in this study

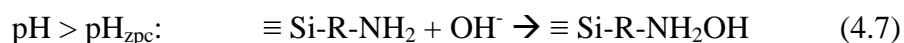
Adsorbents	pH_{zpc}
HMS	5.5
A-HMS	9.5
M-HMS	6.2
OD-HMS	4.4
PAC	9.5
A3M7	6.7
A5M5	8.6
A7M3	8.3
SBA-15	4.0 (Bui and Choi, 2009))
Magnetite	7.8 (Bajpai <i>et al.</i> , 2008)

At this pH value, the positive charge of cationic surface groups and the negative charge of anionic surface groups are balanced. As can be seen in Figure 4.6, the surface charge density decrease as the pH increased from acidic region to neutral pH range. The variations of surface charge at different as expressed in Equation 4.4 and 4.5 were the results of protons gaining or losing from the silanol groups on the surface of HMSs as well as SBA-15. At low pH, surface sites of HMSs are protonated and the surfaces become positively charged; whereas at a high pH, the surface hydroxides lose their protons, and the surfaces become negatively charged. The phenomena occurred as effects of pH for other adsorbents are expressed as following in Equation 4.6 – 4.11.

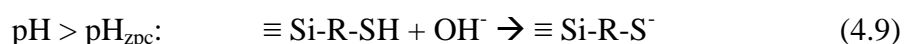
HMS, SBA-15:



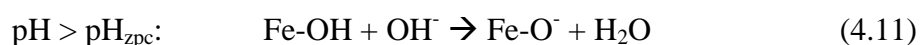
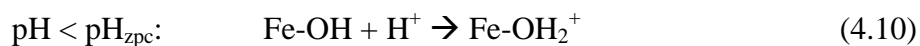
A-HMS:



M-HMS:



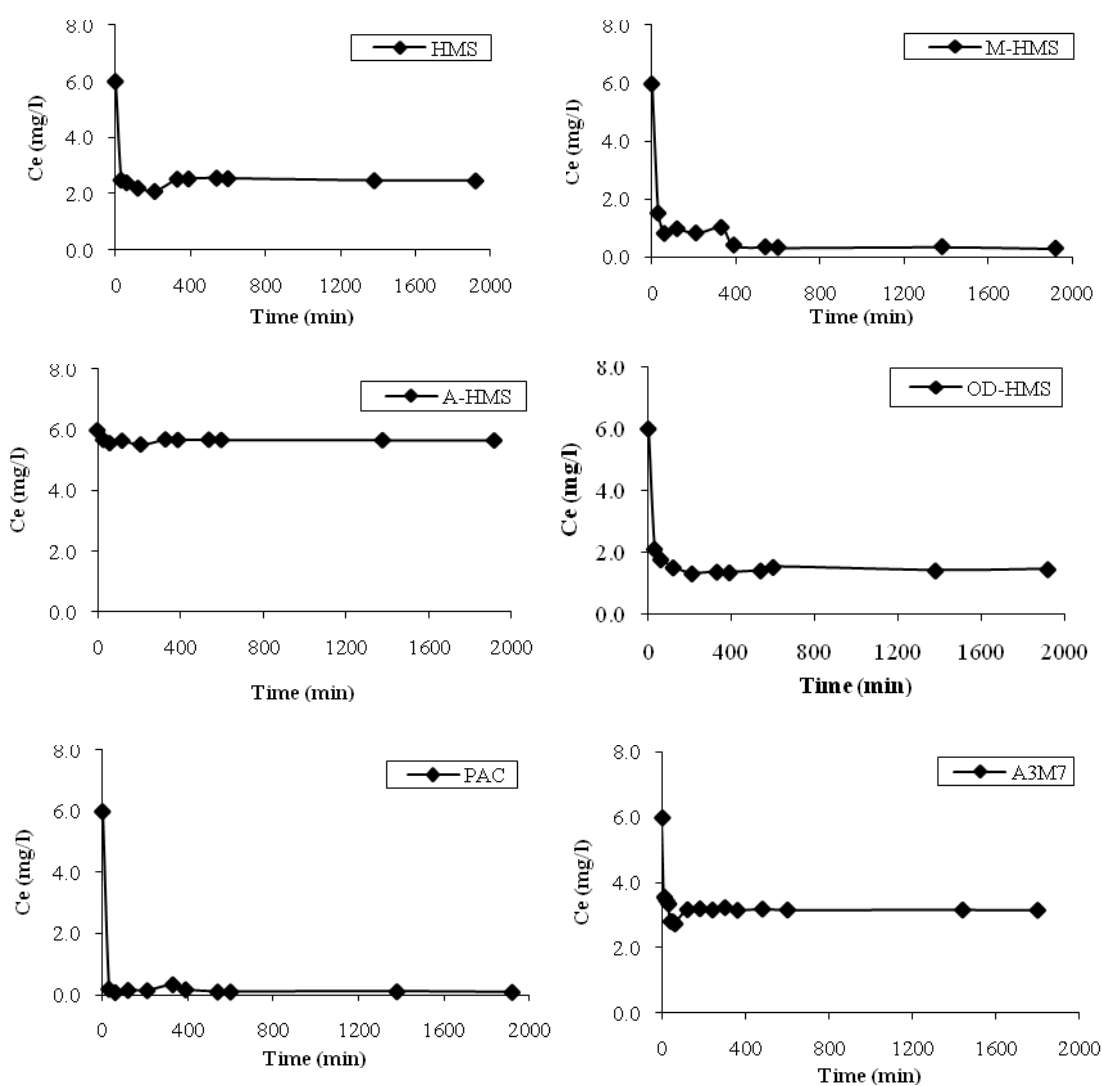
Superparamagnetic magnetite:



The presence of amino-functional groups on surface of HMS provided a higher pH_{zpc} than the pristine HMS. The amino groups were protonated and turned into positively charged on surface. However, surface charge of M-HMS did not obviously change at pH range of 4 – 6.

4.2 Adsorption Kinetic

The adsorption kinetic study of CIP and CBZ were conducted in this section at pH around 7 ± 0.2 with ionic strength of 0.01 M controlled by phosphate buffer. Figure 4.7 displays the kinetic results of CIP on the applied adsorbents. It can be seen that the concentrations of CIP were drastically decreased at first 30 minutes period, except in case of A-HMS. After that, the concentrations were gradually decreased and then achieved the equilibrium stage at approximately 9 hours for HMS, functionalized HMSs, and PAC, while 3 hours for SBA-15 and superparamagnetic magnetite (Fe_3O_4).



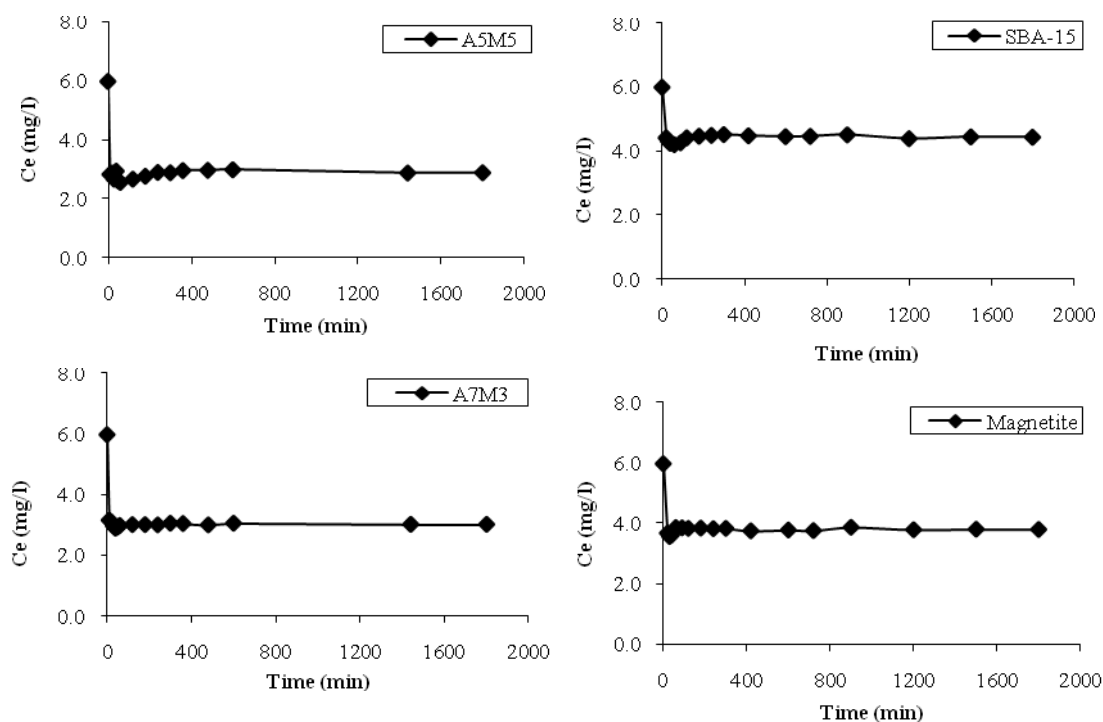
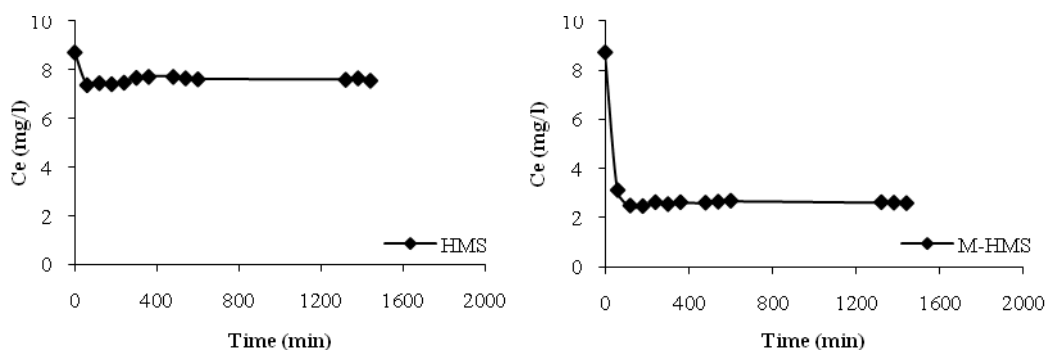


Figure 4.7 Adsorption kinetic results of CIP

Figure 4.8 displays the kinetic results of CBZ for all used adsorbents. It should be noticed that the decreasing of CBZ concentration contained the similar trend with that of CIP. The concentrations were rapidly reduced in the first 30 minutes and then reached the saturation stage at evaluated 9 hours for HMS, functionalized HMSs, and PAC, and approximately 3 hours for SBA-15 and the mesoporous magnetite as well.



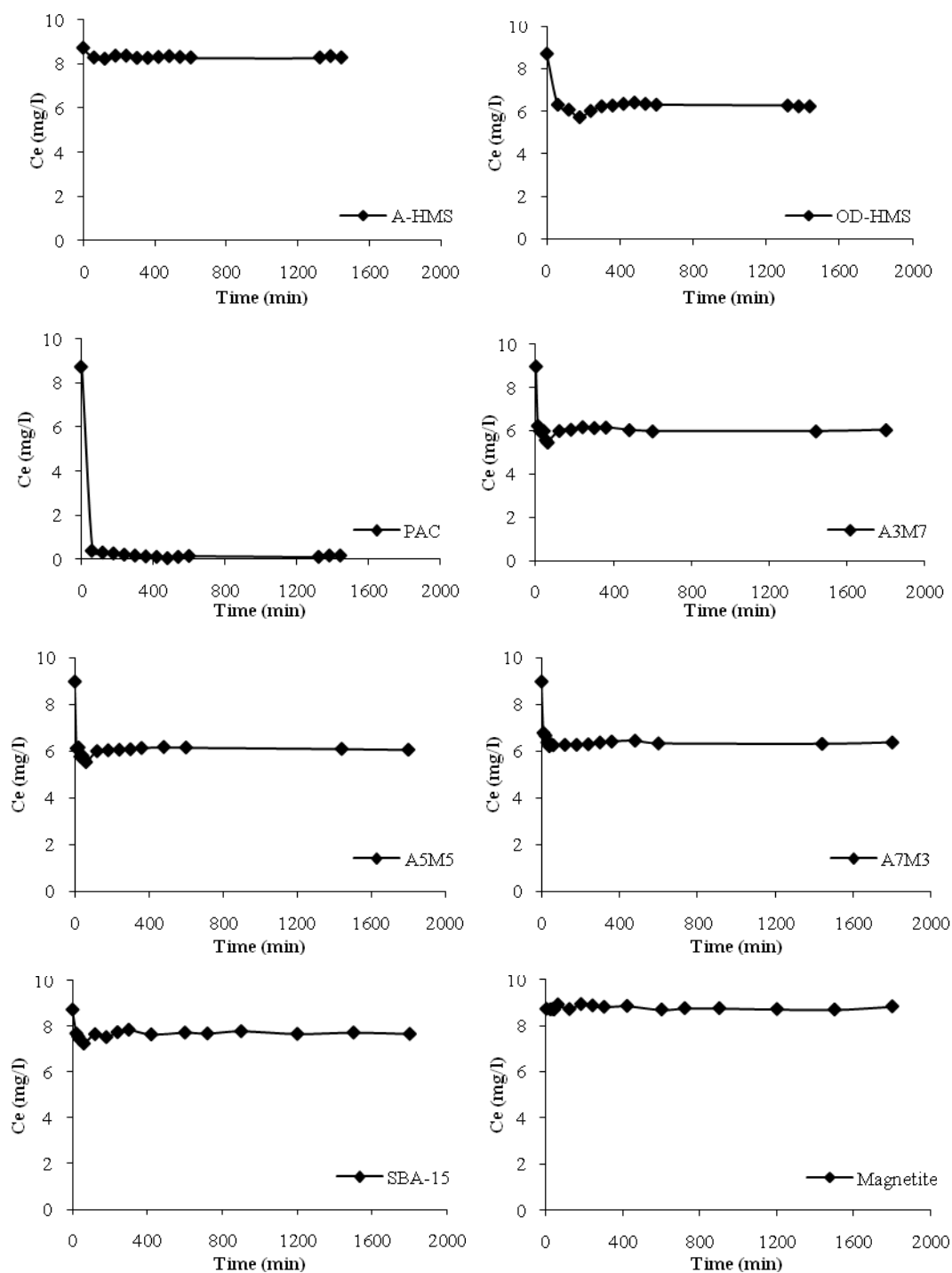


Figure 4.8 Adsorption kinetic results of CBZ

In order to analyze the adsorption rate of CIP and CBZ on the applied adsorbents in this study, the pseudo-first and pseudo-second order model were evaluated based on the experimental results. The pseudo-first order and pseudo-second order kinetic models are expressed in Equation 4.6 and Equation 4.7.

$$\ln(q_e - q_t) = \ln q_e - k_1 t \quad (4.6)$$

$$\frac{t}{q_t} = \frac{1}{2k_2 q_e^2} + \frac{t}{q_e} \quad (4.7)$$

Where, k_1	=	Lagergen rate constant (h^{-1})
k_2	=	Pseudo-second order rate constant ($\text{g} \cdot \text{mg}^{-1} \text{h}^{-1}$)
q_e	=	Amounts of targeted pollutant sorbed at equilibrium (mg/g)
q_t	=	Amounts of targeted pollutant sorbed at time t (mg/g)

The experimental data were plotted between $\ln (q_e - q_t)$ versus time for pseudo-first order rate and between t/q_t versus time for pseudo-second order rate. The calculated kinetic constants of adsorbents for CIP and CBZ are summarized in Table 4.3 and Table 4.4, respectively.

It was found that the experimental data were incompatible with pseudo-first order model. However, the results were fitted with the pseudo-second order model, which meaning that the adsorption kinetic of CIP and CBZ can be described by this model. The experimental q_e values and the calculated q_e obtained from linear plot in Equation (4.7) were compared as shown in Table 4.3 and Table 4.4. The results exhibit very good consistency between the calculated q_e and the experimental one. The pseudo-second order model implied that the adsorption phenomena of both CIP and CBZ were dependent on the quantity of adsorbed target compounds on the adsorbents' surface. Moreover, the adsorption rapidly occurred at the initial stage, and then slower after passing time.

Table 4.3 Kinetics values calculated for CIP adsorption onto HMS, functionalized HMSs, PAC, SBA-15, and superparamagnetic magnetite

Adsorbents	Pseudo-second order			Experimental q_e ($\mu\text{g/g}$)	h ($\mu\text{g/g h}$)
	R^2	k_2 ($\text{g}/\mu\text{g h}$)	Calculated q_e ($\mu\text{g/g}$)		
HMS	0.9992	0.084	1.9650	1.953	0.325
A-HMS	-	-	-	0.242	-
M-HMS	0.9935	0.036	2.6846	2.847	0.261
OD-HMS	0.9997	0.054	2.3469	2.340	0.295
PAC	-	-	-	2.956	-
A3M7	0.9836	0.082	1.6609	1.605	0.227
A5M5	0.9982	0.412	1.6461	1.685	1.117
A7M3	0.9992	0.770	1.5214	1.540	1.783
SBA-15	0.9985	0.347	1.7603	1.788	1.077
Magnetite	-	-	-	2.430	-

Table 4.4 Kinetics values calculated for CBZ adsorption onto HMS, functionalized HMSs, PAC, SBA-15, and superparamagnetic magnetite

Adsorbents	Pseudo-second order			Experimental q_e ($\mu\text{g/g}$)	h ($\mu\text{g/g h}$)
	R^2	k_2 ($\text{g}/\mu\text{g h}$)	Calculated q_e ($\mu\text{g/g}$)		
HMS	-	-	-	0.654	-
A-HMS	-	-	-	0.244	-
M-HMS	0.9993	0.095	3.0931	3.118	0.909
OD-HMS	0.9909	0.049	2.7816	2.957	0.382
PAC	-	-	-	4.279	-
A3M7	0.9824	0.105	1.5748	1.583	0.259
A5M5	0.9930	0.132	1.5775	1.567	0.329
A7M3	0.9946	0.181	1.2572	1.238	0.286
SBA-15	0.9672	0.068	1.5168	1.491	0.157
Magnetite	-	-	-	0.028	-

Furthermore, the initial adsorption rate can also be obtained from this model by calculated from Equation 4.8 as shown in Table 4.3 and Table 4.4.

$$h = k_2 q_e^2 \quad (4.8)$$

Where, h is the initial adsorption rate ($\mu\text{g/g}\cdot\text{h}$). The calculated k_2 values indicated the adsorption rate of adsorbents. High k_2 value implied to high adsorption rate and can rapidly reach the saturation stage. Moreover, it also meant that the adsorbents with high k_2 required higher quantity to equally adsorb with the low k_2 adsorbent. Whereas, the initial adsorption rate (h) mentioned the rate of adsorption at the initial

period, which can be implied to the drastically decrease of CIP and CBZ concentration in the first 30 minutes occurred in this study.

4.3 Adsorption Isotherm

In this part, adsorption mechanisms of CIP and CBZ from aqueous solution onto synthesized HMSs, SBA-15, and superparamagnetic magnetite were investigated. Their adsorption capacities were compared with PAC. Physical characteristics of these materials were determined and discussed for their effects on the adsorption mechanisms. The results from adsorption isotherm were applied with a theoretical evaluation of the surface properties of adsorbents and adsorbate to explain the adsorption capacities and mechanisms. Moreover, the experimental results were fitted to Langmuir and Freundlich isotherm model with linear regression.

4.3.1 Effect of Surface Functional Groups at pH 6.8 – 7.2

The adsorption studies of CIP and CBZ were conducted at pH 6.8 – 7.2 with 0.01 M ionic strength controlled by phosphate buffer. CIP, which has pKa at 6.10 (carboxyl group) and 8.70 (amine group) (Gu and Karthikeyan, 2005), and CBZ, which contained pKa at 2.30 (ketone group) and 13.90 (amine group) (Yu *et al.*, 2008), were in neutral charge species. These two compounds had two pKa values since they can be dissociate at two different functional groups depending on pH of solution. At this pH range, several adsorbents including PAC, A-HMS, A5M5, A7M3, and magnetite provided the positively charged surface, while HMS, M-HMS, OD-HMS, and SBA-15 expressed the negative charge. The neutral species of CIP and CBZ were expected to have low electrostatic attraction with the charged adsorbents and can be neglected. However, CIP and CBZ contained hydrophobic functional groups, which expected to have high affinity with the hydrophobic adsorbents such as PAC, M-HMS, and OD-HMS; whereas, the hydrophilic surface adsorbent tended to have low adsorption with CIP and CBZ. Figure 4.7 displays adsorption isotherms of CIP on all used adsorbents.

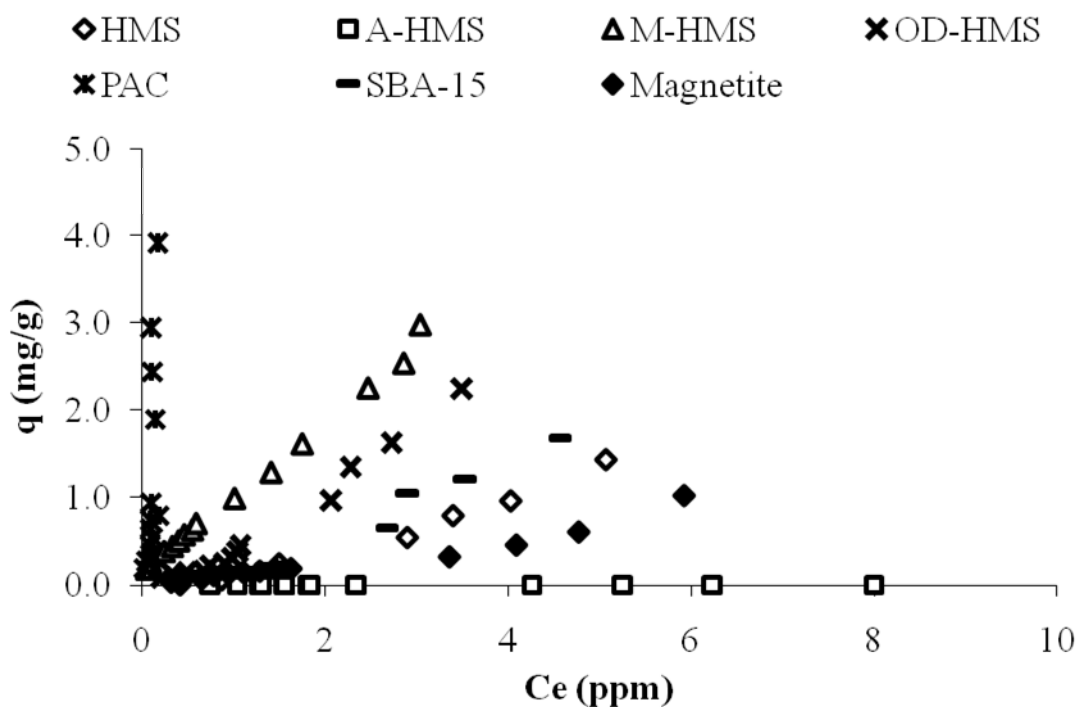


Figure 4.9 Adsorption capacities of CIP on HMS, SF-HMS, PAC, SBA-15, and superparamagnetic magnetite at 25 ± 2 °C, pH 7 ± 2 , and 0.01 M ionic strength

From Figure 4.9, it was found that hydrophobic adsorbents (PAC, M-HMS, OD-HMS) provided higher adsorption capacity than the hydrophilic one (HMS, A-HMS, SBA-15). Note that the molecule dimensions of CIP (0.57 nm in width and 0.95 nm in length) and CBZ (0.72 nm in width and 1.35 nm in length) were smaller than pore size of all adsorbents; therefore, the effects of adsorbents' pore size can be neglected. As mentioned above, the adsorption mechanisms of CIP on the adsorbents' surface tend to be the results of water affinity of adsorbents as well as hydrogen bonding. It should be noted that adsorption of CIP on HMS and SBA-15 due to interaction between silanol groups on surface and intermolecular hydrogen bonding part of CIP molecule might be stronger than hydrogen bonding interacted with amino functional on A-HMS surface. However, the difference of adsorption capacities of HMS and SBA-15, which contained the same functional group: silanol might cause by the difference of specific surface area where SBA-15 had higher area than HMS. Moreover, in case of M-HMS, hydrogen bonding caused by mercapto functional

groups should be suggested to enhance the adsorption capacity comparing with OD-HMS.

Figure 4.10 illustrates the adsorption capacities of all adsorbents per square meter of specific surface area in order to neglect the effect of surface area of adsorbents. According Figure 4.10, it was found that PAC still had highest capacity; whereas, adsorption capacity per area of OD-HMS was relatively close to M-HMS. It indicated that adsorption of CIP was governed by the hydrophobicity of adsorbents as well as hydrogen bonding. Moreover, it can be seen that SBA-15 and HMS provided closely adsorption capacity. Since the silanol groups were presented in both SBA-15 and HMS, the effects of hydrogen bonding on the adsorbents were equally obtained. Moreover, it can be seen from Figure 4.10 that the capacity per area of magnetite was as high as OD-HMS and M-HMS. This might cause from the hydrogen bonding between carboxyl groups on CIP molecule and hydroxyl groups (-OH) on surface of magnetite. The hydroxyl groups can be ionized as in Equation 4.10. However, low specific surface area of magnetite resulted in low adsorption capacity, which was the disadvantage of this material.

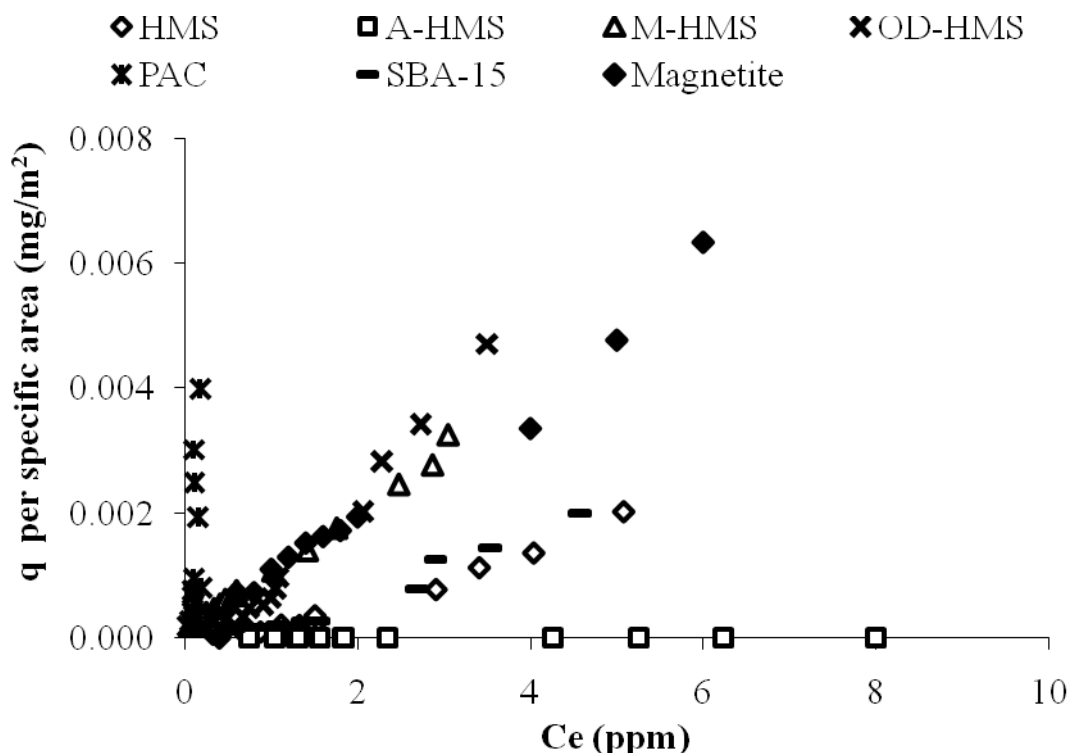


Figure 4.10 Adsorption capacities per specific surface area of CIP on HMS and SF-HMS, PAC, SBA-15, and superparamagnetic magnetite at 25 ± 2 °C, pH 7 ± 2 , and 0.01 M ionic strength

In case of CBZ adsorption, the capacities obtained from adsorbents used in this study had a similar trend with CIP adsorption. Hydrophobicity of materials might play a key role on the adsorption. Moreover, hydrogen bonding between amide groups ($-\text{NH}_2$) on the targeted compound surface that can interact with the surface functional group of materials was mainly responsible for this adsorption (Turku et al., 2007). It can be noticed from Figure 4.11 that CBZ interaction between silanol group on HMS and CBZ might be stronger than hydrogen bonding interacted with amino functional group on A-HMS surface. In addition, CBZ can also interact with mercapto group on M-HMS comparing with the hydrophobic OD-HMS. For superparamagnetic magnetite, the CBZ tend to be not adsorbed by the materials, which might be the results of weak interaction.

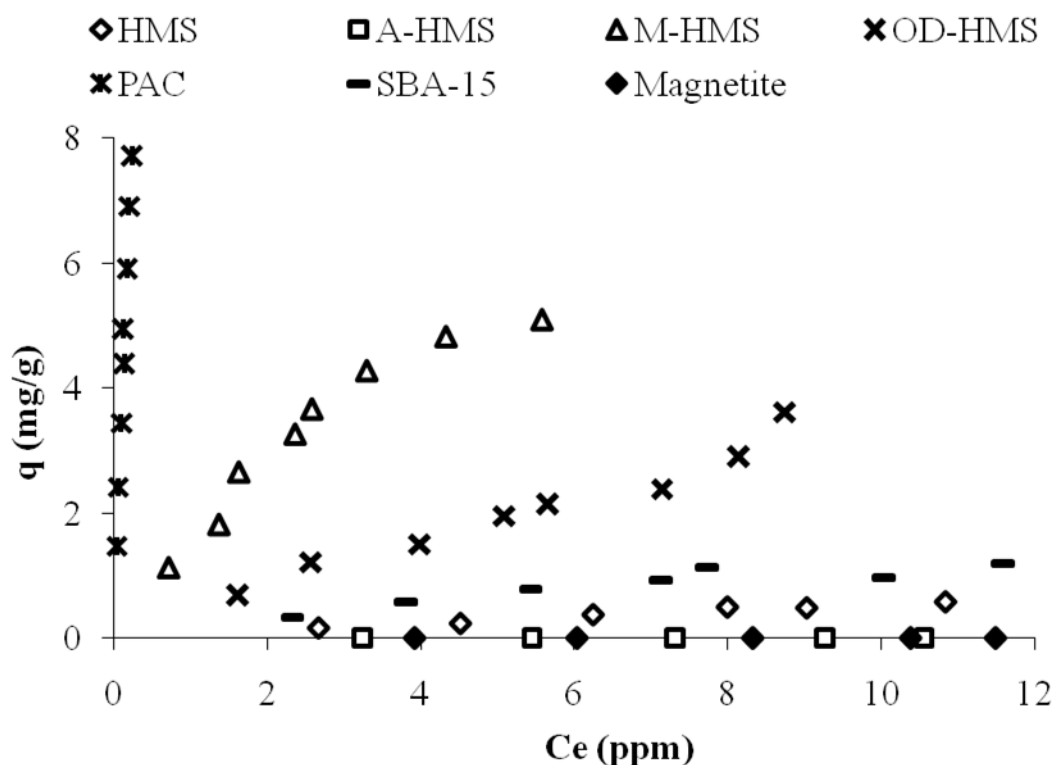


Figure 4.11 Adsorption capacities of CBZ on HMS, SF-HMS, PAC, SBA-15, and superparamagnetic magnetite at 25 ± 2 °C, $\text{pH } 7 \pm 2$, and 0.01 M ionic strength

From Figure 4.12, the adsorption capacities of adsorbents per square meter of specific surface area are shown. From Figure 4.12, PAC contained highest adsorption capacity compared to HMSs. M-HMS and OD-HMS provided relatively close capacity to each other likewise in case of CIP. Hence, the higher capacity of M-HMS than OD-HMS might cause from the difference of specific surface area. Moreover, SBA-15 and HMS provided the same relation with CIP, where the hydrogen bonds interaction between amide group and silanol groups causing the adsorption on these adsorbents.

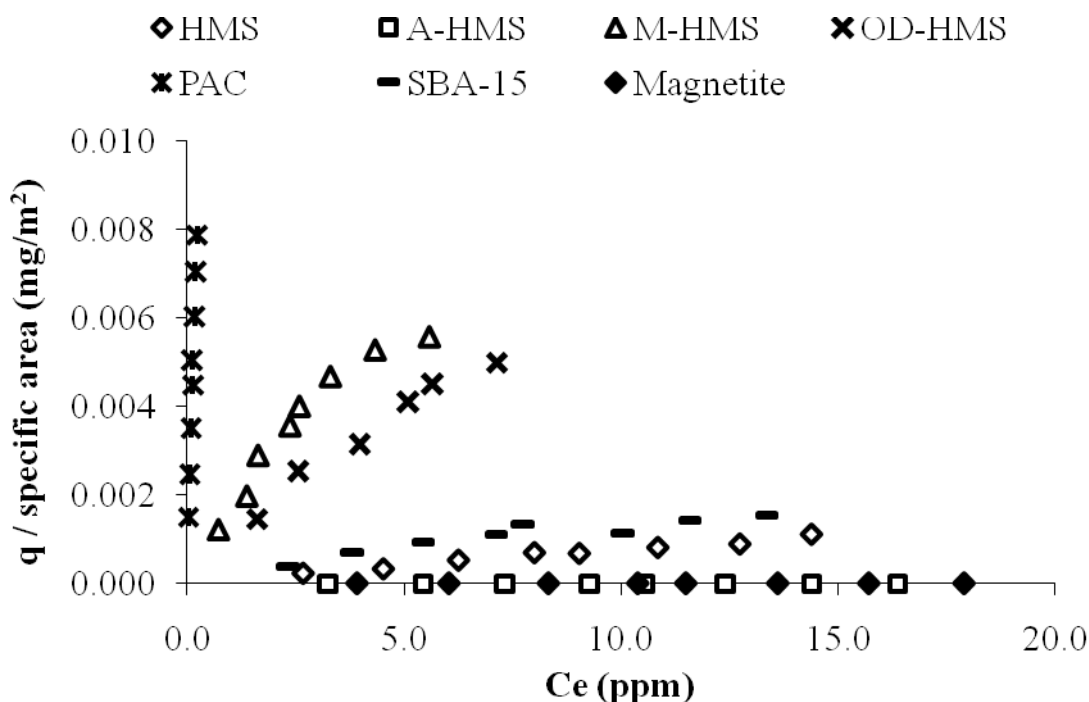


Figure 4.12 Adsorption capacities per specific surface area of CBZ on HMS, SF-HMS, PAC, SBA-15, and superparamagnetic magnetite at 25 ± 2 °C, pH 7 ± 2 , and 0.01 M ionic strength

4.3.2 Effect of surface functional groups density

Figure 4.13 showed the adsorption capacities of CIP on M-HMS, A-HMS, and BF-HMSs. It was found that M-HMS provided highest capacity among them following with A3M7. The capacities of A5M5 and A7M3 were in the same range, while A-HMS did not exhibit the adsorption capacity. These results might correspond to the molar ratios of amino- (N) and mercapto- (S) functional group. It can be noticed that increase of amino functional group ratio resulted in decrease of adsorption capacity; however, in case of A7M3, content of mercapto functional group was raised resulting in higher capacity as same as A5M5. Note that the carboxyl groups on CIP molecule can interact with mercapto group via hydrogen bonding with higher strength than that occur for amino group as mentioned above. From this part, it can be concluded that the content of amino and mercapto functional group affected the adsorption capacity of BF-HMSs. However, mercapto and amino surface functional groups density of all

functionalized HMS were calculated and concluded in Table 4.5. Figure 4.14 displayed the adsorption capacities of CIP on M-HMS, A-HMS, and BF-HMSs per square meter. It was found that M-HMS still provided highest capacity. Nevertheless, the capacity per area of A7M3 was relatively higher than that of A5M5 and A7M3, which quite different from Figure 4.13. Comparing with A3M7 and A5M5, it might be concluded that the presence of amino functional groups can inhibit the adsorption CIP on surface of adsorbents. In case of A-HMS and A7M3, although mercapto functional groups density of M-HMS was lower than A7M3, the adsorption capacity of M-HMS per square meter was still higher than A7M3 due to the presence of high amino functional groups density. From these obtained results, it can be concluded that the specific surface area and densities of surface functional group might play an important role in the adsorption of CIP on BF-HMSs.

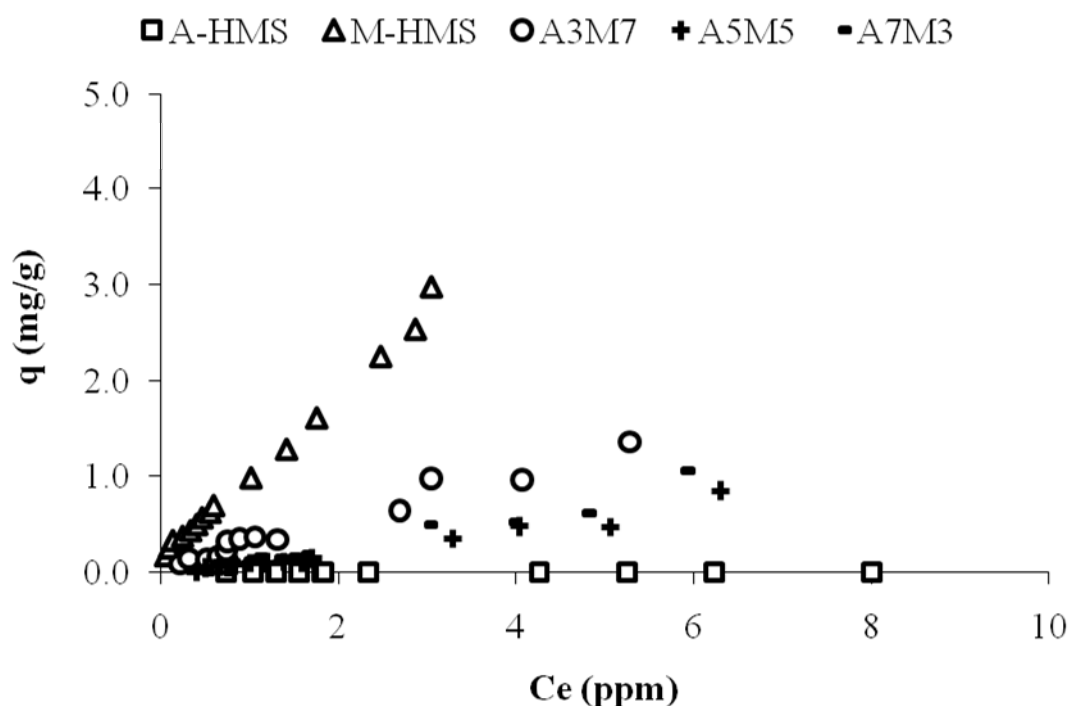
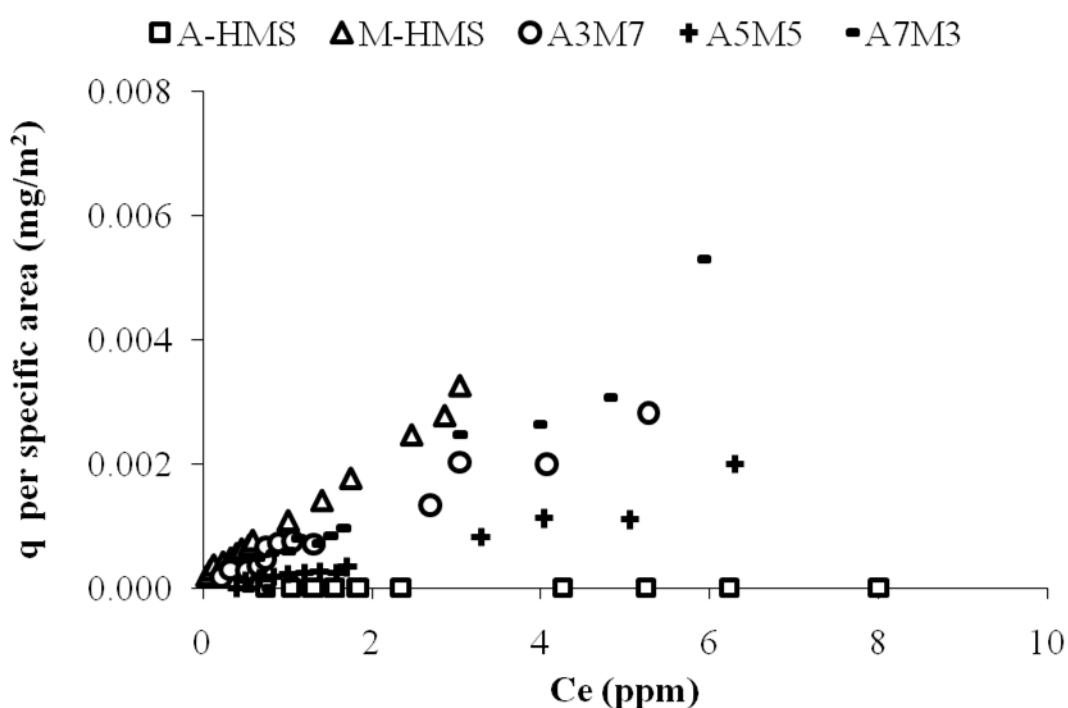


Figure 4.13 Adsorption capacities of CIP on M-HMS, A-HMS, and BF-HMSs at 25 ± 2 °C, $\text{pH } 7 \pm 2$, and 0.01 M ionic strength

Table 4.5 Densities of amino- and mercapto- functional group per area

Adsorbents	S ($\mu\text{mole}/\text{m}^2$)	N ($\mu\text{mole}/\text{m}^2$)
M-HMS	3.39	-
A3M7	4.58	0.90
A5M5	4.39	1.29
A7M3	5.38	4.65
A-HMS	-	3.84

**Figure 4.14** Adsorption capacities per specific surface area of CIP on M-HMS, A3M7, A5M5, A7M3, and A-HMS at 25 ± 2 °C, pH 7 ± 2 , and 0.01 M ionic strength

In case of CBZ adsorption, it was found that M-HMS still had highest adsorption capacity as can be seen in Figure 4.15. Nevertheless, BF-HMSs provided very slightly different capacities. As aforementioned that CBZ tend to be neutral at studied pH, electrostatic interaction might not be considered as the main mechanism. The van der Waals interaction caused by hydrophobic and hydrogen bonding between amide group of CBZ and functional groups of adsorbents may responsible for the adsorption mechanism. However, the strength of hydrogen bonding of amide group (NH_2) of

CBZ with mercapto- functional group of adsorbents might be higher than with amino group; therefore, BF-HMSs, which content relatively close of mercapto group content, resulted in insignificantly different of adsorption capacities.

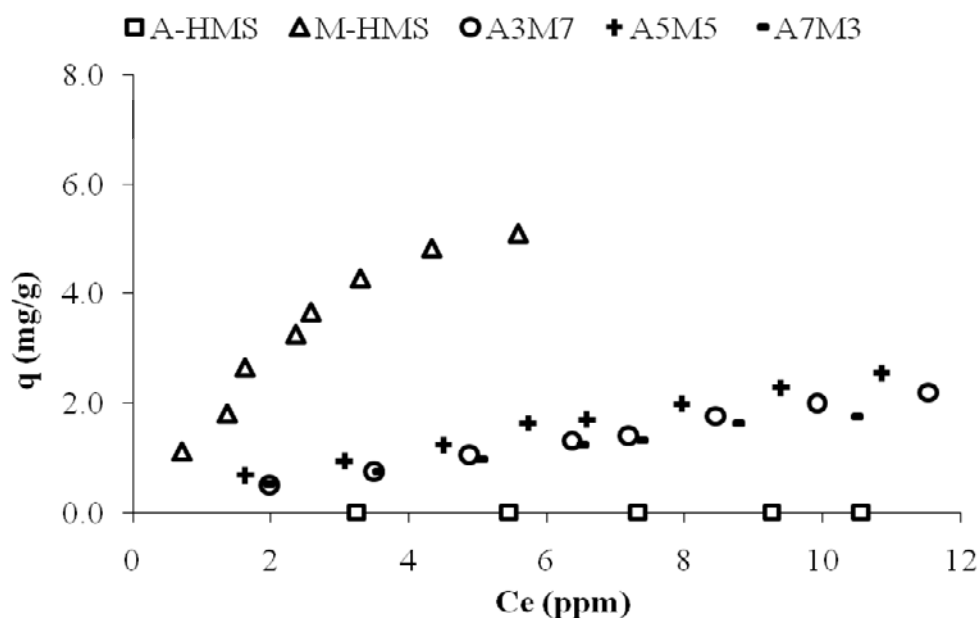


Figure 4.15 Adsorption capacities of CBZ on M-HMS, BF-HMSs, and A-HMS at 25 ± 2 °C, pH 7 ± 2 , and 0.01 M ionic strength

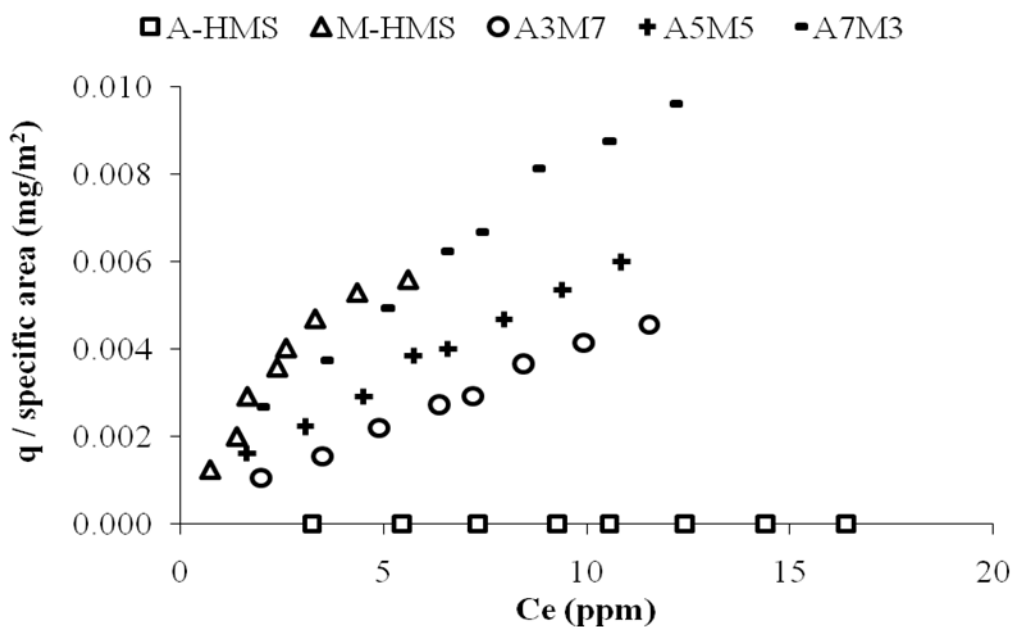


Figure 4.16 Adsorption capacities per specific surface area of CBZ on M-HMS, BF-HMSs, and A-HMS at 25 ± 2 °C, pH 7 ± 2 , and 0.01 M ionic strength

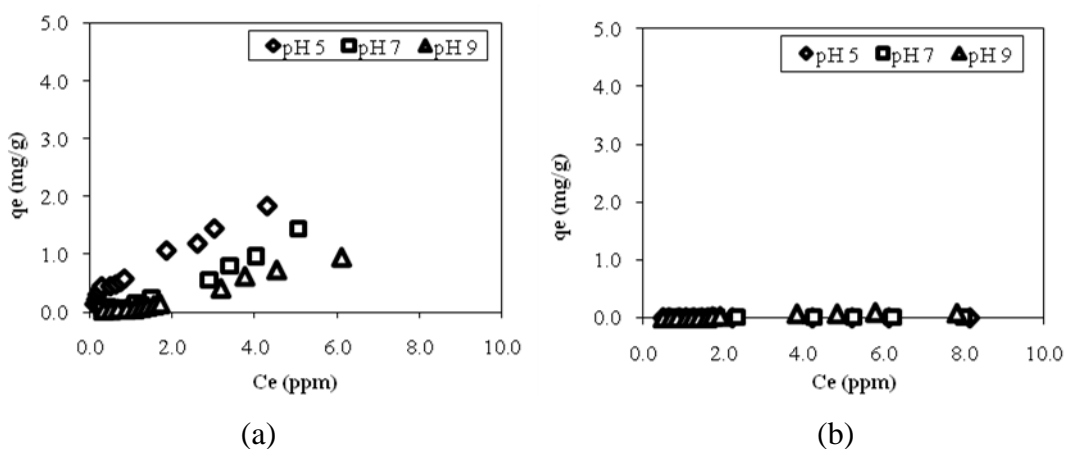
Figure 4.16 illustrated the adsorption capacities per surface area of M-HMS, A-HMS, and BF-HMSs. It can be noticed that capacity per surface area of A7M3 was comparatively close to that of M-HMS. This might be the result of mercapto-functional group content of A7M3 per area, which was highest among the mercapto-containing adsorbents. However, the presence of amino functional groups on functionalized surface might affect to adsorption capacities as same as adsorption of CIP which discussed above. Therefore, it can be concluded that adsorption capacity of CBZ by the BF-HMSs was mainly governed by the content of mercapto-functional group, which can have hydrogen bonding interaction together.

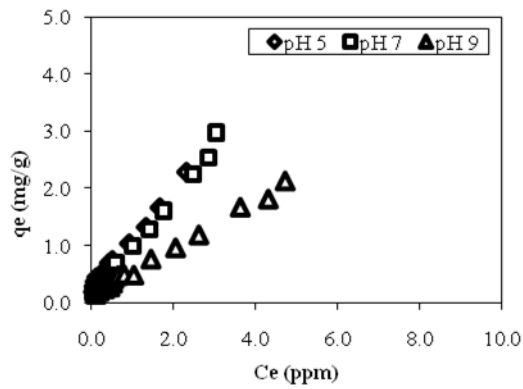
4.4 Adsorption Mechanisms

In order to investigate adsorption mechanism of CIP and CBZ, the effect of pH on adsorption capacity of adsorbents were evaluated and discussed as following.

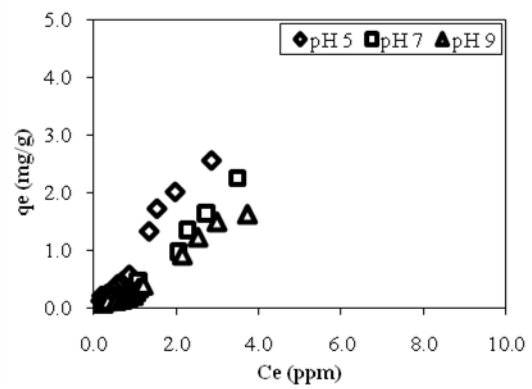
4.4.1 Effect of pH

For comprehending the importance of electrostatic interaction between target compounds and adsorbents, the effect of pH on the adsorption capacity of HMS, SF-HMSs, BF-HMSs, PAC, SBA-15, and magnetite were determined by varying pH of solution to 5, 7, and 9 with 0.01 M, controlled by phosphate buffer.

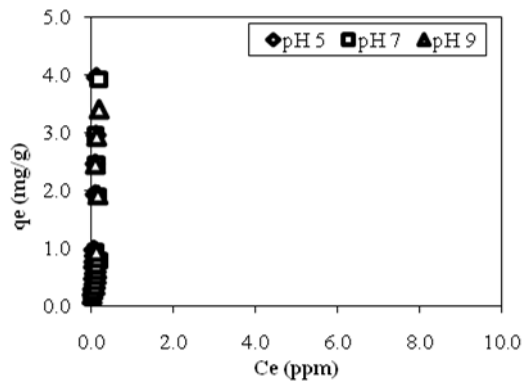




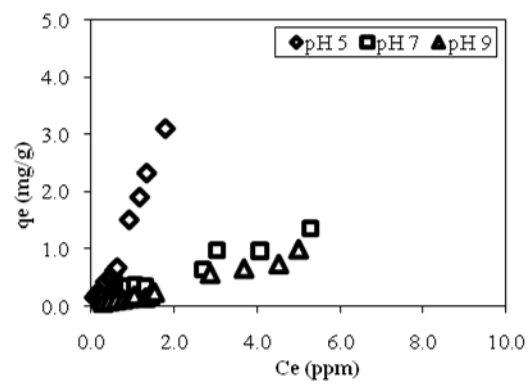
(c)



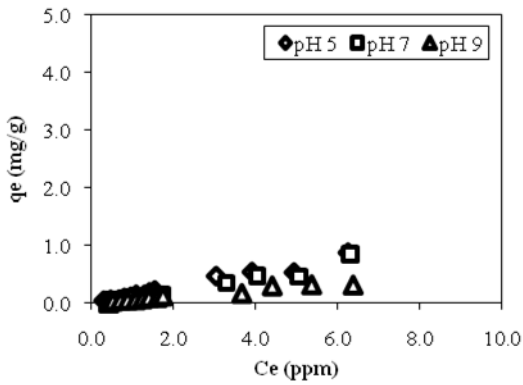
(d)



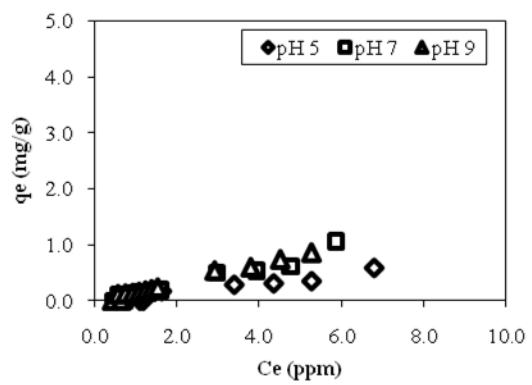
(e)



(f)



(g)



(h)

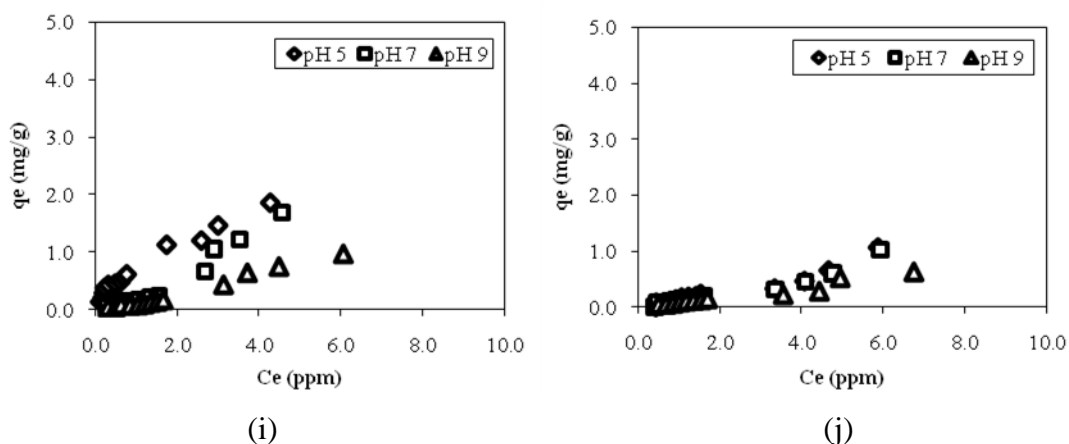
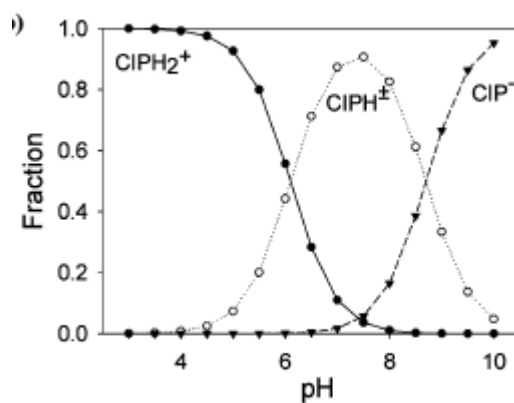


Figure 4.17 Adsorption capacities of CIP on (a) HMS; (b) A-HMS; (c) M-HMS; (d) OD-HMS; (e) PAC; (f) A3M7; (g) A5M5; (h) A7M3; (i) SBA-15; and (j) superparamagnetic magnetite at 25 ± 2 °C and 0.01 M ionic strength

In the studied pH range, CIP provided different types of charge depending on the pH value. The varying of surface charge to pH of solution was illustrated in Figure 2.3 (b) as displayed below (Gu and Karthikeyan, 2005).



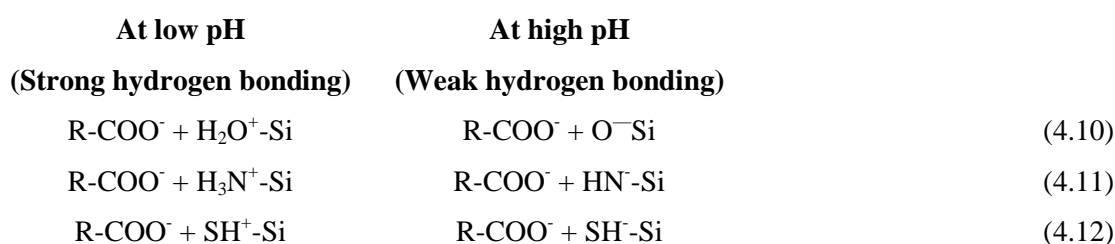
A pH varying also resulted in changing of charge type in adsorbents. The type of charge was dependent on pH_{zpc} of each adsorbent as mentioned before. Types of charge at pH 5, 7, and 9 are summarized in Table 4.6.

Table 4.6 Charge types of studied adsorbents at different pH

Adsorbents	pH _{zpc}	Surface charge		
		pH 5	pH 7	pH 9
HMS	5.5	+	-	-
A-HMS	9.5	+	+	+
M-HMS	6.2	+	-	-
OD-HMS	4.4	-	-	-
PAC	9.5	+	+	+
A3M7	6.7	+	-	-
A5M5	8.6	+	+	-
A7M3	8.3	+	+	-
SBA-15	4.0	-	-	-
Magnetite	7.8	+	+	-

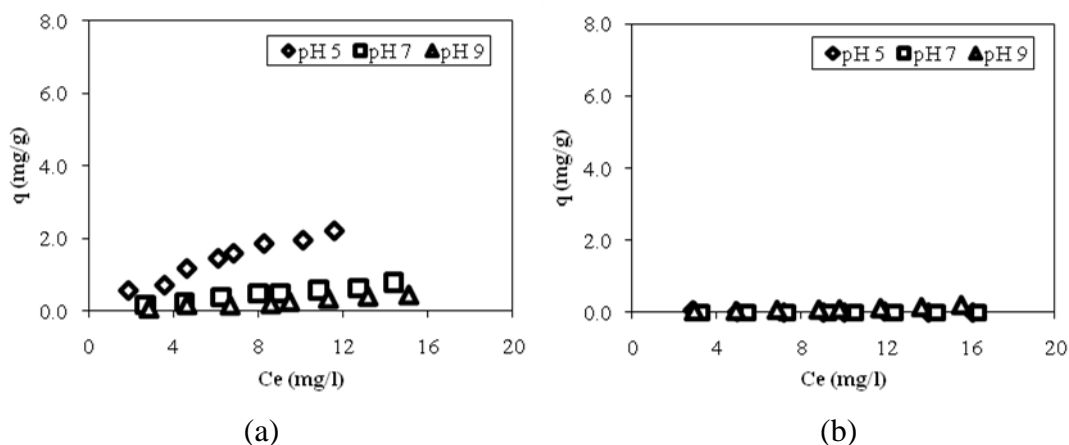
Figure 4.17 (a-j) shows the adsorption capacities of studied adsorbent at varying pH for 5, 7, and 9. It can be firstly seen that the capacities were affected by pH change, except for A-HMS and PAC. Figure 4.17 (a) displays adsorption capacities of HMS at different pH values. It was found that HMS contained weak positive charge at pH 5 that was the same charge type with CIP. The electrostatic repulsion might occur between positive charges in this case as well as at pH 9, where both HMS and CIP were negatively charged. At pH 7, HMS contained negative charge while CIP was in neutral form. The electrostatic attraction between HMS and CIP might happen in this case resulting to enhance the adsorption capacity. However, the results as shown in Figure 4.17 (a) were contrast. The highest adsorption capacity between HMS and CIP occur at pH 5 following by pH 7 and 9. Therefore, it can be concluded from this case that the electrostatic interaction might not affect the adsorption capacity of CIP on HMS. As same as HMS, adsorption capacities of other adsorbents including M-HMS, OD-HMS, A3M7, A5M5, A7M3, SBA-15, and magnetite, can be defined for the same electrostatic interaction impacts by pH varying by means of no electrostatic interaction. It should be noticed that HMS and SBA-15, which contained the same functional group: silanol provided the same trend of adsorption capacity for varied pH. In case of PAC, the adsorption capacity of CIP on PAC was not affected by changing of pH value as can be seen from Figure 4.17 (e), which can be concluded

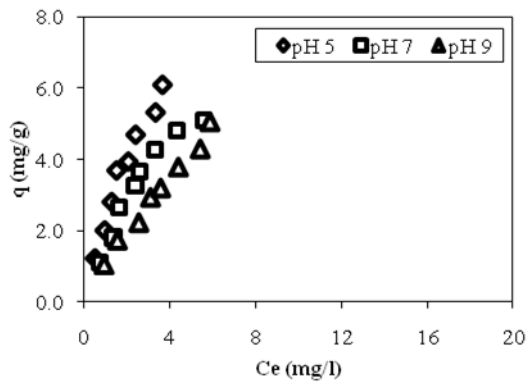
that the electrostatic interaction might not play the important role in this case as well. The main adsorption mechanism might be hydrogen bonding between CIP and adsorbents (i.e. silanol, mercapto, and amino group on synthesized HMSs and Fe-OH on superparamagnetic magnetite), which was weaker at high pH since the increasing of pH might affect to the carboxylic group of CIP (Breda *et al.*, 2009) resulting in decreasing of hydrogen bonding between CIP and surface functional group of adsorbents as displayed in Equation 4.10 – 4.12.



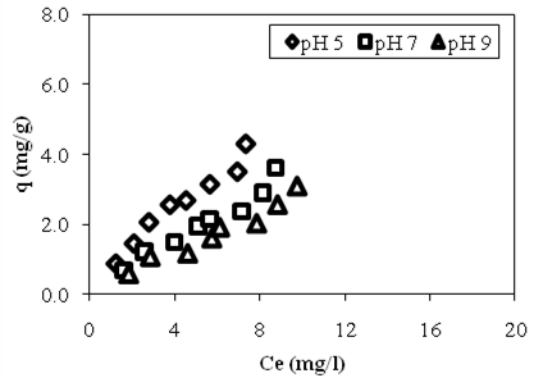
In case of A-HMS, charge density surface can be ionized to be positive at pH around 9; where CIP contained negatively charged, but the effect of attractive interaction between positive surface and negative molecule of CIP still cannot be detect significantly.

For BF-HMSs, the effects of pH value could be defined by the mechanisms occurred to the mercapto and amino-functional group presented on their surface. Van der Waals interaction and Hydrogen bonding might be the main mechanisms as mentioned.

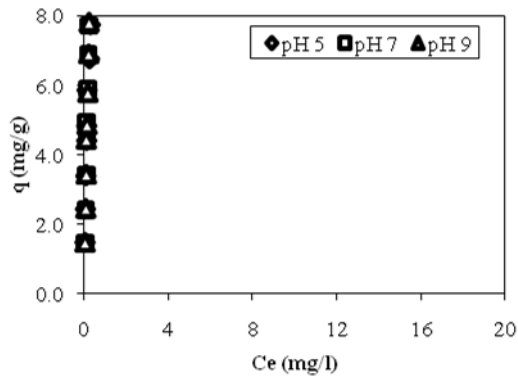




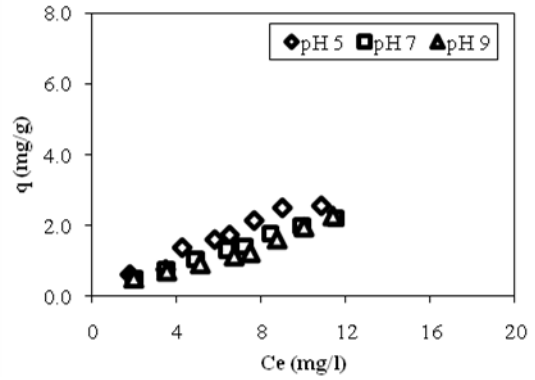
(c)



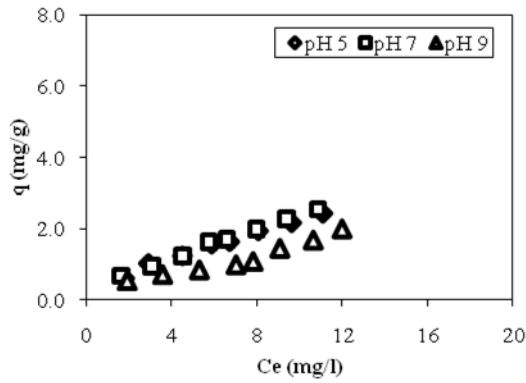
(d)



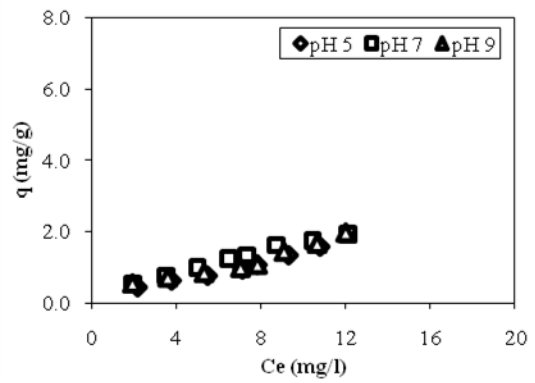
(e)



(f)



(g)



(h)

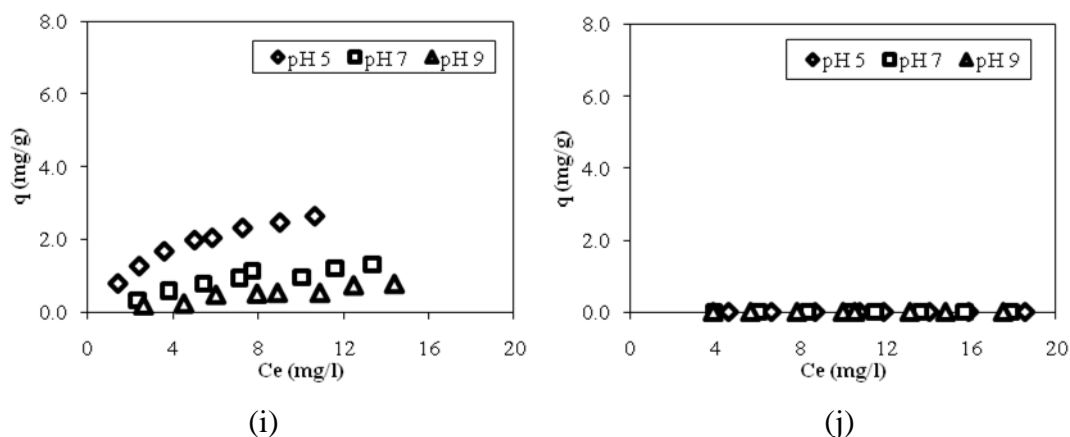


Figure 4.18 Adsorption capacities of CBZ on (a) HMS; (b) A-HMS; (c) M-HMS; (d) OD-HMS; (e) PAC; (f) A3M7; (g) A5M5; (h) A7M3; (i) SBA-15; and (j) superparamagnetic magnetite at 25 ± 2 °C and 0.01 M ionic strength

Figure 4.18 (a-j) illustrated adsorption capacities of CBZ at different pH for adsorbents used in this study. The structure molecule of CBZ was neutral in the studied pH range; hence, electrostatic interaction might not influence the adsorption capacity. From Figure 4.18 (e), it was also found that adsorption capacity of PAC was not impacted by the varying of pH as well as CIP. The adsorption capacities of CBZ on HMS, M-HMS, OD-HMS, A3M7, and SBA-15 provided the similar trend with those of CIP, where the highest capacities were found at pH 5, comparing to pH 7 and 9. The strength of hydrogen bonding at different pH might be responsible for the results. However, A-HMS and superparamagnetic magnetite did not perform the adsorption of CBZ in studied pH range. For BF-HMSs, the difference of adsorption capacities by altering pH values cannot be obviously seen. This might be the results of hydrogen bonding between CBZ structure and functional groups on adsorbents, which was not significantly affected by changing of pH in the studied range. Comparing to other study, adsorption capacity of SBA-15 was high at pH 5 and low at pH 9. This result had a correspondence with Bui and Choi (2009), where the high adsorption capacity was obtained at low pH range.

The results of adsorption capacities of applied adsorbents at pH 5, 7, and 9 were fitted with linear, Langmuir, and Freundlich isotherm model by linear regression in order to

describe the adsorption mechanism occurred in this study. It was found that the obtained experimental data had no relationship with Freundlich isotherm. On the other hand, linear and Langmuir isotherm can be fitted to the results with very high correlation coefficients. The linear regression data fitted with linear and Langmuir isotherm model for CIP and CBZ adsorption were summarized in Table 4.7 and Table 4.8, respectively. Hence, it can be concluded that the adsorption phenomena of CIP and CBZ on all studied adsorbents were dependent on concentration of the targeted pollutants.

Table 4.7 Parameters of Langmuir and linear isotherm model for CIP adsorption on applied adsorbents

Adsorbent pH	Langmuir			Linear	
	q_m	B	R^2	a (slope)	R^2
HMS					
5	2.044	0.648	0.908	0.476	0.873
7	1.601	0.079	0.842	0.232	0.902
9	1.092	0.074	0.912	0.145	0.930
A-HMS					
5	N/A	N/A	N/A	N/A	N/A
7	N/A	N/A	N/A	N/A	N/A
9	N/A	N/A	N/A	N/A	N/A
M-HMS					
5	1.200	5.910	0.923	1.008	0.946
7	1.184	3.163	0.916	0.941	0.979
9	1.151	1.031	0.929	0.452	0.976
OD-HMS					
5	5.978	0.133	0.907	0.924	0.953
7	2.872	0.136	0.929	0.556	0.927
9	2.164	0.149	0.907	0.432	0.939
PAC					
5	3.370	5.634	0.835	24.768	0.731
7	2.993	3.095	0.723	12.207	0.297
9	2.493	3.809	0.774	11.334	0.376
A3M7					
5	1.630	1.200	0.917	1.600	0.952
7	1.349	0.313	0.924	0.265	0.953
9	1.124	0.169	0.966	0.178	0.970

Adsorbent pH	Langmuir			Linear	
	q_m	B	R^2	a (slope)	R^2
A5M5					
5	1.650	0.081	0.932	1.396	0.969
7	1.536	0.064	0.964	0.113	0.938
9	1.237	0.053	0.982	0.055	0.950
A7M3					
5	1.496	0.072	0.943	0.078	0.901
7	1.630	0.095	0.926	0.151	0.935
9	1.796	0.101	0.938	0.160	0.977
SBA-15					
5	2.187	0.620	0.944	0.488	0.843
7	2.029	0.102	0.952	0.314	0.895
9	1.555	0.062	0.915	0.150	0.946
Magnetite					
5	1.464	0.115	0.954	0.146	0.913
7	1.444	0.097	0.937	0.136	0.912
9	1.416	0.066	0.969	0.087	0.930

Table 4.8 Parameters of Langmuir and linear isotherm model for CBZ adsorption on applied adsorbents

Adsorbent pH	Langmuir			Linear	
	q_m	b	R^2	a (slope)	R^2
HMS					
5	4.410	0.075	0.922	0.211	0.963
7	3.913	0.016	0.983	0.055	0.966
9	3.629	0.009	0.932	0.031	0.905
A-HMS					
5	N/A	N/A	N/A	N/A	N/A
7	N/A	N/A	N/A	N/A	N/A
9	N/A	N/A	N/A	N/A	N/A
M-HMS					
5	18.242	0.138	0.989	1.775	0.954
7	15.711	0.107	0.982	1.116	0.899
9	12.422	0.099	0.992	0.857	0.972
OD-HMS					
5	15.000	0.051	0.992	0.579	0.963
7	12.549	0.037	0.984	0.378	0.978
9	11.580	0.030	0.958	0.296	0.976

Adsorbent	Langmuir			Linear		
	pH	q_m	b	R^2	a (slope)	R^2
PAC						
5	55.426	0.762	0.975	31.346	0.868	
7	51.615	0.777	0.986	34.831	0.964	
9	52.083	0.767	0.971	35.207	0.960	
A3M7						
5	6.640	0.054	0.897	0.266	0.930	
7	5.957	0.045	0.988	0.202	0.962	
9	3.645	0.080	0.949	0.191	0.968	
A5M5						
5	5.048	0.078	0.988	N/A	N/A	
7	3.796	0.127	0.965	N/A	N/A	
9	2.199	0.152	0.892	N/A	N/A	
A7M3						
5	2.898	0.078	0.966	0.140	0.953	
7	3.258	0.097	0.978	0.177	0.940	
9	2.199	0.152	0.892	0.159	0.932	
SBA-15						
5	4.375	0.159	0.994	0.306	0.899	
7	4.128	0.039	0.970	0.111	0.824	
9	3.434	0.020	0.930	0.058	0.938	
Magnetite						
5	N/A	N/A	N/A	N/A	N/A	
7	N/A	N/A	N/A	N/A	N/A	
9	N/A	N/A	N/A	N/A	N/A	

CHAPTER V

CONCLUSION AND RECOMMENDATIONS

5.1 Conclusion

The main objectives of this study are to evaluate the possibility of using mesoporous silicates involve HMS, Functionalized HMS (such as single and bi functionalized HMS), SBA-15 and superparamagnetic magnetite (Fe_3O_4) for removal of pharmaceutical residues by adsorption process. The pharmaceutical residues used in this study are ciprofloxacin (CIP) and carbamazepine (CBZ) and their adsorption capacities of ciprofloxacin (CIP) and carbamazepine (CBZ) on all synthesized mesoporous silicates and superparamagnetic magnetite (Fe_3O_4) were compared with powdered activated carbon (PAC) in aqueous phase of each batch condition. Physico-chemical characteristics of these materials were determined and the effects of pH on adsorption phenomena were involved in this study.

From the investigation, functional group modification by co-condensation method caused crystalline structure was lost comparing with pristine HMS. The synthesized HMSs and SBA-15 had their average pore size in the range 2-50 nm which fell in the mesoporous structure category.

The results of kinetic study at pH 7 ± 0.2 were found that the adsorption of CIP and CBZ achieved the saturation stage at 9 hr for synthesized HMSs and PAC; which was longer than that of SBA-15 and superparamagnetic magnetite with 3 hr.

From adsorption isotherm study, it was found that the highest adsorption capacities of CIP and CBZ were obtained from M-HMS; however, its capacity was still lower than PAC. Specific surface area and densities of surface functional group might play an

important role in the adsorption of CIP and CBZ on BF-HMSs. Hydrophobicity and Hydrogen bonding played a key role on the adsorption mechanisms, while the electrostatic interaction might not affect the adsorption capacity. Moreover, the effects of pH on adsorption capacities were determined and found that the capacities was increased at low pH value (pH=5) and lower at high pH (pH=9), which might be the effect of hydrogen bonding strength occurred in each pH value.

5.2 Recommendations

- 5.2.1 Study the effect of selectivity between ciprofloxacin and carbamazepine as well as other pharmaceutical substances on adsorption capacity of HMSs, SBA-15 and superparamagnetic magnetite.
- 5.2.2 Study the effect of coexisting compounds in real pharmaceutical contaminated wastewater onto adsorption capacity of both ciprofloxacin and carbamazepine.
- 5.2.3 Study other factors that might be involved the adsorption capacity; for example, ionic strength and temperature onto adsorption capacity of both ciprofloxacin and carbamazepine.

REFERENCES

- Afkhami, A., Moosavi, R. 2010. Adsorptive removal of Congo red, a carcinogenic textile dye, from aqueous solutions by maghemite nanoparticles. Journal of Hazardous Materials. 174 : 398-403.
- Andreozzi, R., Raffaele, M., and Nicklas, P. 2003. Pharmaceuticals in STP effluents and their solar photodegradation in aquatic environment. Chemosphere. 50 (10) : 1319-1330.
- Beck, J.S., and Vartuli, J. C. 1996. Recent advances in the synthesis, characterization and applications of mesoporous molecular sieves. Current Science. 1: 76-87.
- Bertschy, G., Bryois, Ch., Bondolfi, G., Velardi, A., Burdy, Ph., Dascal, D., Martinet, C., Baetting, D., and Baumann, P. 1997. The Association Carbamazepine-Mianserin in opiate withdrawal: A Double Blind Pilot Study Versus Clonidine. Pharmacological Research. 35 (5) : 451-456.
- Boxall, A.B.A. 2004. The environmental side effects of medication. Rev. Environ. Contam. Toxicol. 180 : 1.
- Brain, R.A., Johnson, D.J., Richards, S.M., Hanson, M.L., Sanderson, H., Lam, M.W., Young, C., Mabury, S.A., Sibley, P.K., and Solomin, K.R. 2004. Microcosm evaluation of the effects of an eight pharmaceutical mixture to the aquatic macrophytes *Lemna gibba* and *Myriophyllum sibiricum*. Aquatic Toxicology. 70 (1): 23-40.
- Brain, R.A., Johnson, D.J., Richards, S.M., Sanderson, H., Sibley, P.K., and Solomin, K.R. 2004. Effects of 25 pharmaceutical compounds to *Lemna gibba* using a seven-day static-renewal test. Environmental toxicology and chemistry. 23 (2): 371-382.
- Bruce, I.J., Taylor, J., Todd, M., Davies, M.J., Borioni, E., Sangregorio, C., and Sen, T. 2004. Synthesis, characterisation and application of silica-magnetite nanocomposites. Journal of Magnetism and Magnetic Materials. 284: 145-160.
- Bui, T.X. and Choi, H. 2009. Adsorptive removal of selected pharmaceuticals by mesoporous silica SBA-15. J. Hazard Mater. 168: 602-608.

- Carballa, M., Omil, F., and Lema, J.M. 2005. Removal of cosmetic ingredients and pharmaceuticals in sewage primary treatment. Water Research. 39 (19) : 4790-4796.
- CBSNews. Probe: Pharmaceuticals In Drinking Water. [Online]. 2008. Available from: <http://www.cbsnews.com/stories/2008/03/10/health/main392>. [2009, September 20].
- Chong, A.S.M., Zhao, X.S., and Lu, G.Q. 2004. Surface functionalization of ordered nanoporous silicates. Nanoporous materials- Science and Engineering, Imperial Coll. Press. p. 393-426.
- Comerton, A.M., Andrews, R.C., Bagley, D.M., and Hao, C. 2008. The rejection of endocrine disrupting and pharmaceutically active compounds by NF and RO membranes as a function of compound and water matrix properties. Journal of Membrane Science. 313 (1-2): p. 323-335.
- Cordova-Kreylos, A.L. and Scow, K.M. 2007. Effects of ciprofloxacin on salt marsh sediment microbial communities. ISME J. 1(7) : 585-595.
- Diwan, V., Tamhankar, A.J., Aggrawal, M., Sen, S., Khandal, R. K., Lundborg, C. S. 2009. Detection of antibiotics in hospital effluents in India. Current Science J. 97 (12) : 1752-1755.
- Drewes, J.E., Heberer, T., Redderson, K. 2002. Fate of pharmaceuticals during indirect potable reused. Water Sci. Technol. 46 :73-80.
- Duong, H.A., Pham, N.H., Nguyen, H.T., Hoang, T.T., Pham, H.V., Pham, V.C., Berg, M., Giger, W., and Alder, A.C. 2008. Occurrence, fate and antibiotic resistance of fluoroquinolone antibacterials in hospital wastewaters in Hanoi, Vietnam. Chemosphere. 72(6) : 968-973.
- Durdureanu-Angheluta, A., Ardeleanu, R., Pinteala, M., Harabagiu, V., Chiriac, H., and Simionescu, B.C. 2008. Silane covered magnetite particles preparation and characterization. Digest Journal of Nanomaterials and Biostructures. 3 (1): 33-40.
- Eckel, W.P., Ross, B., and Isensee, R.K. 1993. Pentobarbital found in ground water. Ground water. 31(5): 801-804.
- Fent, K., Weston, A.A., and Caminada, D. 2006. Ecotoxicology of human pharmaceuticals. Aquatic Toxicology. 76(2) : 122-159.

- Giger, W., Alder, A.C., Golet, E.M., Kohler, H.E., Mcardell, C.S., Molinar E., Siegrist, H., and Suter M.J.-F. 2003. Occurrence and Fate of Antibiotics as Trace Contaminants in Wastewaters, Sewage Sludges, and Surface Waters. CHIMIA International Journal for Chemistry. 57: 485-491.
- Golet, E.M., Alder, A., Hartmann, A., Ternes, T.A., and Giger, W. 2001. Trace Determination of Fluoroquinolone Antibacterial Agents in Urban Wastewater by Solid-Phase Extraction and Liquid Chromatography with Fluorescence Detection. Analytical Chemistry. 73(15): 3632-3638.
- Gu, C. and Karthikeyan, K.G. 2005. Sorption of the Antimicrobial Ciprofloxacin To Aluminum and Iron Hydrous Oxides. Environmental Science & Technology. 39(23) : 9166-9173.
- Gupta, A.K. and Gupta, M. 2005. Synthesis and surface engineering of iron oxide nanoparticles for biomedical applications. Biomaterials. 26(18): 3995-4021.
- Halling-Sørensen, B., Holten Lutzhoft, H.-C., Andersen, H.R., and Ingerslev, F. 2000. Environmental risk assessment of antibiotics: comparison of mecillinam, trimethoprim and ciprofloxacin. J Antimicrob Chemother. 46: 53-58.
- Hartmann, A., Golet, E.M., Gartsler, S., Alder, A.C., Koller, T., and Widmer, R.M. 1999. Primary DNA Damage But Not Mutagenicity Correlates with Ciprofloxacin Concentrations in German Hospital Wastewaters. Archives of Environmental Contamination and Toxicology. 36(2): 115-119.
- Heberer, T., Reddersen, K., and Mechlinski, A. 2002. From municipal sewage to drinking water: fate and removal of pharmaceutical residues in the aquatic environment in urban areas. Water Science and Technology. 46(3): 81-88.
- Hektoen, H., Berge, J.A., Hormazabal, V., and Yndestad, M. 1995. Persistence of antibacterial agents in marine sediments. Aquaculture. 133(3): 175-184.
- Ho, Y.-S. 2006. Review of second-order models for adsorption systems. Journal of Hazardous Materials. 136(3): 681-689.
- Holm, J.V., Rugge, K., Bjerg, P.L., and Christensen, T.H. 1995. Occurrence and distribution of pharmaceutical organic compounds in the groundwater downgradient of a landfill. Environ. Sci. Technol. 29: 1415-1420.

- Hu, J., Chen, G., and Lo, I.M.C. 2006. Selective Removal of Heavy Metals from Industrial Wastewater Using Maghemite Nanoparticle: Performance and Mechanisms. Journal of Environmental Engineering. 132(7) : 709-715.
- Imperor-Clerc, M., Davidson, P., and Davidson A. 2000. Existence of a Microporous Corona around the Mesopores of Silica-Based SBA-15 Materials Templated by Triblock Copolymers. Journal of the American Chemical Society. 122(48): 11925-11933.
- Jolivet, J.-P., Tronc, É., and Chanéac, C. 2002. Synthesis of iron oxide-based magnetic nanomaterials and composites. Comptes Rendus Chimie. 5(10): 659-664.
- Kim, D.H., Lee, S.H., Im, K.H., Kim K.M., Shim, I.B., Lee, M.H., and Lee, Y.K. 2006. Surface-modified magnetite nanoparticles for hyperthermia: Preparation, characterization, and cytotoxicity studies. Current Applied Physics: 681: e242-e246.
- Kim, Y., Choi, K., Jung, J., Park, S., Kim, P.G., and Park, J. 2007. Aquatic toxicity of acetaminophen, carbamazepine, cimetidine, diltiazem and six major sulfonamides, and their potential ecological risks in Korea. Environment International. 33(3): 370-375.
- Larsson, D.G.J., de Pedro, C., and Paxeus, N. 2007. Effluent from drug manufactures contains extremely high levels of pharmaceuticals. Journal of Hazardous Materials. 148(3): 751-755.
- Lee, B.H., Kim, Y.H., Lee, H.J., and Yi, J.H. 2001. Synthesis of functionalized porous silicas via templating method as heavy metal ion adsorbents: the introduction of surface hydrophilicity onto the surface of adsorbents. Microporous Mesoporous Mater. 50 (1): 77-90.
- Liu, X., Ma, Z., Xing, J., and Liu, H. 2004. Preparation and characterization of amino-silane modified superparamagnetic silica nanospheres. Journal of Magnetism and Magnetic Materials. 270: 1-6.
- Ma, Z. and Liu, H. 2007. Synthesis and surface modification of magnetic particles for application in biotechnology and biomedicine. China Particuology. 5(1-2): 1-10.

- Mestre, A.S., Pires, J., Nogueira, J.M.F., and Carvalho, A.P. 2007. Activated carbons for the adsorption of ibuprofen. Carbon. 45(10) : 1979-1988.
- Miao, X.-S., Bishay, F., Chen, M., and Metcalfe, C.D. 2004. Occurrence of Antimicrobials in the Final Effluents of Wastewater Treatment Plants in Canada. Environmental Science & Technology. 38(13): 3533-3541.
- Mompelat, S., Le Bot, B., and Thomas, O. 2009. Occurrence and fate of pharmaceutical products and by-products, from resource to drinking water. Environment International. 35(5): 803-814.
- Montgomery, S.A., Schatzberg, A.F., Guelfi, J.D., Nemeroff, C., Swann, A., and Zaiecka, J. 2000. Pharmacotherapy of depression and mixed states in bipolar disorder. Journal of Affective Disorders. 59(1): S39-S56.
- Musson, S.E. and Townsend, T.G. 2009. Pharmaceutical compound content of municipal solid waste. Journal of Hazardous Materials. 162(2-3): 730-735.
- Nakata, H., Kannan, K., Jones, P.D., and Giesy, J.P. 2005. Determination of fluoroquinolone antibiotics in wastewater effluents by liquid chromatography-mass spectrometry and fluorescence detection. Chemosphere. 58(6): 759-766.
- Oetken, M., Nentwig, G., Löffler, D., Ternes, T., and Oehlmann, J. 2005. Effects of Pharmaceuticals on Aquatic Invertebrates. Part I. The Antiepileptic Drug Carbamazepine. Archives of Environmental Contamination and Toxicology. 49(3): 353-361.
- Ort, C., Lawrence, M.G., Reungoat, J., Eaglesham, G., Carter, S., and Keller, J. **In Press**. Determining the fraction of pharmaceutical residues in wastewater originating from a hospital. Water Research. **Corrected Proof**.
- Pe´rez-Quintanilla, del Hierro, I., Fajardo, M., and Sierra, I. 2006. Mesoporous silica functionalized with 2-mercaptopyridine: Synthesis, characterization and employment for Hg(II) adsorption. Microporous and Mesoporous Materials. 89: 58–68.
- Per-ake, J., Ottoson, J., Lindberg, R., Stenstrom, T., Johansson, M., Tysklind, M., Winner, M., and Olsen, B. 2004. Fluoroquinolone Antibiotics in a Hospital Sewage Line; Occurrence, Distribution and Impact on Bacterial Resistance. Scandinavian Journal of Infectious Diseases. 36: 752-755.

- Punyapalukul, P. 2004. Removal of alkylphenol polyethoxyates using hexagonal mesoporous silicates, Doctoral dissertation. Department of Urban Environment Graduate School of Engineering University of Tokyo.
- Punyapalukul, P., and Takizawa, S. 2004. Effect of organic grafting modification of hexagonal mesoporous silicate on haloacetic acid removal. Environ. Eng. Forum. 44: 247–256.
- Punyapalukul, P. and Takizawa, S. 2006. Selective adsorption of nonionic surfactant on hexagonal mesoporous silicates (HMSs) in the presence of ionic dyes. Water Research. 40(17): 3177-3184.
- Punyapalukul, P., Soonglerdsongpha, S., Kanlayaprasit, C., Ngamcharussrivichai, C., and Khaodhiar, S. 2009. Effects of crystalline structures and surface functional groups on the adsorption of haloacetic acids by inorganic materials. Journal of Hazardous Materials. 171(1-3) : 491-499.
- Putra, E.K., Pranowo, R., Sunarso, J., Indraswati, N., and Ismadji, S. 2009. Performance of activated carbon and bentonite for adsorption of amoxicillin from wastewater: Mechanisms, isotherms and kinetics. Water Research. 43(9): 2419-2430.
- Renew, J.E. and Huang, C.-H. 2004. Simultaneous determination of fluoroquinolone, sulfonamide, and trimethoprim antibiotics in wastewater using tandem solid phase extraction and liquid chromatography-electrospray mass spectrometry. Journal of Chromatography A. 1042(1-2): 113-121.
- Rouquerol, F., Rouquerol, J., and Sing, K. 1999. Adsorption by powder and porous solids: principles, Methodology and applications. London: Academic press.
- Sacher, F., Lange, F.T., Brauch, H.-J., and Blankenhorn, I. 2001. Pharmaceuticals in groundwaters: Analytical methods and results of a monitoring program in Baden-Württemberg, Germany. Journal of Chromatography A. 938(1-2): 199-210.
- Scheytt, T.J., Mersmann, P., and Heberer, T. 2006. Mobility of pharmaceuticals carbamazepine, diclofenac, ibuprofen, and propyphenazone in miscible-displacement experiments. Journal of Contaminant Hydrology. 83(1-2): 53-69.

- Sternebring, B., Liden, A., Andersson, K., and Melander, A. 1992. Carbamazepine kinetics and adverse effects during and after ethanol exposure in alcoholics and in healthy volunteers. European Journal of Clinical Pharmacology. 43(4): 393-397.
- Sukul, P. and Spiteller, M. 2007. Fluoroquinolone Antibiotics in the Environment. Reviews of Environmental Contamination and Toxicology. 191: 131-162.
- Sun, Y.K., Ma, M., Zhang, Y., and Gu, N. 2004. Synthesis of nanometer-size maghemite particles from magnetite. Colloids and Surfaces. 245: 15–19.
- Tanev, P.T. and Pinnavaia, T.J. 1996. Mesoporous Silica Molecular Sieves Prepared by Ionic and Neutral Surfactant Templating: A Comparison of Physical Properties. Chemistry of Materials. 8 (8): 2068-2079.
- Ternes, T. 2000. Pharmaceuticals and metabolites as contaminants of the aquatic environment. In Keith, L.H.N. et al. (eds.), An overview in Symposia Papers Presented before the division Environmental Chemistry American Chemistry Society. pp. 98-100. San Francisco.
- Ternes, T.A. 1998. Occurrence of drugs in German sewage treatment plants and rivers. Water Research. 32(11): 3245-3260.
- Tixier, C., Singer, H.P., Oellers, S., and Muller, S.R. 2003. Occurrence and Fate of Carbamazepine, Clofibric Acid, Diclofenac, Ibuprofen, Ketoprofen, and Naproxen in Surface Waters. Environmental Science & Technology. 37(6): 1061-1068.
- Wako Pure Chemical Industries. 2004. Material Safety Data Sheets " Carbamazepine". (Unpublished Manuscript).
- Wako Pure Chemical Industries. 2005. Material Safety Data Sheets " Ciprofloxacin Hydrochloride Monohydrate". (Unpublished Manuscript).
- Wang, C., Ao, Y., Wang, P., Qian, J., Hou, J., and Zhang, S. **In Press**. A simple method for preparation of superparamagnetic porous silica. Journal of Alloys and Compounds. **Corrected Proof**.
- Willis, B. Type of magnetisms Magnet maddness. [Online]. 2002. Available from: <http://www.worsleyschool.net/science/files/magnet/types/ofmagnetism.html> [2010, January 20].

- Wong, M.S., and Knowles, W.V. 2004. Surfactant-templated mesostructured materials: synthesis and compositional control. Nanoporous materials- Science and Engineering. In G.Q.a.Z. Lu, (ed.), pp. 897. London: Imperial Coll. Press.
- Woo, K. and Lee, H.J.H.J., 2004. Synthesis and magnetism of hematite and maghemite nanoparticles. Journal of Magnetism and Magnetic Materials, 2004. 272–276: e1155–e1156.
- Xu, X., Wang, J., Yang, C., Wu, H., and Tang, F. 2009. Sol-gel formation of [gamma]-Fe₂O₃/SiO₂ nanocomposites: Effects of different iron raw material. Journal of Alloys and Compounds. 468(1-2): 414-420.
- Yamamoto, H., Nakamura, Y., Moriguchi, S., Nakamura, Y., Honda, Y., Tamura, I., Hirata, Y., Hayashi, A., and Sekizawa, J. 2009. Persistence and partitioning of eight selected pharmaceuticals in the aquatic environment: Laboratory photolysis, biodegradation, and sorption experiments. Water Research. 43(2): 351-362.
- Yang, C., Jia, X., Cao, Y., and He, N. 2002. Effect of Functionalization Conditions on Loadings of Basic Functional Groups in Hexagonal Mesoporous Silica. 8th International Conference on Electronic Materials (IUMRS-ICEM 2002). Xi'an :China.
- Yuan, P., Liu, D., Fan, M., Yang, D., Zhu, R., Ge, F., Zhu, R., and He, H. 2010. Removal of Hexavalent Chromium (Cr (VI)) form aqueous solution by the diatomite-supported / unsupported magnetic nanoparticle. Journal of Hazardous Materials. 173: 614-621.
- Zuccato, E., Castiglioni, S., and Fanelli, R. 2005. Identification of the pharmaceuticals for human use contaminating the Italian aquatic environment. Journal of Hazardous Materials. 122(3): 205-209.
- Zurita, J.L., Repetto, G., Jos, A., Salguero, M., Lopez-Artiguez, M., and Camean, M. 2007. Toxicological effects of the lipid regulator gemfibrozil in four aquatic systems. Aquatic Toxicology. 81(1): 106-115.
- Zhang, Y., Gei□en, S-U., and Gal, C. 2008. Carbamazepine and diclofenac : Removal in wastewater treatment plant and occurrence in water bodies. Chemosphere. 73: 1151-1161.

APPENDICES

APPENDIX A

Characterization of physico-chemical properties of HMSs

Table A-1 Nitrogen content on HMSs

Adsorbents	Nitrogen content (mg)	Weight (g)	Overall nitrogen content (g/g)	% Nitrogen
A3M7	0.7329	0.1200	0.0061	0.6108
A5M5	0.9249	0.1200	0.0077	0.7708
A7M3	1.4310	0.1100	0.0130	1.3009
A-HMS	1.5531	0.1100	0.0141	1.4119

Table A-2 Nitrogen content on HMSs

Adsorbents	Nitrogen content (mg)	Weight (g)	Overall nitrogen content (g/g)	% Nitrogen
M-HMS	0.0105	0.1057	0.0992	9.9243
A3M7	0.0072	0.1008	0.0709	7.0933
A5M5	0.0064	0.1076	0.0599	5.9891
A7M3	0.0033	0.1015	0.0326	3.2640

Table A-3 Surface charge of PAC

Sample	pH	Surface charge (C/g)
1	9.78	-21.0795
2	9.63	-7.6424
3	9.51	-3.3454
4	9.47	-1.0167
5	9.38	1.1597
6	9.30	2.8946
7	9.21	4.6074
8	9.08	8.4962
9	8.30	19.7073

Table A-4 Surface charge of HMS

Sample	pH	Surface charge (C/g)
1	3.39	20.6894
2	3.60	8.8539
3	3.78	7.3326
4	4.06	2.1769
5	4.37	1.5538
6	4.99	-0.0495
7	5.42	-0.0857
8	5.97	-2.0218
9	6.70	-8.4018
10	7.24	-20.5957
11	8.23	-33.4557
12	8.56	-54.5800
13	8.94	-115.0719

Table A-5 Surface charge of A-HMS

Sample	pH	Surface charge (C/g)
1	9.67	-21.6759
2	9.60	-7.6125
3	9.58	-2.9676
4	9.57	-0.6363
5	9.53	1.6316
6	9.51	3.5461
7	9.50	5.3390
8	9.38	9.0818
9	9.38	19.9328

Table A-6 Surface charge of M-HMS

Sample	pH	Surface charge (C/g)
1	8.63	-24.0164
2	7.56	-9.5771
3	7.01	-4.7963
4	6.62	-2.3749
5	6.14	-0.0338
6	4.96	1.4146
7	4.40	1.9738
8	3.97	2.5858
9	3.45	2.3544

Table A-7 Surface charge of OD-HMS

Sample	pH	Surface charge (C/g)
1	8.75	-21.0023
2	7.42	-9.3215
3	6.96	-8.7532
4	6.54	-7.3215
5	5.83	-2.1132
6	4.76	-0.0321
7	4.31	1.9758
8	3.88	2.5953
9	3.21	3.0154

Table A-8 Surface charge of A3M7

Sample	pH	Surface charge (C/g)
1	8.56	-24.2884
2	7.85	-9.4485
3	7.39	-4.7962
4	7.09	-2.4298
5	6.77	-0.0053
6	6.62	1.9320
7	6.41	3.8733
8	6.21	7.7682
9	5.13	18.834

Table A-9 Surface charge of A5M5

Sample	pH	Surface charge (C/g)
1	9.37	-23.4226
2	9.17	-8.9258
3	9.11	-4.3742
4	9.09	-1.8768
5	9.03	0.5108
6	8.90	2.3656
7	8.81	4.2612
8	8.87	8.1223
9	8.57	19.7511

Table A-10 Surface charge of A7M3

Sample	pH	Surface charge (C/g)
1	8.76	-23.7093
2	8.52	-9.4174
3	8.37	-4.7039
4	8.38	-2.3164
5	8.30	0.0938
6	8.25	2.0308
7	8.18	3.9713
8	8.08	7.8548
9	7.68	19.3987

APPENDIX B

Adsorption kinetic and isotherm results

Table B-1 Kinetic study results of CIP on HMS, SF-HMSs, and PAC for 6 mg/l initial concentration

Time (min)	Ce (mg/l)				
	HMS	A-HMS	M-HMS	OD-HMS	PAC
0	5.99	5.99	5.99	5.99	5.99
30	2.48	5.66	1.51	2.10	0.18
60	2.39	5.55	0.80	1.76	0.07
120	2.20	5.63	0.97	1.50	0.15
210	2.08	5.50	0.82	1.30	0.14
330	2.52	5.68	1.01	1.36	0.33
390	2.53	5.66	0.40	1.34	0.16
540	2.55	5.67	0.34	1.40	0.09
600	2.54	5.66	0.32	1.51	0.09
1380	2.46	5.65	0.35	1.40	0.10
1920	2.45	5.64	0.29	1.44	0.08

Table B-2 Kinetic study results of CIP on BF-HMS, SBA-15 and superparamagnetic mesoporous magnetite for 6 mg/l initial concentration

Time (min)	Ce (mg/l)				
	A3M7	A5M5	A7M3	SBA-15	Magnetite
0	5.99	5.99	5.99	5.98	5.98
10	3.54	2.84	3.15	4.41	3.66
20	3.43	2.88	3.09	4.31	3.55
30	3.33	2.67	2.96	4.23	3.60
40	2.79	2.95	2.88	4.19	3.85
50	2.78	2.62	2.92	4.25	3.84
60	2.72	2.56	2.97	4.41	3.82
120	3.16	2.67	3.00	4.46	3.83
180	3.18	2.77	3.00	4.48	3.81
240	3.15	2.90	2.99	4.51	3.82
300	3.22	2.89	3.05	4.47	3.74
360	3.14	2.97	3.04	4.44	3.77
480	3.18	2.97	2.99	4.45	3.75
600	3.15	2.99	3.05	4.50	3.86
1440	3.15	2.88	3.01	4.38	3.78
1800	3.14	2.89	3.01	4.43	3.80

Table B-3 Kinetic study results of CBZ on HMS, SF-HMSs, and PAC for 9 mg/l initial concentration

Time (min)	Ce (mg/l)				
	HMS	A-HMS	M-HMS	OD-HMS	PAC
0	8.70	8.70	8.70	8.70	8.70
60	7.39	8.27	3.10	6.31	0.39
120	7.47	8.21	2.48	6.07	0.31
180	7.43	8.35	2.46	5.72	0.28
240	7.49	8.35	2.61	6.01	0.22
300	7.68	8.25	2.53	6.23	0.18
360	7.72	8.25	2.61	6.27	0.14
480	7.72	8.29	2.59	6.35	0.12
540	7.66	8.33	2.63	6.40	0.06
600	7.62	8.29	2.67	6.35	0.12
1320	7.60	8.27	2.61	6.31	0.16
1380	7.66	8.27	2.59	6.27	0.12
1440	7.56	8.33	2.57	6.23	0.18

Table B-4 Kinetic study results of CBZ on BF-HMS, SBA-15 and superparamagnetic mesoporous magnetite for 9 mg/l initial concentration

Time (min)	Ce (mg/l)				
	A3M7	A5M5	A7M3	SBA-15	Magnetite
0	8.98	8.98	8.98	8.73	8.73
10	6.25	6.11	6.78	7.68	8.71
20	6.01	6.15	6.66	7.54	8.72
30	5.99	5.76	6.37	7.41	8.70
40	6.01	5.80	6.21	7.24	8.93
50	5.60	5.64	6.29	7.65	8.72
60	5.48	5.52	6.25	7.52	8.94
120	6.01	5.99	6.27	7.74	8.88
180	6.07	6.03	6.27	7.84	8.82
240	6.19	6.05	6.29	7.64	8.86
300	6.15	6.07	6.37	7.72	8.70
360	6.17	6.13	6.40	7.68	8.76
480	6.05	6.17	6.44	7.78	8.76
600	5.99	6.15	6.33	7.66	8.72
1440	5.99	6.09	6.31	7.72	8.70
1800	6.05	6.05	6.37	7.66	8.84

Table B-5 Adsorption isotherm results of CIP on HMS at pH 5, 7, and 9

C ₀ (mg/l)	q _e (mg/g)		
	pH 5	pH 7	pH 9
0.40	0.134	0.040	0.030
0.60	0.211	0.075	0.040
0.80	0.298	0.069	0.055
1.00	0.369	0.065	0.050
1.20	0.442	0.074	0.055
1.40	0.445	0.145	0.075
1.60	0.475	0.140	0.100
1.80	0.520	0.149	0.120
2.00	0.575	0.250	0.145
4.00	1.065	0.550	0.410
5.00	1.187	0.800	0.618
6.00	1.449	0.968	0.728
8.00	1.840	1.440	0.948

Table B-6 Adsorption isotherm results of CIP on A-HMS at pH 5, 7, and 9

C_0 (mg/l)	q_e (mg/g)		
	pH 5	pH 7	pH 9
0.40	0.000	0.000	0.000
0.60	0.000	0.000	0.000
0.80	0.000	0.000	0.000
1.00	0.000	0.000	0.000
1.20	0.000	0.000	0.000
1.40	0.000	0.000	0.000
1.60	0.000	0.000	0.000
1.80	0.000	0.000	0.025
2.00	0.000	0.000	0.030
4.00	0.000	0.000	0.074
5.00	0.000	0.000	0.075
6.00	0.000	0.000	0.098
8.00	0.000	0.000	0.083

Table B-7 Adsorption isotherm results of CIP on M-HMS at pH 5, 7, and 9

C ₀ (mg/l)	q _e (mg/g)		
	pH 5	pH 7	pH 9
0.40	0.183	0.174	0.12
0.60	0.277	0.255	0.20
0.80	0.362	0.333	0.33
1.00	0.440	0.376	0.46
1.20	0.485	0.435	0.52
1.40	0.530	0.500	0.56
1.60	0.608	0.569	0.66
1.80	0.690	0.625	0.81
2.00	0.739	0.696	1.04
3.00	1.034	0.985	1.46
4.00	1.322	1.282	2.06
5.00	1.665	1.609	2.63
7.00	2.291	2.248	3.64
8.00	2.579	2.532	4.32
9.00	3.027	2.973	4.73

Table B-8 Adsorption isotherm results of CIP on OD-HMS at pH 5, 7, and 9

C ₀ (mg/l)	q _e (mg/g)		
	pH 5	pH 7	pH 9
0.40	0.114	0.089	0.079
0.60	0.202	0.134	0.123
0.80	0.239	0.153	0.125
1.00	0.278	0.163	0.150
1.20	0.328	0.228	0.179
1.40	0.407	0.250	0.215
1.60	0.453	0.305	0.284
1.80	0.491	0.380	0.350
2.00	0.570	0.460	0.395
4.00	1.327	0.968	0.920
5.00	1.722	1.350	1.230
6.00	2.015	1.635	1.500
8.00	2.562	2.244	1.630

Table B-9 Adsorption isotherm results of CIP on PAC at pH 5, 7, and 9

C ₀ (mg/l)	q _e (mg/g)		
	pH 5	pH 7	pH 9
0.40	0.194	0.189	0.190
0.60	0.290	0.270	0.277
0.80	0.373	0.351	0.351
1.00	0.471	0.445	0.450
1.20	0.560	0.542	0.540
1.40	0.673	0.649	0.632
1.60	0.764	0.746	0.727
1.80	0.866	0.791	0.830
2.00	0.970	0.942	0.940
4.00	1.925	1.893	1.920
5.00	2.453	2.439	2.450
6.00	2.950	2.950	2.935
8.00	3.945	3.913	3.405

Table B-10 Adsorption isotherm results of CIP on A3M7 at pH 5, 7, and 9

C ₀ (mg/l)	q _e (mg/g)		
	pH 5	pH 7	pH 9
0.40	0.158	0.090	0.055
0.60	0.224	0.140	0.080
0.80	0.284	0.139	0.100
1.00	0.337	0.172	0.114
1.20	0.429	0.226	0.138
1.40	0.457	0.322	0.177
1.60	0.536	0.350	0.144
1.80	0.620	0.368	0.187
2.00	0.680	0.342	0.235
4.00	1.514	0.644	0.565
5.00	1.910	0.978	0.655
6.00	2.330	0.965	0.735
8.00	3.105	1.360	0.995

Table B-11 Adsorption isotherm results of CIP on A5M5 at pH 5, 7, and 9

C ₀ (mg/l)	q _e (mg/g)		
	pH 5	pH 7	pH 9
0.40	0.045	0.000	0.000
0.60	0.060	0.050	0.035
0.80	0.060	0.065	0.045
1.00	0.093	0.078	0.054
1.20	0.113	0.093	0.057
1.40	0.149	0.099	0.074
1.60	0.148	0.108	0.094
1.80	0.189	0.104	0.095
2.00	0.223	0.144	0.125
4.00	0.472	0.349	0.165
5.00	0.544	0.479	0.295
6.00	0.535	0.470	0.315
8.00	0.880	0.850	0.310

Table B-12 Adsorption isotherm results of CIP on A7M3 at pH 5, 7, and 9

C ₀ (mg/l)	q _e (mg/g)		
	pH 5	pH 7	pH 9
0.40	0.000	0.000	0.000
0.60	0.000	0.000	0.000
0.80	0.005	0.100	0.114
1.00	0.000	0.113	0.123
1.20	0.000	0.118	0.134
1.40	0.104	0.158	0.154
1.60	0.134	0.143	0.178
1.80	0.165	0.169	0.201
2.00	0.174	0.194	0.230
4.00	0.290	0.496	0.535
5.00	0.314	0.529	0.595
6.00	0.355	0.615	0.735
8.00	0.595	1.060	0.855

Table B-13 Adsorption isotherm results of CIP on SBA-15 at pH 5, 7, and 9

C ₀ (mg/l)	q _e (mg/g)		
	pH 5	pH 7	pH 9
0.40	0.139	0.060	0.035
0.60	0.206	0.080	0.040
0.80	0.293	0.119	0.074
1.00	0.378	0.145	0.065
1.20	0.432	0.143	0.070
1.40	0.455	0.170	0.090
1.60	0.485	0.165	0.115
1.80	0.555	0.219	0.135
2.00	0.615	0.225	0.160
4.00	1.125	0.660	0.425
5.00	1.197	1.050	0.633
6.00	1.459	1.214	0.743
8.00	1.85	1.686	0.963

Table B-14 Adsorption isotherm results of CIP on superparamagnetic magnetite at pH 5, 7, and 9

C ₀ (mg/l)	q _e (mg/g)		
	pH 5	pH 7	pH 9
0.40	0.000	0.000	0.000
0.60	0.079	0.070	0.050
0.80	0.084	0.069	0.055
1.00	0.108	0.105	0.070
1.20	0.138	0.123	0.090
1.40	0.170	0.145	0.110
1.60	0.183	0.155	0.120
1.80	0.195	0.164	0.130
2.00	0.235	0.185	0.150
4.00	0.330	0.320	0.225
5.00	0.464	0.455	0.284
6.00	0.654	0.604	0.525
8.00	1.062	1.022	0.628

Table B-15 Adsorption isotherm results of CBZ on HMS at pH 5, 7, and 9

C ₀ (mg/l)	q _e (mg/g)		
	pH 5	pH 7	pH 9
0.50	0.032	0.013	0.003
0.70	0.093	0.056	0.033
0.90	0.123	0.084	0.075
1.50	0.246	0.178	0.153
2.50	0.493	0.146	0.104
3.00	0.572	0.167	0.086
5.00	0.719	0.238	0.189
7.00	1.176	0.378	0.176
9.00	1.454	0.499	0.211
10.00	1.593	0.487	0.273
12.00	1.859	0.583	0.358
14.00	1.952	0.638	0.422
16.00	2.208	0.795	0.460

Table B-16 Adsorption isotherm results of CBZ on A-HMS at pH 5, 7, and 9

C ₀ (mg/l)	q _e (mg/g)		
	pH 5	pH 7	pH 9
0.50	0.003	0.000	0.013
0.70	0.009	0.000	0.023
0.90	0.023	0.000	0.025
1.50	0.046	0.000	0.033
2.50	0.043	0.000	0.034
3.00	0.061	0.000	0.040
5.00	0.014	0.000	0.052
7.00	0.000	0.000	0.082
9.00	0.000	0.000	0.093
10.00	0.000	0.000	0.102
12.00	0.028	0.000	0.132
14.00	0.000	0.000	0.161
16.00	0.000	0.000	0.221

Table B-17 Adsorption isotherm results of CBZ on M-HMS at pH 5, 7, and 9

C ₀ (mg/l)	q _e (mg/g)		
	pH 5	pH 7	pH 9
0.50	0.166	0.40	0.015
0.70	0.223	0.46	0.089
0.90	0.283	0.60	0.117
1.50	0.513	0.73	0.363
2.50	0.993	0.79	0.791
3.00	1.216	1.123	1.033
5.00	1.999	1.814	1.728
7.00	2.796	2.652	2.223
9.00	3.683	3.260	2.934
10.00	3.932	3.662	3.196
12.00	4.685	4.275	3.787
14.00	5.311	4.821	4.298
16.00	6.086	5.092	5.059

Table B-18 Adsorption isotherm results of CBZ on OD-HMS at pH 5, 7, and 9

C_0 (mg/l)	q_e (mg/g)		
	pH 5	pH 7	pH 9
0.50	0.147	0.028	0.005
0.70	0.204	0.099	0.070
0.90	0.264	0.128	0.098
1.50	0.494	0.283	0.248
2.50	0.826	0.624	0.543
3.00	0.877	0.694	0.589
5.00	1.452	1.215	1.084
7.00	2.064	1.502	1.179
9.00	2.566	1.956	1.614
10.00	2.690	2.153	1.929
12.00	3.154	2.380	2.043
14.00	3.514	2.903	2.583
16.00	4.314	3.613	3.113

Table B-19 Adsorption isotherm results of CBZ on PAC at pH 5, 7, and 9

C ₀ (mg/l)	q _e (mg/g)		
	pH 5	pH 7	pH 9
0.50	0.246	0.244	0.244
0.70	0.341	0.340	0.345
0.90	0.443	0.443	0.446
1.50	0.735	0.732	0.746
2.50	1.248	1.248	1.227
3.00	1.481	1.470	1.477
5.00	2.441	2.417	2.456
7.00	3.394	3.443	3.436
9.00	4.410	4.388	4.442
10.00	4.834	4.942	4.861
12.00	5.860	5.913	5.785
14.00	6.758	6.903	6.896
16.00	7.741	7.710	7.809

Table B-20 Adsorption isotherm results of CBZ on A3M7 at pH 5, 7, and 9

C ₀ (mg/l)	q _e (mg/g)		
	pH 5	pH 7	pH 9
0.50	0.242	0.196	0.162
0.70	0.320	0.255	0.230
0.90	0.366	0.300	0.270
1.50	0.447	0.356	0.271
2.50	0.562	0.433	0.363
3.00	0.614	0.507	0.520
5.00	0.761	0.747	0.726
7.00	1.376	1.058	0.930
9.00	1.605	1.316	1.150
10.00	1.735	1.408	1.245
12.00	2.145	1.768	1.631
14.00	2.505	1.999	1.975
16.00	2.562	2.200	2.288

Table B-21 Adsorption isotherm results of CBZ on A5M5 at pH 5, 7, and 9

C ₀ (mg/l)	q _e (mg/g)		
	pH 5	pH 7	pH 9
0.50	0.232	0.04	0.209
0.70	0.303	0.16	0.228
0.90	0.324	0.32	0.247
1.50	0.447	0.73	0.310
2.50	0.601	1.43	0.478
3.00	0.606	0.683	0.532
5.00	1.028	0.945	0.703
7.00	1.242	1.235	0.835
9.00	1.573	1.636	0.979
10.00	1.642	1.700	1.071
12.00	1.950	1.990	1.437
14.00	2.180	2.278	1.669
16.00	2.448	2.547	1.984

Table B-22 Adsorption isotherm results of CBZ on A7M3 at pH 5, 7, and 9

C ₀ (mg/l)	q _e (mg/g)		
	pH 5	pH 7	pH 9
0.50	0.230	0.212	0.194
0.70	0.189	0.222	0.189
0.90	0.178	0.224	0.229
1.50	0.197	0.268	0.324
2.50	0.377	0.472	0.463
3.00	0.432	0.532	0.532
5.00	0.624	0.747	0.703
7.00	0.759	0.985	0.835
9.00	0.937	1.245	0.979
10.00	1.073	1.333	1.071
12.00	1.345	1.625	1.437
14.00	1.591	1.750	1.669
16.00	1.637	1.918	1.984

Table B-23 Adsorption isotherm results of CBZ on SBA-15 at pH 5, 7, and 9

C ₀ (mg/l)	q _e (mg/g)		
	pH 5	pH 7	pH 9
0.50	0.165	0.044	0.017
0.70	0.225	0.094	0.048
0.90	0.289	0.140	0.067
1.50	0.510	0.239	0.091
2.50	0.669	0.281	0.157
3.00	0.790	0.332	0.181
5.00	1.269	0.588	0.234
7.00	1.676	0.780	0.482
9.00	1.985	0.937	0.513
10.00	2.047	1.130	0.537
12.00	2.320	0.964	0.533
14.00	2.468	1.198	0.746
16.00	2.644	1.301	0.787

Table B-24 Adsorption isotherm results of CBZ on superparamagnetic magnetite at pH 5, 7, and 9

C ₀ (mg/l)	q _e (mg/g)		
	pH 5	pH 7	pH 9
0.50	0.000	0.000	0.000
0.70	0.000	0.000	0.000
0.90	0.000	0.000	0.000
1.50	0.000	0.000	0.000
2.50	0.000	0.000	0.000
3.00	0.000	0.000	0.000
5.00	0.000	0.000	0.000
7.00	0.000	0.000	0.000
9.00	0.000	0.000	0.000
10.00	0.000	0.000	0.000
12.00	0.000	0.000	0.000
14.00	0.000	0.000	0.000
16.00	0.000	0.000	0.000

BIOGRAPHY

Name: Miss Thitikamon Sitthisorn

Date of birth: June 29th, 1980

Birth place: Chiang Mai

Education: 2007 Bachelor's Degree of Science in Environmental Science
Department of General Science, Faculty of Science,
Chulalongkorn University.

2008 Enrolled in Master's Degree student of Science in
Environmental management (International Program),
Graduated School, Chulalongkorn University.

Presentation: 9th National Environmental Conference in Title of "Removal
of Ciprofloxacin by Adsorption on Mesoporous silicate"
March 24-27th, 2010. Ubonrachathani province.

Current address: 50/1 Sanamkeera road Subdistrict Naimuang
District Muang Lamphun province 51000

E-mail: thitikamon_s@hotmail.com